

# Robust control of the Kuramoto-Sivashinsky equation

*Using  $\mu$ -synthesis to provide robust performance and a priori stability guarantees for the KS equation*

R.J. Baaij

August 15, 2017



**Robust control of the  
Kuramoto-Sivashinsky equation**  
Using  $\mu$ -synthesis to provide robust performance and a priori  
stability guarantees for the KS equation

MASTER OF SCIENCE THESIS

For obtaining the degree of Master of Science in Aerospace Engineering  
at Delft University of Technology

R.J. Baaij

August 15, 2017



**Delft University of Technology**

Copyright © R.J. Baaij  
All rights reserved.

DELFT UNIVERSITY OF TECHNOLOGY  
DEPARTMENT OF  
CONTROL AND SIMULATION

The undersigned hereby certify that they have read and recommend to the Faculty of Aerospace Engineering for acceptance a thesis entitled “**Robust control of the Kuramoto-Sivashinsky equation**” by **R.J. Baaij** in partial fulfillment of the requirements for the degree of **Master of Science**.

Dated: August 15, 2017

Readers:

---

Dr.ir. C.C. de Visser

---

Ir. H.J. Tol

---

Dr. M. Kotsonis

---

Dr.ir. Q.P. Chu



---

# Contents

<b>1</b>	<b>Introduction</b>	<b>1</b>
1-1	Background . . . . .	1
1-2	Research question and objective . . . . .	3
1-3	Structure . . . . .	4
<b>I</b>	<b>Scientific Paper</b>	<b>5</b>
<b>II</b>	<b>Literature Study</b>	<b>33</b>
<b>2</b>	<b>Literature Review</b>	<b>35</b>
2-1	Modeling fluid flows . . . . .	35
2-1-1	The Kuramoto-Sivashinky equation . . . . .	36
2-2	Model reduction methods . . . . .	38
2-2-1	Reduced order modeling . . . . .	38
2-2-2	The multivariate B-spline . . . . .	39
2-2-3	Use in literature . . . . .	39
2-3	Control frameworks . . . . .	40
2-3-1	Generic control configuration . . . . .	40
2-3-2	$H_2$ -controller . . . . .	41
2-3-3	$H_\infty$ -controller . . . . .	41
2-3-4	Controller synthesis in literature . . . . .	42
2-4	Robust control . . . . .	43
2-4-1	Uncertainties . . . . .	43
2-4-2	Generalized robust control problem . . . . .	45
2-5	Comparing robust control methods . . . . .	47

<b>III</b>	<b>Methodology</b>	<b>51</b>
<b>3</b>	<b>Methodology</b>	<b>53</b>
3-1	Reduced Order Models . . . . .	53
3-1-1	Proper Orthogonal Decomposition . . . . .	53
3-1-2	Balanced truncation . . . . .	54
3-1-3	Balanced Proper Orthogonal Decomposition . . . . .	55
3-1-4	Galerkin projection and the multivariate B-spline . . . . .	57
3-2	Control framework synthesis . . . . .	60
3-2-1	The LQG problem . . . . .	60
3-2-2	General $H_\infty$ algorithm . . . . .	61
3-3	Advanced robust control methods . . . . .	62
3-3-1	Structured singular value synthesis . . . . .	63
3-3-2	Signal based approach . . . . .	64
3-3-3	$H_\infty$ loop-shaping . . . . .	64
<b>IV</b>	<b>Conclusions and Recommendations</b>	<b>69</b>
<b>4</b>	<b>Conclusion</b>	<b>71</b>
<b>5</b>	<b>Recommendations</b>	<b>73</b>
	<b>Bibliography</b>	<b>75</b>

---

# Chapter 1

---

## Introduction

According to the United States Energy Information Administration (EIA) the annual world jet fuel consumption is estimated around two billion barrels per year. A slight decrease in aircraft drag could thus save millions of dollars. Hence, many researchers dedicate their work to the development of Active Flow Control (AFC) systems. The concept of AFC focuses on the control of fluid flows using active control systems in order to improve flow properties. Within the field of flow control, the focus has shifted from optimal to robust control. Robust control is required to account for dissimilarities between the model and the physical system. This thesis will investigate the possibility of implementing a robust controller using  $\mu$ -synthesis, accounting for structured parametric uncertainty. This type of uncertainty potentially requires a large effort to model, especially for the complex systems often encountered in flow control (Skogestad & Postlethwaite, 2001, p. 352). However, the work of this thesis proves that modeling for structured parametric uncertainty is not only feasible in the context of flow control, but that robust  $\mu$ -controllers show significant performance improvements with respect to the commonly used optimal LQG controller.

### 1-1 Background

When air flows along the airfoil of a wing, the interaction with the wing causes a transition from laminar to turbulent flow. This turbulent flow is not desirable, as it causes skin-friction drag. Once the flow has reached a turbulent state, it becomes very difficult to control. However, the flow can be controlled during the transition phase from laminar to turbulent flow. This transition phase is initiated by small growing wave-packets, convectively propagating downstream, and they are called Tollmien-Schlichting waves. The transition from laminar to turbulent flow can be delayed by damping these waves, effectively reducing drag.

Active flow control distinguishes itself from passive flow control by the fact that an external power source is used to control the flow. Examples of passive flow might be the dimples on a golf ball or the vortex generators on an aircraft wing. Active flow control uses an actuator to actively influence the flow. An example of an active flow controller is a plasma actuator

that forms a low-temperature plasma between two electrodes, ionizing and accelerating air molecules passing through the plasma. The flow needs to be modeled in order for such a controller to be able to predict the state of the system. Only then does the actuator know when and how it should control the flow.

Modeling a fluid flow is done using a set of Partial Differential Equations (PDEs). Fluid flow is described using the Navier-Stokes (NS) equations. It is however not uncommon for the designer to select a different PDE that mimics specific flow characteristics. A good example of such an equation is the Kuramoto-Sivashinsky equation. The Kuramoto-Sivashinsky (KS) equation is a one-dimensional PDE and, when linearized, consisting of a base flow velocity term and two viscosity terms. It describes numerous physical phenomena, such as instabilities in laminar flame fronts (Sivashinsky, 1977), phase dynamics in reaction-diffusion systems (Kuramoto & Tsuzuki, 1976) and, relevant to our case, convective flows propagating growing disturbances downstream (Fabbiane et al., 2014).

In order to apply controller synthesis methods to a PDE such as the KS equation, the equation needs to be discretized and transformed to a state space system. For high order models, model reduction needs to be applied in order to make controller design computationally tractable. Commonly used methods for model reduction are Proper Orthogonal Decomposition (POD), Balanced Truncation (BT) and Balanced POD (BPOD). In this thesis, a new method for model reduction developed by Tol, Visser, & Kotsonis (2016) is used to model the KS equation. Using this method, an explicit finite dimensional representation of the KS equation is obtained, resulting in a state-space system which can be used for controller synthesis.

Optimal control methods such as LQG control have long been used to control fluid flows. This is often done in feedforward configuration, where the sensor is placed upstream of the actuator and a model is used to predict the state of the flow when it reaches the actuator. In this configuration, optimal control is used since it has very good nominal performance characteristics and is relatively easy to implement. The downside of optimal control in this configuration is that it is very sensitive to perturbations in the plant. The sensor is upstream from the actuator and predicts the state of the signal at the location of the actuator. However, a small difference in for example the base flow velocity would result in an erroneous prediction, potentially amplifying the signal instead of damping it. Uncertainty in the parameters is one of the main reasons that the effects of robust control should be investigated.

When modeling for robust control, two types of uncertainty are distinguished. Model uncertainty is defined as the uncertainty introduced due to approximation and truncation errors that are caused by model reduction or discretization. Real uncertainty is caused by a difference between the model and the physical system in the sense that there is uncertainty in parameters such as the Reynolds number. These real uncertainties are described using structured parametric uncertainty, which is difficult to model due to the complexity of the models used to describe fluid flows. Robust control frameworks have previously been implemented for flow control, but they rarely take into account real uncertainties (Baramov et al., 2002, 2004; Chen & Rowley, 2013; Jones et al., 2015; Flinois & Morgans, 2016).

This thesis aims to show that by use of the state-modeling framework from Tol, de Visser and Kotsonis (2016), explicit finite dimensional representations can be obtained for all differential operators in the KS equation Tol, Visser, & Kotsonis (2016). These representations determine how the parameters from the equation are mapped to the state space equations, defining the structure in which the uncertainty appears in the model. This uncertainty is incorporated

into the model using a procedure based on the work of Gu, Petkov and Konstantinov (2005) (Gu et al., 2005, p. 101-162). A robust control method specifically developed for structured parametric uncertainty is used to synthesize a  $\mu$ -controller in feedback configuration. This controller is then compared to an optimal LQG controller showing that when the plant is perturbed, the robust controller is able to maintain performance while the optimal controller suffers significant loss in performance, proving that robust control outperforms optimal control in presence of uncertainty.

## 1-2 Research question and objective

Recent work by Tol, Visser, & Kotsonis (2016) at the Faculty of Aerospace Engineering at the TU Delft has provided a new methodology for model reduction of linear parabolic PDEs using Multivariate B-Splines (MBSs) on triangulations. Subsequently, using balanced truncation, a model reduction was performed for which an  $H_2$  optimal controller was designed (Tol, Kotsonis, et al., 2016). The work of this thesis contributes to the further development of this control framework in the sense that in the model as presented by Tol, Kotsonis, et al. (2016) real uncertainties have not yet been addressed. The objective for this research reads as follows:

*Develop a robust control framework for the Kuramoto-Sivashinsky equation, discretized using multivariate B-splines, by accounting for parametric uncertainties and analyzing its robust stability and performance characteristics.*

The goal of this thesis is to develop a control framework for fluid flows which provides *a priori* stability guarantees with respect to the robustness of the model. To limit the scope of this thesis, the controller will be designed for the KS equation. Furthermore, in order to prove its robustness, a controller designed using the framework will be benchmarked to analyze the robust stability and performance characteristics of the controller.

The objective as stated above provides a general direction for the research. A set of research questions provides a more direct frame of reference which allows for effective research. The main research question for this thesis is stated as follows:

*How can parametric uncertainty be used in the implementation of a robust control method for the KS equation, such that it provides robust performance characteristics and a priori stability guarantees for a pre-defined set of perturbed plants.*

This main research question has been divided into four subquestions to provide a structured approach:

- I *How should parametric uncertainty be represented in the model after discretization of the Kuramoto-Sivashinsky equation?*
- II *What robust control method should be used for implementing parametric uncertainty?*
- III *How does accounting for parametric uncertainty increase the robust performance characteristics of the system?*
- IV *What stability guarantees can be provided when using feedback control.*

These four questions cover the main subjects of the thesis: structured parametric uncertainties, the robust control framework, robust performance characteristics and robust stability guarantees. Finding the answers to these questions will consequently lead to answering the research question.

## 1-3 Structure

This thesis is structured into four parts. The first part contains the main contribution of this thesis, the scientific paper called *Using  $\mu$ -synthesis to provide stability guarantees and robust performance for the KS-equation*. The second part contains a literature study reviewing the KS equation, different Reduced Order Model (ROM) methods and comparing the different applications of optimal and robust control frameworks. The third part provides a theoretical background to the different model reduction and control methods used in this thesis. The final part contains the conclusions and recommendations of this study.

**Part I**

**Scientific Paper**



# Using $\mu$ -synthesis to provide robust performance and a priori stability guarantees for the KS-equation

R. J. Baaij\*, H. J. Tol† and C. C. de Visser‡

*Delft University of Technology, Mekelweg 2, 2628 CD, Delft, The Netherlands.*

Dissimilarities between an active flow control model and the physical system can be accounted for by use of a robust controller. Modeling errors and uncertainty in the parameters cause controller performance to decrease, and, in some cases, can even destabilize the closed-loop system. This paper shows that, whilst  $H_2$  optimal control provides excellent nominal performance, perturbations in the plant cause significant degradation of robust performance. In an effort to increase the robustness, structured parametric uncertainty is accounted for in the model and used to design a  $\mu$ -controller for the Kuramoto-Sivashinsky equation. To this end, the structure in which the uncertainty presents itself is derived from the partial differential equation and its discretization. This proves that  $\mu$ -synthesis is feasible for active flow control applications, showing that robust performance can be maintained in the presence of perturbations in the plant and guaranteeing robust stability for an acceptable range of uncertainty. Future research should include mixed feedback-feedforward or aggregated actuator/sensor configurations, which could further increase robust performance and stability characteristics.

## Nomenclature

$x$	Dimensionless spatial coordinate	$l$	Control penalty
$v$	Dimensionless velocity	$\gamma$	Expected signal-to-noise ratio
$t$	Dimensionless time	$\sigma$	Variance
$v'$	Velocity perturbation	$E$	Relative energy reduction
$\mathcal{V}$	Steady state velocity	$T(s)$	Closed-loop transfer function
$\mathcal{P}$	Energy ratio	$G(s)$	Open-loop transfer function
$\mathcal{R}$	Reynolds-number-like coefficient	$K(s)$	Controller transfer function
$\omega$	Temporal frequency	$\mathcal{S}(s)$	Sensitivity function
$\alpha$	Spatial wave number	$p_{\mathcal{V}}, p_{\mathcal{P}}, p_{\mathcal{R}}$	Relative perturbation
$q$	Temporal expansion coefficient vector	$p$	Relative combined perturbation
$u$	Control input	$\delta_{\mathcal{V}}, \delta_{\mathcal{P}}, \delta_{\mathcal{R}}$	Uncertainty
$y$	Sensor output	$\delta$	Combined uncertainty
$z$	Control objective	$\Delta_{\mathcal{V}}, \Delta_{\mathcal{P}}, \Delta_{\mathcal{R}}$	Uncertainty block
$A$	State matrix	$\Delta$	Combined uncertainty block
$B$	Input matrix	$\mathbf{\Delta}$	Uncertainty set
$C$	Output matrix	$\mu$	Structured singular value
$D$	Feedthrough matrix	$\delta_{\max}$	Maximum allowed perturbation
$A_{\mathcal{V}}, A_{\mathcal{P}}, A_{\mathcal{R}}$	Mapping matrices	$x_a$	Actuator position
$w_n$	Sensor noise	$x_s$	Sensor position
$w_d$	External disturbance	$\delta_x$	Distance between sensor and actuator
$T$	Simulation time		

\*MSc Student, Control & Simulation Department, Faculty of Aerospace Engineering, Kluyverweg 1, Delft, The Netherlands.

†PhD Student, Control & Simulation Department, Faculty of Aerospace Engineering, Kluyverweg 1, Delft, The Netherlands,

AIAA Student Member

‡Assistant Professor, Control & Simulation Department, Faculty of Aerospace Engineering, Kluyverweg 1, Delft, The Netherlands, AIAA Member

## I. Introduction

Due to the complexity of the Navier-Stokes Equations and the lack of computational power available, active flow control has long been out of the reach of the fluid mechanics community. However, its potential to control turbulence and, with that, reduce drag, has stimulated the disciplines of control theory and fluid mechanics to join forces. This paper positions itself in the field of control of boundary layer flows. In the boundary layer over a flat plate, a transition takes place from laminar flow to turbulent flow. During this transition, growing perturbations are convectively propagating downstream, eventually causing turbulence. Control of these so-called Tollmien-Schlichting (TS) waves allows for damping of the growth of the perturbation, delaying transition and thus reducing overall turbulence.<sup>1</sup>

The field of flow control has recently seen a shift in design philosophy.<sup>2</sup> Whereas earlier work mainly consists of optimal control methods with a focus on performance, recent research often recommends the implementation of robust controllers. Optimal control techniques like Linear Quadratic Regulator (LQR)/Linear Quadratic Gaussian (LQG) control have long been preferred because they are relatively easy to implement and because of their excellent (optimal) nominal performance characteristics.<sup>3</sup> The  $H_2$  optimal control framework has hence successfully been implemented for many different models and used in combination with a wide spread of modeling techniques.<sup>4-7</sup> However, optimal control also has a number of downsides. One disadvantage is that  $H_2$  optimal controllers do not have guaranteed stability margins.<sup>8</sup> This does however make them very well suited for implementation in feedforward configuration in a convective system, where the actuator cannot destabilize the system.<sup>9</sup> The other disadvantage of the  $H_2$  optimal control framework, especially in feedforward setting, is that it is highly sensitive to uncertainties. A small difference in the model would cause an erroneous prediction, potentially amplifying the perturbation instead of damping it. These two disadvantages are the main reasons that robust control methods are being implemented in flow control. However, a robust controller *can maintain performance* as the plant is perturbed while also *guaranteeing that the system will be stable* under such perturbation. Skogestad and Postlethwaite (2001) suggest that these are two of the three fundamental reasons to use feedback control [10, p. 24]. However, in feedback configuration, an erroneous actuation due to uncertainty in the plant will come back to the sensor, increasing the error and potentially destabilizing the plant. Since the  $H_2$  control framework cannot provide stability guarantees, its implementation in a feedback configuration cannot guarantee that the system will remain stable. This suggests that a robust controller which does provide *a priori* stability guarantees could be used to control the system in a feedback configuration.

Robustness is key to controlling a system where there are dissimilarities between the physical system and the model. Whenever some kind of approximation or discretization is applied, a small amount of uncertainty is introduced, potentially destabilizing the system. This kind of model uncertainty is not explicitly accounted for in the model, but it is modeled using a general class of uncertainty. The most straightforward method of accounting for this general uncertainty is the design of a (sub)-optimal  $H_\infty$  controller. Its synthesis method is very similar to the LQG problem, only introducing an extra worst-case disturbance term in the cost function. Research has shown that in a feedback setting, such an  $H_\infty$  (sub)-optimal controller can significantly outperform an  $H_2$  optimal controller.<sup>11</sup> If even more information about the uncertainty is available, this information can be used to design less conservative controllers. To this end, normalized coprime factor uncertainty is commonly modeled using Glover & McFarlane's  $H_\infty$  loop-shaping procedure.<sup>12</sup> This method for robust control design has previously been used to parametrize the unmodelled dynamics after a low-order approximation of the Navier-Stokes Equations.<sup>13</sup> Other research has combined this method with the  $\nu$ -gap, in order to guarantee the stability of such a low-order system.<sup>14,15</sup> However, while model uncertainty indeed can increase the system's overall robustness, it fails to capture specific physical uncertainty such as a change in Reynolds number.

In order to model for real uncertainties, it is necessary to know how a specific uncertainty is explicitly introduced in the model. Skogestad (2001) correctly observes that this method "potentially [...] yields better designs, but may require a much larger effort in terms of uncertainty modeling, especially if parametric uncertainty is considered [10, p. 352]." Flow control usually yields relatively high-order models that include discretization and model reduction steps, making it difficult for explicit uncertainty modeling. For this reason, parametric uncertainty modeling has not been done in the context of flow control. However, this methodology has proven successful for other problems. Research shows examples of robust feedback linearization, using parametric uncertainty for reactor tanks, proving that it is feasible for small systems with two states.<sup>16</sup> Other research shows that for more complex problems, such as the design of a robust controller for a blended wing body aircraft, the controller synthesis becomes computational infeasible due to sheer size of the controller.<sup>17</sup>

However, this paper aims to prove *that structured parametric uncertainty can be modeled for flow control applications, improving robust performance for uncertainty in specific parameters, whilst providing a priori stability guarantees.*

In this paper, a robust controller is synthesized with the objective to control boundary layer flow. Fluid flow is commonly described by the Navier-Stokes equations, but, due to their complexity, it is not uncommon for the designer to select a Partial Differential Equation (PDE) which mimics specific flow characteristics. The linearized Kuramoto-Sivashinsky (KS) equation shows similar characteristics as the initial stage of transition of the flow over a flat plate. It is a one-dimensional equation, which, when linearized, consists of a base flow velocity term and two viscosity terms. It is driven by three parameters: the steady state velocity  $\mathcal{V}$ , the ratio between energy production and dissipation  $\mathcal{P}$ , and Reynolds-number-like parameter  $\mathcal{R}$ . This paper shows that by use of the state-modeling framework from Tol, de Visser and Kotsonis (2016), explicit finite dimensional representations can be obtained for all differential operators.<sup>18</sup> These representations determine how each parameter is mapped to the state space equations. With a procedure based on the work of Gu, Petkov and Konstantinov [19, p. 101-162], the uncertainty is incorporated into the model, mapping the uncertainty parameters using the structure defined by the differential operator representations. This results in an uncertainty model which is used to synthesize a  $\mu$ -controller in feedback configuration. A comparison between the LQG controller and the  $\mu$ -controller shows that when the plant is perturbed, the robust controller is able to maintain performance while the optimal controller suffers significant loss in performance.

This paper is organized as follows. Section II provides an outline of the model, the discretization of the model, and the setting in which the controllers are compared. In Section III, an LQG controller is synthesized, and it is shown that the system suffers from significant performance loss when the plant is perturbed with parametric uncertainty. Section IV shows how the parametric uncertainty is modeled and used to synthesize a  $\mu$ -controller. Finally, Section V compares the two control methods, proving that robust control outperforms optimal control in presence of uncertainty. This paper ends with conclusions and recommendations in Sections VI and VII.

## II. Modeling

In order to represent the Tollmien-Schlichting waves in a flat-plate boundary layer, the linearized Kuramoto-Sivashinsky (KS) equation is discretized in such a way that multiple control methods can be implemented. This section will explain why the KS equation has been selected, how the Multivariate B-Spline (MBS) method is used to discretize the Partial Differential Equation (PDE), and how the control framework and layout have been set up.

### A. The Kuramoto-Sivashinsky equation

The KS equation is a one-dimensional (1D) PDE that describes numerous physical phenomena, such as instabilities in laminar flame fronts,<sup>20</sup> phase dynamics in reaction-diffusion systems<sup>21</sup> and, relevant to our case, convective flows propagating disturbances downstream.<sup>6</sup> The non-linearized KS equation reads

$$\frac{\partial \tilde{v}}{\partial \tilde{t}} + \tilde{v} \frac{\partial \tilde{v}}{\partial \tilde{x}} = -\tilde{\eta} \frac{\partial^2 \tilde{v}}{\partial \tilde{x}^2} - \tilde{\mu} \frac{\partial^4 \tilde{v}}{\partial \tilde{x}^4} \quad (1)$$

with time  $\tilde{t}$ , spatial coordinate  $\tilde{x}$  and velocity perturbation  $\tilde{v}$ . In this equation,  $\tilde{\eta}$  and  $\tilde{\mu}$  are two viscosity parameters. By introducing a reference length  $\tilde{l}$  and a reference velocity  $\tilde{V}$ , where

$$x = \frac{\tilde{x}}{\tilde{l}}, \quad v = \frac{\tilde{v}}{\tilde{V}}, \quad t = \frac{\tilde{V}}{\tilde{v}} \tilde{t} \quad (2)$$

the equation can be made dimensionless. Also, two parameters  $\mathcal{R} = \frac{\tilde{V} \tilde{l}^3}{\tilde{\mu}}$  and  $\mathcal{P} = \frac{\tilde{\eta} \tilde{l}^2}{\tilde{\mu}}$  are introduced.  $\mathcal{R}$  is a Reynolds-number-like coefficient, and  $\mathcal{P}$  controls the ratio between energy production and dissipation. The dimensionless form of the KS equation then reads:

$$\frac{\partial v}{\partial t} + v \frac{\partial v}{\partial x} = -\frac{1}{\mathcal{R}} \left( \mathcal{P} \frac{\partial^2 v}{\partial x^2} + \frac{\partial^4 v}{\partial x^4} \right) \quad (3)$$

If it is then assumed that the system is close to a steady state solution  $\mathcal{V}(x) = \mathcal{V}$ , the KS equation can be linearized using the perturbation  $v'(x, t)$ :

$$v(x, t) = \mathcal{V} + \varepsilon v'(x, t) \quad (4)$$

where  $V$  can be considered the baseflow velocity. Combining Equation (3) and Equation (4) results in the following linearized KS equation:

$$\frac{\partial v'}{\partial t} = -\mathcal{V} \frac{\partial v'}{\partial x} - \frac{1}{\mathcal{R}} \left( \mathcal{P} \frac{\partial^2 v'}{\partial x^2} + \frac{\partial^4 v'}{\partial x^4} \right). \quad (5)$$

As shown by Fabbiane, Semarero, Bagheri and Henningson (2014), using the right parameters, this PDE can be used to represent Tollmien-Schlichting waves.<sup>6</sup> The parameters are set at  $\mathcal{V} = 0.4$ ,  $\mathcal{P} = 0.05$  and  $\mathcal{R} = 0.25$  as to closely mimic the Blasius boundary layer at a local Reynolds number of  $\text{Re}_\delta = 1000$ .

## B. Discretization

The linearized KS equation as described in Equation (5) is a continuous PDE. In order to allow for control design, a finite dimensional approximation of the equation will be derived. The work of Tol, de Visser and Kotsonis (2016) introduces a method by which a parabolic PDE can be transformed into a state-space formulation.<sup>18</sup> As this paper aims to focus on the control methods applied to the KS equation, this section only addresses the most relevant elements of this method. The general idea of this methodology is that the system is projected onto a triangulation of discontinuous piecewise polynomial functions and combined with smoothness properties and boundary conditions. This results in a state-space system with the general notation:

$$\dot{q} = Aq + Bu \quad (6)$$

$$y = Cq \quad (7)$$

where  $q$  is a vector containing the temporal expansion coefficients of the splines and  $u$  represents the control input. The state matrix  $A$  corresponds to the set of linearized differential operators defined as

$$Av' = \left[ -\mathcal{V} \frac{\partial}{\partial x} - \frac{1}{\mathcal{R}} \left( \mathcal{P} \frac{\partial^2}{\partial x^2} + \frac{\partial^4}{\partial x^4} \right) \right] v' \quad (8)$$

and  $B$  corresponds to the mapping of the forcing function used for control of the system. The state matrix  $A$  is generated by a series of linear transformations applied to the parameters  $\mathcal{V}$ ,  $\mathcal{P}$  and  $\mathcal{R}$ . This will become relevant once the subject of structured parametric uncertainty is introduced, as the linearized operators represent the structure of how the parameters are mapped to the state matrix.

The discretization method of Tol, de Visser and Kotsonis (2016) introduces a generic framework that can be used to discretize a parabolic PDE using Galerkin projection on a set of multivariate B-splines. Using this method, explicit finite dimensional representations are obtained for all differential operators in Equation (8).<sup>18</sup> When this method is applied to the KS equation, the differential operators can be written as invariant matrices

$$A_{\mathcal{V}} v' = \frac{\partial}{\partial x} v' \quad (9)$$

$$A_{\mathcal{P}} v' = \frac{\partial^2}{\partial x^2} v' \quad (10)$$

$$A_{\mathcal{R}} v' = \frac{\partial^4}{\partial x^4} v' \quad (11)$$

Due to the linearity of the linearized KS equation, these operators can be substituted into Equation (8), showing that the state matrix of our system is a linear function of the parameters  $\mathcal{V}$ ,  $\mathcal{P}$  and  $\mathcal{R}$ .

$$Av' = \left[ -\mathcal{V} A_{\mathcal{V}} - \frac{1}{\mathcal{R}} (\mathcal{P} A_{\mathcal{P}} + A_{\mathcal{R}}) \right] v' \quad (12)$$

where the partial state matrices describe how the parameters from the KS equation are mapped to the state matrix of our state space system. This means that the state matrix is scaled by each parameter individually and the scaling is mapped by a matrix we have explicitly derived. This property will become very useful when modeling for uncertainty, which is described in detail in Section IV.

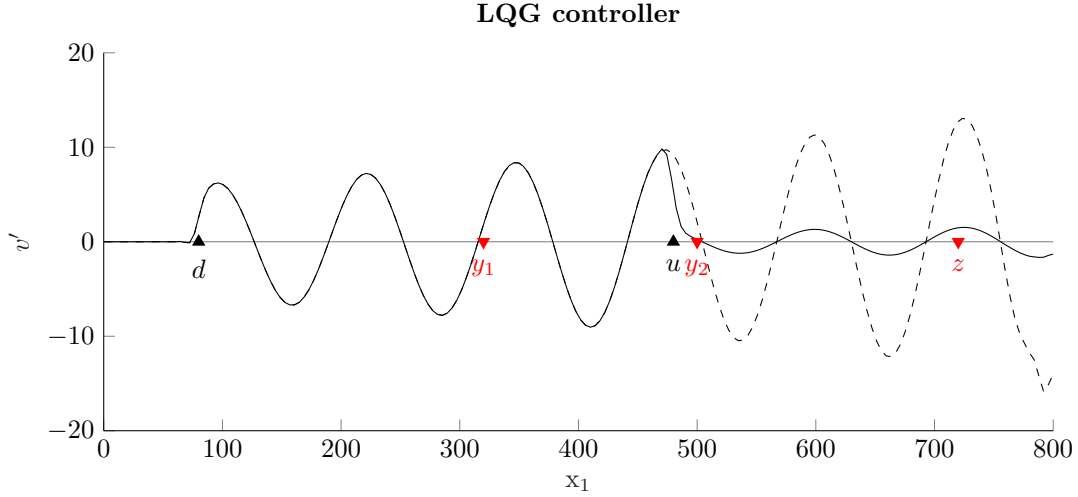


Figure 1: The system is controlled using three sensors  $y_1$ ,  $y_2$  and  $z$  and two actuators  $d$  and  $u$ . Due to the convective property of the KS equation, a growing perturbation propagates downstream showing temporal instability.

### C. Layout

The layout of the system has been modeled after the layout suggested by Fabbiane (2014).<sup>6</sup> The domain in which the perturbation is simulated is defined by  $x \in [0, 800]$ . On this domain we define two actuators at  $x_d = 80$  and  $x_u = 480$  and three sensors at  $x_{y_1} = 320$ ,  $x_{y_2} = 492$  and  $x_z = 720$ , as is shown in Figure 1. Combined with the control input from Equation (6), the linearized KS equation then reads

$$\frac{\partial v'}{\partial t} = -\mathcal{V} \frac{\partial v'}{\partial x} - \frac{1}{\mathcal{R}} \left( \mathcal{P} \frac{\partial^2 v'}{\partial x^2} + \frac{\partial^4 v'}{\partial x^4} \right) + f'(x, t) \quad (13)$$

where the forcing function  $f'(x, t)$  contains both actuators

$$f'(x, t) = b_d(x)w_d(t) + b_u(x)u(t) \quad (14)$$

where  $b_d(x)$  and  $b_u(x)$  map the external disturbance  $d(t)$  and the control input  $u(t)$  to the system respectively. The spatial distribution of the actuators are represented by Gaussian distributions, both with  $\sigma = 4$  and amplified by a factor 2.5. The Gaussian distribution implies that the actuator  $b_u$  controls the system by localized volume forcing.<sup>5</sup> In the physical model it is obviously unknown how the external disturbance  $w_d(t)$  enters the system, so the Gaussian distribution here is used as a modeling assumption.<sup>6</sup>

For control purposes, we define three outputs for this system

$$y_1(t) = \int c_{y_1}(x)v'(x, t)dx + w_n(t) \quad (15)$$

$$y_2(t) = \int c_{y_2}(x)v'(x, t)dx + w_n(t) \quad (16)$$

$$z(t) = \int c_z(x)v'(x, t)dx \quad (17)$$

The first output is defined as a point sensor at  $x_{y_1} = 320$  and will be used for state estimation for the feedforward controller presented in Section III. The second output is defined as point sensor at  $x_{y_2} = 492$  and is used by the feedback controller presented in Section IV. Both sensors are influenced by a sensor noise  $w_n(t)$  defined as white Gaussian noise with mean  $\mu = 0$  and standard deviation  $\sigma = 1$ . The third output is a point sensor far downstream of the actuators ( $x_z = 720$ ), used as a control objective for the design of both control configurations.

We now combine Equations (13) to (17) and discretize the system using a spline base of 49 splines, consisting of sixth degree, 1D polynomials with third order continuity according to the methodology described

in Section B. This yields the following state space system

$$\dot{q} = Aq + B_d w_d + B_u u \quad (18)$$

$$z = C_z q + l u \quad (19)$$

$$y = \begin{cases} C_{y_1} q + \gamma w_n & \text{in feedforward configuration} \\ C_{y_2} q + \gamma w_n & \text{in feedback configuration} \end{cases} \quad (20)$$

where  $q \in \mathbb{R}^{147}$  is a vector containing al de B-spline coefficients. The external disturbance  $w_d$  and the control input  $u$  are mapped to the B-spline coefficients by the vectors  $B_d$  and  $B_u$  and the output matrices  $C_z$ ,  $C_{y_1}$  and  $C_{y_2}$  approximate the integrals described by Equations (15) to (17). The control penalty  $l$  and expected signal-to-noise ratio  $\gamma$  will later on be used to tune the controller.

### III. Feedforward control

Studies have shown that in the context of flow control, the best performance in terms of amplitude reduction is achieved when using feedforward control, and, due to the absence of feedback, the system cannot be destabilized by the controller.<sup>3</sup> However, when nominal plant is perturbed, the lack of feedback results in significant performance degradation. This section will present the implementation of an optimal controller in feedforward setting, and will also show how the performance of the controller decreases as parametric uncertainty is introduced.

#### A. $H_2$ /LQG controller

We often see the use of  $H_2$  optimal control frameworks in flow control. Optimal control is based on finding a control law that minimizes a certain cost function. These methods tend to have very good performance characteristics, but do not provide stability guarantees.<sup>8</sup> However, as will be explained in Section E, robust stability is not an issue for feedforward control. Hence  $H_2$  optimal control is very well suited for this problem. The objective of the  $H_2$  control problem is to minimize the energy in the transfer function between the disturbance and the control objective. This problem is often solved using the LQG problem, which is the time-domain equivalent of  $H_2$  optimal control. It combines the LQR with a Kalman estimator to find an optimal controller for a linear system perturbed by white Gaussian noise. This section describes how the LQG controller is implemented for the KS equation.

In the feedforward configuration, the sensor used to estimate the state is placed upstream of the actuator. Therefore, the system described by Equations (18) to (20) can be written as

$$\dot{q} = Aq + B_d w_d + B_u u \quad (21)$$

$$z = C_z q + l u \quad (22)$$

$$y = C_y q + \gamma w_n \quad (23)$$

Our problem is then defined as to find a controller  $u = Ky$  that minimizes the objective function that describes the  $H_2$  norm of the system, defined as

$$J = E \left\{ \lim_{T \rightarrow \infty} \frac{1}{T} \int_0^T [q^T C_z q + u^T l u] dt \right\} \quad (24)$$

The block diagram corresponding with this problem is shown in Figure 2. If we define the error signal  $z$  as

$$z = \begin{bmatrix} C_z & 0 \\ 0 & l \end{bmatrix} \begin{bmatrix} q \\ u \end{bmatrix} \quad (25)$$

and the stochastic inputs as

$$\begin{bmatrix} w_d \\ w_n \end{bmatrix} = \begin{bmatrix} B_d & 0 \\ 0 & \gamma \end{bmatrix} w \quad (26)$$

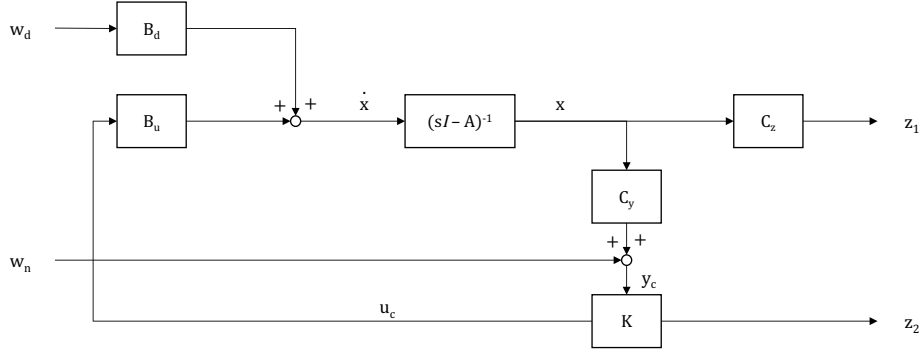


Figure 2: Block diagram for the LQG problem

we can represent the LQG problem as an  $H_2$  optimal control problem, resulting in the cost function

$$J = E \left\{ \lim_{T \rightarrow \infty} \frac{1}{T} \int_0^T z(t)^T z(t) dt \right\} \quad (27)$$

The generalized plant can now be written as

$$P = \left[ \begin{array}{c|cc} A & B_1 & B_2 \\ \hline C_1 & D_{11} & D_{12} \\ C_2 & D_{21} & D_{22} \end{array} \right] = \left[ \begin{array}{c|cc|c} A & B_d & 0 & B_u \\ \hline C_z & 0 & 0 & 0 \\ 0 & 0 & 0 & l \\ \hline C_y & 0 & \gamma & 0 \end{array} \right] \quad (28)$$

Solving the LQG problem can be split up in two independent problems using the separation principle as described in [10, pp. 354]. The first step is to determine the optimal controller for a deterministic LQR problem and the second step is to determine the optimal state estimator. The final step is then to combine the optimal state estimator and the optimal state feedback into an LQG controller.

The control feedback  $K$  is computed using a simple LQR controller to optimize the objective function described by Equation (24). This is done by solving the Riccati equation such that the control signal is equal to  $u = -Kq$ , where

$$K = R^{-1} B^T X \quad (29)$$

and  $X = X^T \geq 0$  is the solution to the algebraic Riccati equation

$$A^T X + X A - X B R^{-1} B^T X + Q = 0 \quad (30)$$

The next step is to compute the estimation feedback gain  $L$  using a Kalman estimator. The Kalman filter has the following structure:

$$\dot{\hat{q}} = A\hat{q} + Bu + L(y - C\hat{q}) \quad (31)$$

The optimal estimation feedback gain is given by

$$L = Y C^T V^{-1} \quad (32)$$

where again we find  $T = Y^T \geq 0$  using the algebraic Riccati equation

$$Y A^T + A Y - Y C^T V^{-1} C Y + W = 0 \quad (33)$$

Finally steps 1 and 2 are combined to create the following compensator:

$$\begin{aligned} \dot{\hat{q}} &= (A - BK - LC)\hat{q} + Ly \\ u &= K\hat{q} \end{aligned} \quad (34)$$

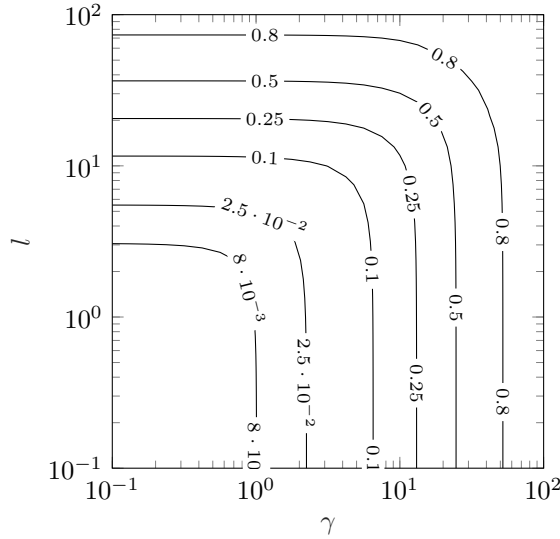


Figure 3: Nominal controller performance measured in  $E$ , subject to varying design parameters  $l$  and  $\gamma$

The closed-loop dynamics can now be described as

$$\frac{d}{dt} \begin{bmatrix} q \\ q - \hat{q} \end{bmatrix} = \begin{bmatrix} A - BK & BK \\ 0 & A - LC \end{bmatrix} \begin{bmatrix} q \\ q - \hat{q} \end{bmatrix} + \begin{bmatrix} B_d & 0 \\ 0 & \gamma \end{bmatrix} \begin{bmatrix} w_d \\ w_n \end{bmatrix} \quad (35)$$

This system provides an optimal control signal  $u$  proportional to the estimate flow  $\hat{q}$  using signals from the measurement  $y$ .

## B. Parameter selection

The LQG controller synthesis is subject to two tuning parameters, the control penalty  $l$  and the expected signal-to-noise ratio  $\gamma$ .<sup>7</sup> These parameters define how the state feedback gain and the estimator feedback gain behave within the model. A high control penalty  $l$  results in a less aggressive state feedback gain  $K$ , and a high signal-to-noise ratio results in a less aggressive estimator feedback gain  $L$ . Tuning of the control penalty influences the performance of the system. Increasing the control penalty will lead to a smaller control effort, which is favourable. Tuning of the expected signal-to-noise ratio determines how much noise the system expects. This is a form of robust control, as noise is a form of uncertainty. Increasing  $\gamma$  would thus lead to a more robust design. Figure 3 shows the results of a parametric study, where controllers have been designed for varying values of  $l$  and  $\gamma$ . The controller performance for each setting is defined as the ratio between the 2-norm of the closed-loop system to the 2-norm of the open-loop system. This ratio represents the size of the perturbation that remains after control is applied relative to the size of the uncontrolled perturbation. Throughout the rest of this paper the following definition of relative energy reduction  $E$  is used:

$$E = \frac{\|T_{zw}\|_2^2}{\|G_{zw}\|_2^2}. \quad (36)$$

From Figure 3 it becomes clear that both tuning parameters can be harmlessly increased along the contour until the curve in the plot is reached. For a focus on control effort minimization, the design point should be selected on the left-hand side of the curve in the contour. On the other hand, if the goal is to design a more robust controller, the design point should be selected on the right-hand side of the curve in the contour. Since our objective is the latter, the rest of this chapter will work with a controller designed at  $l = 1$ ,  $\gamma = 1$ , resulting in a controller with an excellent performance of  $E = 0.008$ .

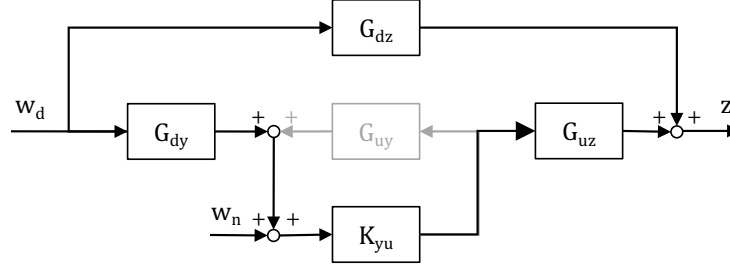


Figure 4: Transfer function diagram for the feedforward configuration.

### C. Robust stability

As explained in Section A, the aim of the control design is to find a compensator  $\mathcal{K}_{yu}(s)$  such that

$$u = \mathcal{K}_{yu}y \quad (37)$$

describes the optimal control input. The transfer function of the closed-loop system from the disturbance  $w_d$  to the output  $z$  is then given by

$$\frac{z(s)}{w_d(s)} = G_{zw}(s) + \frac{G_{uz}(s)\mathcal{K}_{yu}(s)G_{wy}(s)}{1 - G_{uy}(s)\mathcal{K}_{yu}(s)} \quad (38)$$

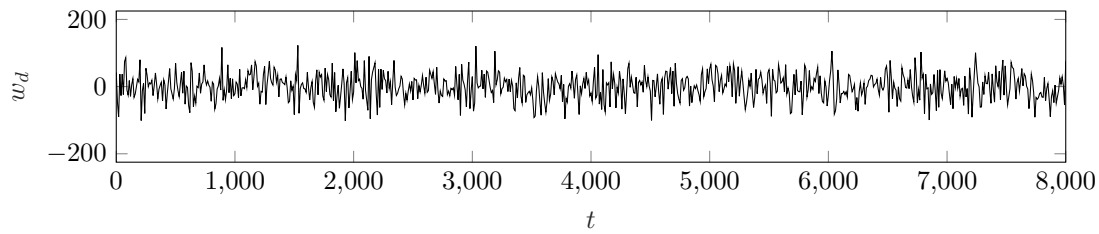
The block diagram for this relation is shown in Figure 4. The main difference between the feedforward case and the feedback case is that, due to the convective nature of the system, we find that  $G_{uy} \approx 0$ . This is because the actuator is downstream of the sensor, and therefore, an erroneous actuator input cannot be fed back into the sensor, destabilizing the system. From this follows that, if the closed-loop system has nominal stability, a feedforward system must achieve robust stability. This can be confirmed when looking at Equation (38), and more specifically, the denominator of the second term. If this denominator, defined as the sensitivity function  $\mathcal{S}(s)$ , becomes very small, the closed-loop transfer function would become very large, destabilizing the system. However, if  $G_{uy} \approx 0$ , we find

$$\mathcal{S}(s) = \frac{1}{1 - G_{uy}(s)\mathcal{K}_{yu}(s)} \approx 1 \quad (39)$$

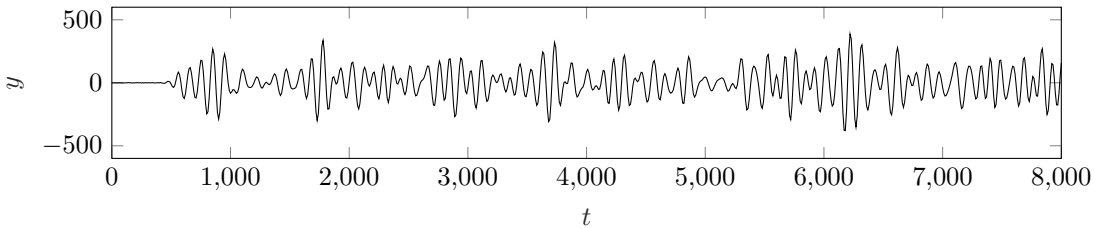
Hence we can conclude that robust stability is not a problem for feedforward systems.

### D. Nominal performance

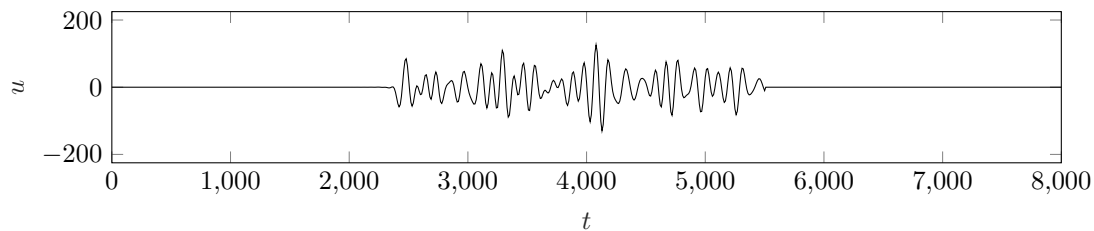
Optimal control is very useful due to its nominal performance characteristics. As described in Section B, the tuning parameters have been selected at  $l = 1$  and  $\gamma = 1$  resulting in a relative energy reduction of  $E = 0.008$ . To illustrate the performance of the controller, a simulation was executed in feedforward configuration. Figure 1 describes the input and output signals. The plant is excited by an external disturbance  $w_d$ , a Gaussian white noise signal with variance  $\sigma_d = 40$ , as shown in Figure 5a. The signal enters the system at  $x = 80$ , with an actuator modeled as a Gaussian distribution with a spatial variance  $\sigma_x = 10$ . As shown by Belson et al. (2013), the combination of a Gaussian distributed actuator and a point sensor provides good results for both feedforward and feedback configuration.<sup>9</sup> This configuration is hence used for the synthesis of both the feedforward controller and, in Section IV, the feedback controller. Better results could potentially be achieved with more advanced actuator/sensor combinations, but this is outside the scope of this research. The point sensor used to generate the Kalman estimate is placed at  $x = 320$ , and the signal measured by the sensor is shown in Section D. The time delay between the start of the simulation and the signal reaching the sensor shows the convective property of the system. The actuator, placed at  $x = 480$  is only activated for  $t \in [2500, 5500]$ , to clearly illustrate the difference between the controlled and uncontrolled signal. As expected from the relative energy reduction  $E = 0.008$ , the control input, shown in Section D, cancels the



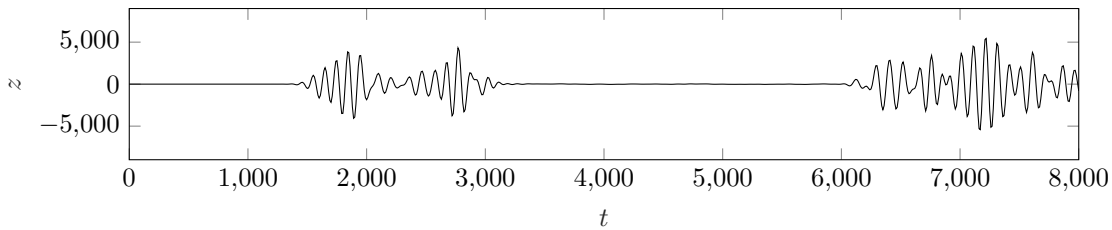
(a) External disturbance  $w_d$  entering the system at  $x = 80$



(b) Sensor output  $y$  observed at  $x = 320$



(c) Control input  $u$  provided by actuator at  $x = 480$



(d) Control objective  $z$  observed at  $x = 720$

Figure 5: Input and output signals of the feedforward system controlled using an LQG controller, where the control input is active for  $t \in [2500, 5500]$ .

external disturbance almost completely. Figure 5d confirms this, as the control objective signal  $z$  is reduced significantly for  $t \in [3000, 6000]$ . The slight time delay is again caused by the convective properties of the system.

### E. Robust performance

An LQG controller in feedforward configuration is rather sensitive to disturbances. Especially uncertainty in the plant cause significant decrease in energy reduction. When the external disturbance reaches the sensor  $y$ , the controller generates an estimate of the model, which is then used to predict the shape and size of the disturbance at the actuator. If this model does not correctly represent the physical system, the physical signal is likely not to correspond to the modeled signal. It is not hard to imagine that an error in the base flow velocity  $\mathcal{V}$  can easily reduce the performance, as the right perturbation will render the modeled signal out of phase with the actual signal, possibly even increasing the disturbance instead of decreasing it.

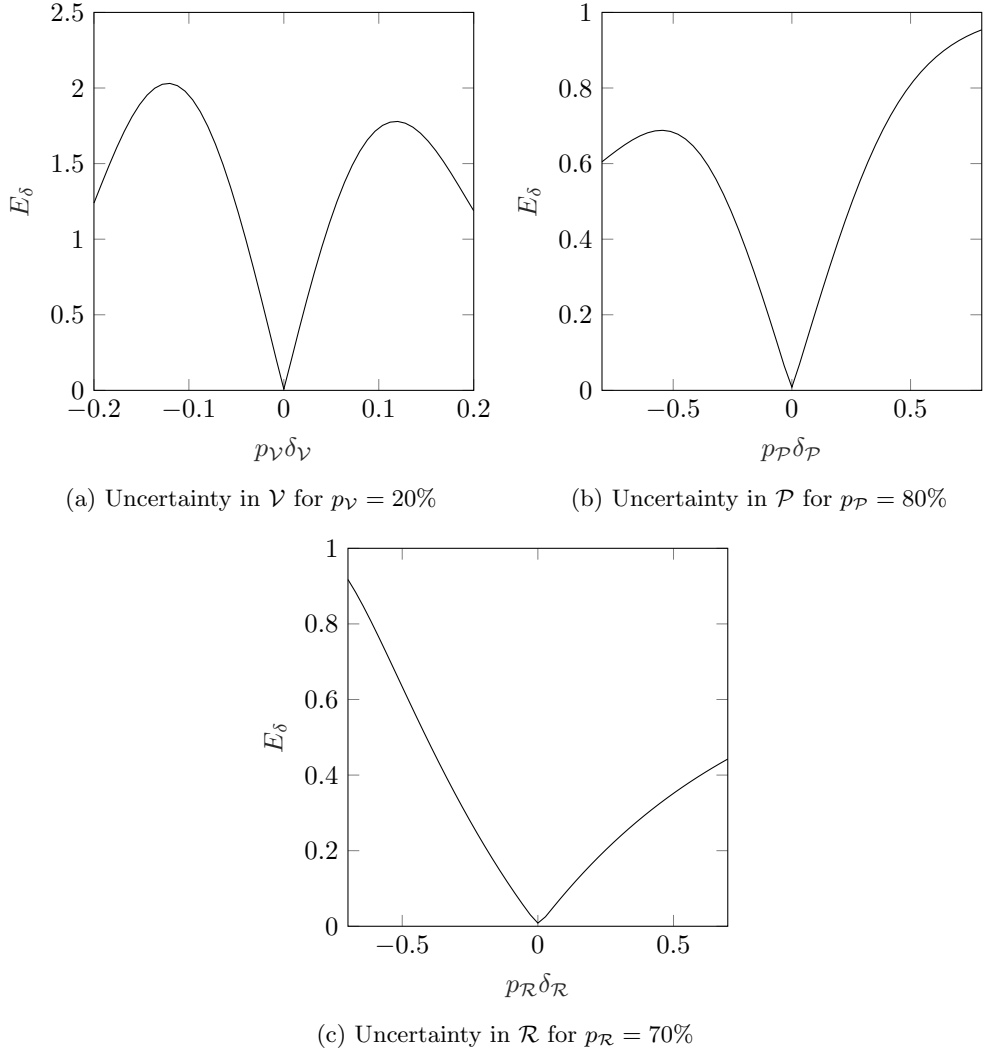


Figure 6: Sensitivity of the closed-loop system, measured in relative perturbed energy reduction  $E_{\delta}$ , to uncertainty in the system parameters  $\mathcal{V} = 0.4$ ,  $\mathcal{P} = 0.05$  and  $\mathcal{R} = 0.25$  where  $|\delta_{\mathcal{V}}, \delta_{\mathcal{P}}, \delta_{\mathcal{R}}| \leq 1$ .

To test the sensitivity of the closed-loop system under the influence of uncertainty, a perturbation is introduced to the parameters of the KS equation. This uncertainty is described by

$$\mathcal{V}_p = \mathcal{V}(1 + \delta_{\mathcal{V}} p_{\mathcal{V}}) \quad (40)$$

$$\mathcal{P}_p = \mathcal{P}(1 + \delta_{\mathcal{P}} p_{\mathcal{P}}) \quad (41)$$

$$\mathcal{R}_p = \mathcal{R}(1 + \delta_{\mathcal{R}} p_{\mathcal{R}}) \quad (42)$$

where the nominal values of the system parameters are  $\mathcal{V} = 0.4$ ,  $\mathcal{P} = 0.05$  and  $\mathcal{R} = 0.25$ . The maximum amount of perturbation allowed for a certain parameter can be selected using the relative perturbations  $p_{\mathcal{V}}$ ,  $p_{\mathcal{P}}$ ,  $p_{\mathcal{R}}$ , where multiplication with an arbitrary  $|\delta_{\mathcal{V}}, \delta_{\mathcal{P}}, \delta_{\mathcal{R}}| \leq 1$  can create an infinite amount of possible uncertainties. The state matrix for the perturbed plant is then described by

$$A_p = \mathcal{V}(1 + p_{\mathcal{V}} \delta_{\mathcal{V}}) A_{\mathcal{V}} + \frac{1}{\mathcal{R}(1 + p_{\mathcal{R}} \delta_{\mathcal{R}})} (\mathcal{P}(1 + p_{\mathcal{P}} \delta_{\mathcal{P}}) A_{\mathcal{P}} + A_{\mathcal{R}}) \quad (43)$$

The performance of the system is described by the relative energy reduction of the closed-loop system to the open-loop system  $E$ , according to

$$E = \frac{\|T_{zw}\|_2^2}{\|G_{zw}\|_2^2} \quad (44)$$

Table 1: Combined uncertainty for different values of  $\delta$

$\delta$	10%	25%	50%	100%
$\delta \begin{bmatrix} p_{\mathcal{V}} \\ p_{\mathcal{P}} \\ p_{\mathcal{R}} \end{bmatrix}$	$\begin{bmatrix} 0.4\% \\ -5.4\% \\ 8\% \end{bmatrix}$	$\begin{bmatrix} 1\% \\ -14\% \\ 20\% \end{bmatrix}$	$\begin{bmatrix} 2\% \\ -27\% \\ 40\% \end{bmatrix}$	$\begin{bmatrix} 4\% \\ -54\% \\ 80\% \end{bmatrix}$

To illustrate the sensitivity of each parameter to a perturbation in the plant,  $E_{\delta}$  is determined for the system while introducing a perturbation to the respective parameters. Figure 6 shows how the performance of the system degrades under this uncertainty for each individual parameter.

From this sensitivity analysis we find that uncertainty in the baseflow velocity  $\mathcal{V}$  results in the largest decrease in relative energy reduction. Only a perturbation of 2% in this parameter causes the relative energy reduction to degrade from  $E = 0.008$  to  $E = 0.5$ . This is a lot compared to the other parameters,  $\mathcal{P}$  and  $\mathcal{R}$ , which encounter this kind of performance degradation under 27% and 40% uncertainty respectively.

In practice, an uncertainty in one of the parameters seldom interacts with the system without affecting the other parameters. Hence, when analyzing the sensitivity of the system to uncertainty in its parameters, not only the individual sensitivities, but the effect of the combined uncertainties should be addressed. We know for example from the Blasius equation that the baseflow velocity is dependent on the Reynolds number, which means that, for the KS equation, an uncertainty in  $\mathcal{R}$  would always come hand in hand with an uncertainty in  $\mathcal{V}$ . In order to properly analyze the system under a combined perturbation, a vector is introduced that simultaneously perturbs each parameter. This vector is defined as

$$p = \begin{bmatrix} p_{\mathcal{V}} \\ p_{\mathcal{P}} \\ p_{\mathcal{R}} \end{bmatrix} \quad (45)$$

The amount of combined uncertainty can then be described by multiplying this vector by a single  $|\delta| \leq 1$ . By varying the different values for  $p_{\mathcal{V}}$ ,  $p_{\mathcal{P}}$  and  $p_{\mathcal{R}}$ , the relative perturbation can be selected. This is important, because as noted before, the system is much more sensitive to a perturbation in the base flow velocity  $\mathcal{V}$  with respect to the other two parameters. Hence, for future reference, the ratio of the three relative perturbations has been selected equal to their sensitivity to a unit disturbance  $\delta_{\mathcal{V}}, \delta_{\mathcal{P}}, \delta_{\mathcal{R}} = 1$ . As the system should be robust against a worst-case disturbance, it was investigated what combination of  $\delta_{\mathcal{V}}$ ,  $\delta_{\mathcal{P}}$  and  $\delta_{\mathcal{R}}$  resulted in the highest loss in performance. Analysis showed that the combination  $[\delta_{\mathcal{V}} \ \delta_{\mathcal{P}} \ \delta_{\mathcal{R}}] = [1 \ -1 \ 1]$  resulted in the worst case uncertainty. Hence, for analysis, the combined uncertainty vector is defined with the uncertainty distribution as shown in Table 1.

Analysis of the closed-loop system under combined uncertainty resulted in a relative energy reduction of 100% under 50% uncertainty. This means that for a combined uncertainty of  $\delta = 0.5$  the controller is entirely ineffective, resulting in an energy reduction of  $E = 1$ . In practice however, this is not expected to occur frequently. For the respective parameters, this corresponds with a combined worst-case perturbation of

$$\delta \begin{bmatrix} p_{\mathcal{V}} \\ -p_{\mathcal{P}} \\ p_{\mathcal{R}} \end{bmatrix} = 0.5 \begin{bmatrix} 4\% \\ -54\% \\ 80\% \end{bmatrix} = \begin{bmatrix} 2\% \\ -27\% \\ 40\% \end{bmatrix} \quad (46)$$

The loss of performance due to a perturbation as described above illustrates why it is necessary to investigate the possibility of more robust controllers for flow control applications.

#### IV. Feedback control

In the previous section it became evident that feedforward control is very sensitive with respect to parametric uncertainty. As uncertainty is always present, a method should be developed to account for this. This section presents a method that addresses parametric uncertainty using the structure in which it appears, and then compares the robust feedback controller to the previously designed LQG/feedforward controller.

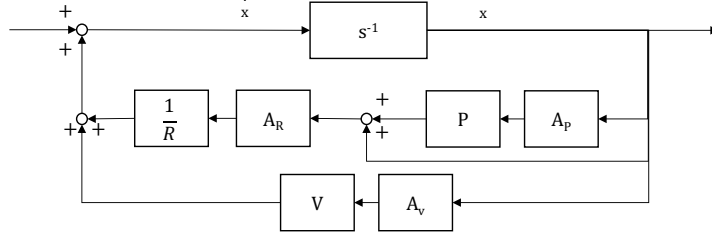


Figure 7: Block diagram of the decomposed state matrix  $A$ . The state matrix is obtained by integration, and multiplication of parameters with their corresponding differential operator matrix.

## A. Uncertainty

Structured uncertainty incorporates knowledge of how the uncertainty is structured in the design of the controller. This potentially results in a less conservative controller while still being able to guarantee robust stability. One specific form of structured uncertainty is parametric uncertainty. With parametric uncertainty, it is known how the parameters affect the model, but their value is uncertain. It is quantified using the assumption that their deviation from the nominal value is known. An uncertain parameter  $\alpha$  can then be described as

$$\alpha_p = \bar{\alpha}(1 + p_\alpha \delta_\alpha) \quad (47)$$

where  $\bar{\alpha}$  is the mean parameter value,  $p_\alpha \in [0 \ 1]$  the relative uncertainty in the parameter, and  $\delta_\alpha$  is a real scalar satisfying  $|\delta_\alpha| \leq 1$ . From Equation (12), we know that uncertainty in the parameters from the KS equation results in a linear perturbation of the state-matrix  $A$ . This is applied to the KS equation by looking at how the state matrix is built up:

$$\dot{q} = \left( \mathcal{V}A_{\mathcal{V}} + \frac{1}{\mathcal{R}} (\mathcal{P}A_{\mathcal{P}} + A_{\mathcal{R}}) \right) q \quad (48)$$

This equation can be pulled apart into different blocks and combined as a block diagram as presented in Figure 7. When introducing uncertainty to the parameters, the blocks from Figure 7 need to be replaced by blocks which include the uncertainty. To that end, the parameters will be represented as Linear Fractional Transformations (LFTs), a configuration used to show how uncertainty affects the system.<sup>19</sup> This can be done either by upper LFTs or lower LFTs, denoted by  $F_u$  and  $F_l$  respectively. Uncertainty in the parameter  $\mathcal{R}$  is introduced as an inverse multiplicative perturbation. We can thus rewrite the parameter  $\mathcal{R}$  as

$$\frac{A_{\mathcal{R}}}{\mathcal{R}(1 + p_{\mathcal{R}}\delta_{\mathcal{R}})} = \frac{A_{\mathcal{R}}}{\mathcal{R}} - \frac{A_{\mathcal{R}}}{\mathcal{R}} p_{\mathcal{R}}\delta_{\mathcal{R}}(1 + p_{\mathcal{R}}\delta_{\mathcal{R}})^{-1} = F_u(M_{mi}, \delta_{\mathcal{R}}) \quad (49)$$

with the corresponding inverse multiplicative input perturbation matrix

$$M_{mi} = \begin{bmatrix} -p_{\mathcal{R}} & \frac{A_{\mathcal{R}}}{\mathcal{R}} \\ -p_{\mathcal{R}} & \frac{A_{\mathcal{R}}}{\mathcal{R}} \end{bmatrix} \quad (50)$$

The parameters  $\mathcal{V}$  and  $\mathcal{P}$  with their uncertainty can also be represented by the upper LFTs  $F_u(M_{\mathcal{V}}, \delta_{\mathcal{V}})$  and  $F_u(M_{\mathcal{P}}, \delta_{\mathcal{P}})$  where

$$M_{\mathcal{V}} = \begin{bmatrix} 0 & A_{\mathcal{V}}\mathcal{V} \\ p_{\mathcal{V}} & A_{\mathcal{V}}\mathcal{V} \end{bmatrix}, \quad \text{and} \quad M_{\mathcal{P}} = \begin{bmatrix} 0 & A_{\mathcal{P}}\mathcal{P} \\ p_{\mathcal{P}} & A_{\mathcal{P}}\mathcal{P} \end{bmatrix} \quad (51)$$

The block diagram of the state matrix with the LFTs included is shown in Figure 8. These LFTs can now be used to connect the uncertain variables  $\delta_{\mathcal{V}}$ ,  $\delta_{\mathcal{P}}$  and  $\delta_{\mathcal{R}}$  with the parameters using the following set of matrix equalities:

$$\begin{bmatrix} y_{\mathcal{V}} \\ v_{\mathcal{V}} \end{bmatrix} = \begin{bmatrix} 0 & A_{\mathcal{V}}\mathcal{V} \\ p_{\mathcal{V}} & A_{\mathcal{V}}\mathcal{V} \end{bmatrix} \begin{bmatrix} u_{\mathcal{V}} \\ q \end{bmatrix} \quad \begin{bmatrix} y_{\mathcal{P}} \\ v_{\mathcal{P}} \end{bmatrix} = \begin{bmatrix} 0 & A_{\mathcal{P}}\mathcal{P} \\ p_{\mathcal{P}} & A_{\mathcal{P}}\mathcal{P} \end{bmatrix} \begin{bmatrix} u_{\mathcal{P}} \\ q \end{bmatrix} \quad \begin{bmatrix} y_{\mathcal{R}} \\ v_{\mathcal{R}} \end{bmatrix} = \begin{bmatrix} -p_{\mathcal{R}} & \frac{1}{\mathcal{R}} \\ -p_{\mathcal{R}} & \frac{1}{\mathcal{R}} \end{bmatrix} \begin{bmatrix} u_{\mathcal{R}} \\ A_{\mathcal{R}}q + v_{\mathcal{R}} \end{bmatrix}$$

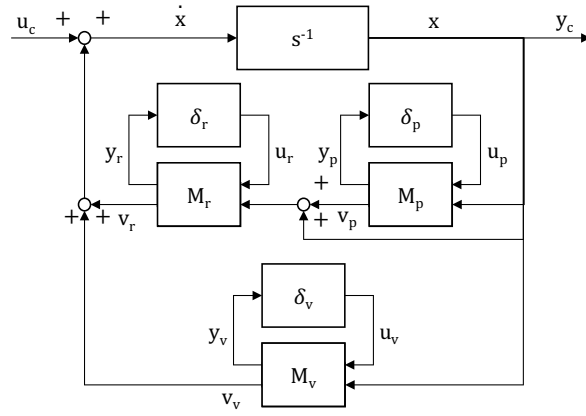


Figure 8: Block diagram of the state matrix  $A$  with Linear Fractional Transformations

$$\begin{aligned} u_{\mathcal{V}} &= \delta_{\mathcal{V}} y_{\mathcal{V}} \\ u_{\mathcal{P}} &= \delta_{\mathcal{P}} y_{\mathcal{P}} \\ u_{\mathcal{R}} &= \delta_{\mathcal{R}} y_{\mathcal{R}} \end{aligned}$$

Now, combining these results with the information we can find in Figure 8 and stating that  $y_c = q$  we obtain the following set of equations:

$$\begin{aligned} \dot{q} &= v_{\mathcal{R}} + v_{\mathcal{V}} + u_c & y_c &= q \\ y_{\mathcal{V}} &= \mathcal{V}q & v_{\mathcal{V}} &= p_{\mathcal{V}}u_{\mathcal{V}} + A_{\mathcal{V}}\mathcal{V}q \\ y_{\mathcal{P}} &= \mathcal{P}q & v_{\mathcal{P}} &= p_{\mathcal{P}}u_{\mathcal{P}} + A_{\mathcal{P}}\mathcal{P}q \\ y_{\mathcal{R}} &= -p_{\mathcal{R}}u_{\mathcal{R}} + \frac{1}{\mathcal{R}}(A_{\mathcal{R}}q + v_{\mathcal{P}}) & v_{\mathcal{R}} &= -p_{\mathcal{R}}u_{\mathcal{R}} + \frac{1}{\mathcal{R}}(A_{\mathcal{R}}q + v_{\mathcal{P}}) \end{aligned}$$

where

$$\dot{q} = -p_{\mathcal{R}}u_{\mathcal{R}} + \frac{1}{\mathcal{R}}(A_{\mathcal{R}}q + p_{\mathcal{P}}u_{\mathcal{P}}) + p_{\mathcal{V}}u_{\mathcal{V}} + A_{\mathcal{V}}\mathcal{V}q + A_{\mathcal{P}}\mathcal{P}q + u_c.$$

The set of equations above can now be combined with Equation (48) to create a state space system taking into account the uncertainty of the parameters. This uncertainty model is shown in Equation (52).

$$\begin{bmatrix} \dot{q} \\ y_{\mathcal{V}} \\ y_{\mathcal{P}} \\ y_{\mathcal{R}} \\ y_c \end{bmatrix} = \begin{bmatrix} A & p_{\mathcal{V}} & \frac{p_{\mathcal{P}}}{\mathcal{R}} & -p_{\mathcal{R}} & 1 \\ \hline A_{\mathcal{V}}\mathcal{V} & 0 & 0 & 0 & 0 \\ A_{\mathcal{P}}\mathcal{P} & 0 & 0 & 0 & 0 \\ \frac{A_{\mathcal{P}}\mathcal{P} + A_{\mathcal{R}}}{\mathcal{R}} & 0 & \frac{p_{\mathcal{P}}}{\mathcal{R}} & -p_{\mathcal{R}} & 0 \\ \hline 1 & 0 & 0 & 0 & 0 \end{bmatrix} \begin{bmatrix} q \\ u_{\mathcal{V}} \\ u_{\mathcal{P}} \\ u_{\mathcal{R}} \\ u_c \end{bmatrix} \quad (52)$$

## B. Generalized plant

Now that the uncertainty is incorporated into the model, our state-space equations are similar to the feed-forward configuration, but now the uncertainty is added, and the sensor is placed slightly downstream of the actuator. The resulting set of equations is:

$$\dot{q} = Aq + B_{\delta}u_{\delta} + B_d w_d + B_u u \quad (53)$$

$$y_{\delta} = C_{\delta}q + D_{\delta}u_{\delta} \quad (54)$$

$$z = C_z q + l u \quad (55)$$

$$y = C_y q + \gamma w_n \quad (56)$$

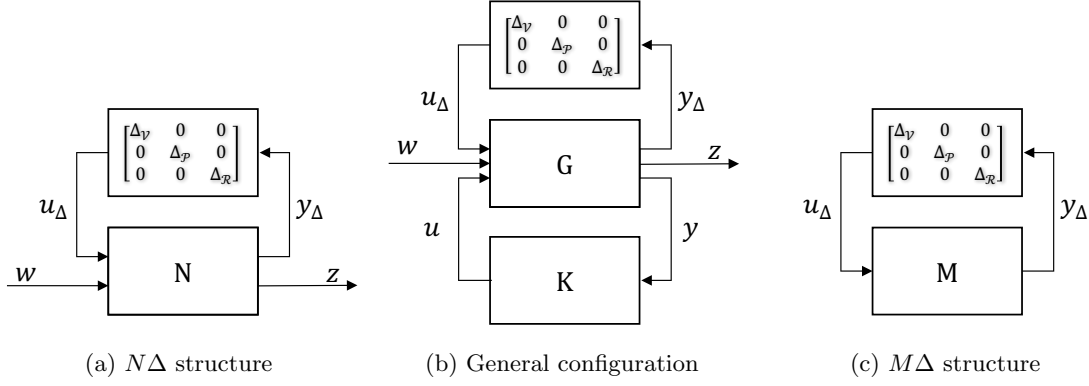


Figure 9: Control configurations used for (a) robust performance analysis (b) controller synthesis and (c) robust stability analysis.

If we now combine the feedback control configuration with the model uncertainty we obtain a following generalized plant.

$$P = \left[ \begin{array}{c|cc} A & B_1 & B_2 \\ \hline C_1 & D_{11} & D_{12} \\ C_2 & D_{21} & D_{22} \end{array} \right] = \left[ \begin{array}{c|cccccc} A & p_{\mathcal{V}} & \frac{p_{\mathcal{P}}}{\mathcal{R}} & -p_{\mathcal{R}} & B_d & 0 & B_u \\ \hline A_{\mathcal{V}}\mathcal{V} & 0 & 0 & 0 & 0 & 0 & 0 \\ A_{\mathcal{P}}\mathcal{P} & 0 & 0 & 0 & 0 & 0 & 0 \\ \frac{A_{\mathcal{P}}\mathcal{P}+A_{\mathcal{R}}}{\mathcal{R}} & 0 & \frac{p_{\mathcal{P}}}{\mathcal{R}} & -p_{\mathcal{R}} & 0 & 0 & 0 \\ C_z & 0 & 0 & 0 & 0 & 0 & 0 \\ 0 & 0 & 0 & 0 & 0 & 0 & l \\ \hline C_y & 0 & 0 & 0 & 0 & \gamma & 0 \end{array} \right] \quad (57)$$

This plant now contains the state matrix, the uncertainty of the system, the performance requirements and the mapping of the actuators and sensors.

For the feedback configuration, the sensor and actuator location needs to be determined with some precision. Obviously the perturbation enters the system at  $B_u$ , far upstream of the actuator. The control objective  $C_z$  is also located far downstream. However, as Belson et al. (2013) showed, for a feedback configuration the sensor is to be placed close to the actuator, as the controller needs to be able to sense the effect of the control input on the signal. If the sensor is placed too far downstream, the estimator cannot determine its effectiveness, rendering the feedback loop ineffective. This is quantified by the sensitivity of the system, which increases significantly as the sensor is placed further downstream from the actuator.<sup>9</sup>

### C. $H_{\infty}$ optimal control

As shown in Section III, the  $H_2$  optimal control framework generally provides excellent performance. Next to having poor robust performance, its largest weakness is that no stability guarantees can be provided. For the feedforward case, which has inherent robust stability, this is not that big of an issue. However, when designing a controller for a feedback configuration, this issue becomes one of the main design considerations. Since the feedback loop can render the system unstable, we need some kind of stability guarantees. Other control methods, based on robust design philosophies, can however provide stability guarantees. This section introduces the  $H_{\infty}$  optimal control framework, which is rather similar to the  $H_2$  optimal control framework and is used as a basis for many more advanced control methods. As the  $H_{\infty}$  optimal control synthesis merely aims to shape the transfer function, no actual uncertainty is incorporated in the plant. Hence, the same generalized plant is used for the controller synthesis:

$$P = \left[ \begin{array}{c|cc} A & B_1 & B_2 \\ \hline C_1 & D_{11} & D_{12} \\ C_2 & D_{21} & D_{22} \end{array} \right] = \left[ \begin{array}{c|ccc} A & B_d & 0 & B_u \\ \hline C_z & 0 & 0 & 0 \\ 0 & 0 & 0 & l \\ \hline C_y & 0 & \gamma & 0 \end{array} \right] \quad (58)$$

The  $H_\infty$  control framework aims to find all stabilizing controllers  $K$  that minimize

$$\|F_l(P, K)\|_\infty = \max_\omega (F_l(P, K)(j, \omega)) \quad (59)$$

In practice that means that if this norm is minimized, the peak value over the transfer function from  $w_d$  to  $z$  is reduced. The algorithm presented by Doyle, Glover, Khargonekar and Francis (1989) does not minimize this objective function, as much as tries to find a bound for the objective function according to  $\|F_l(P, K)\|_\infty < \gamma_\infty$ .<sup>22</sup> Just like the algorithm for the  $H_2$  controller, the algorithm requires the solutions of two Riccati equations. The optimal state feedback controller  $F_\infty$  is found by solving the Riccati equation, such that the control signal is equal to

$$u = F_\infty q \quad (60)$$

where  $F_\infty = -(D_{12}^T D_{12})^{-1} B_2^T X_\infty$  and  $X_\infty \geq 0$  is a solution to the algebraic Riccati equation

$$A^T X_\infty + X_\infty A + C_1^T C_1 + X_\infty (\gamma_\infty^{-2} B_1 B_1^T - B_2 B_2^T) X_\infty = 0 \quad (61)$$

such that  $A + (\gamma_\infty^{-2} B_1 B_1^T - B_2 B_2^T) X_\infty$  is stable. Then, the optimal estimator is given by

$$\begin{aligned} \dot{\hat{q}} &= A\hat{q} + L_\infty [y - C_y \hat{q}] \\ \hat{z} &= C_z \hat{q} \end{aligned} \quad (62)$$

where  $L_\infty = Y_\infty C_2^T (D_{21} D_{21}^T)^{-1}$  and  $Y_\infty > 0$  is a solution to the algebraic Riccati equation

$$A Y_\infty + Y_\infty A^T + B_1 B_1^T + Y_\infty (\gamma_\infty^{-2} C_1^T C_1 - C_2^T C_2) Y_\infty = 0 \quad (63)$$

such that  $A + Y_\infty (\gamma_\infty^{-2} C_1^T C_1 - C_2^T C_2)$  is stable. If for the two Riccati solutions  $X_\infty$  and  $Y_\infty$  holds that

$$\rho(X_\infty Y_\infty) < \gamma_\infty^2 \quad (64)$$

where  $\rho(X_\infty Y_\infty)$  denotes the maximum eigenvalue of  $XY$ , we can write  $Z_\infty = (I - \gamma_\infty^{-2} X_\infty Y_\infty)$ . Combining these steps results in the following state estimator and state feedback:

$$\dot{\hat{q}} = A\hat{q} + \gamma_\infty^{-2} B_1 B_1^T X_\infty \hat{q} + B_2 u + Z_\infty L_\infty (C_2 \hat{q} - y) \quad (65)$$

$$u = F_\infty \hat{q} \quad (66)$$

The algorithm presented above, constructs a controller which achieves the  $H_\infty$  bound for a given  $\gamma_\infty > 0$ . Optimizing the controller is done by iteration on  $\gamma_\infty$ , trying to find the minimum achievable  $H_\infty$  norm  $\gamma_\infty^{\min}$  while simultaneously minimizing the objective function and maximizing the worst-case disturbance. This is done by performing a bisection, testing each value of  $\gamma_\infty$  for whether it is greater or smaller than  $\gamma_\infty^{\min}$ . As mentioned before, this controller does not actually take into account the structured uncertainty, and hence its implementation results in relatively poor performance and stability. However, it is a very useful tool for selecting the controller which provides the best  $H_\infty$  norm of the system at hand, which is why it is often used in combination with other robust control methods.

#### D. $\mu$ -synthesis

In order to generate a controller which provides stability guarantees and also has acceptable performance characteristics, more advanced control methods can be applied. These methods combine the knowledge about the structure in which the uncertainty enters the system to synthesize a less conservative controller. As explained in Section B, the structure of which uncertainty in the parameters enters the system is explicitly derived from the differential operators. Hence, we can use  $\mu$ -synthesis to account for structured uncertainty in our controller design.

The objective for  $\mu$ -synthesis is to design a controller that is robust while under the influence of a relative amount of uncertainty defined by  $p_V$ ,  $p_P$  and  $p_R$ . In order to see how the system performs in the presence of uncertainty, we define the plant  $M = F_l(G, K)$

$$M = \begin{bmatrix} M_{11} & M_{12} \\ M_{21} & M_{22} \end{bmatrix} \quad (67)$$

which is nothing more than the LFT of the open-loop plant and the controller. The design method then uses the  $M\Delta$  structure (Figure 9c) to determine the stability of the system under the influence of uncertainty set  $\Delta$  defined by

$$\Delta := \left\{ \begin{bmatrix} \Delta_{\mathcal{V}} & 0 & 0 & 0 \\ 0 & \Delta_{\mathcal{P}} & 0 & 0 \\ 0 & 0 & \Delta_{\mathcal{R}} & 0 \\ 0 & 0 & 0 & \Delta_F \end{bmatrix} : \Delta_{\mathcal{V}}, \Delta_{\mathcal{P}}, \Delta_{\mathcal{R}} \in \mathbb{R}^{n \times n}, \Delta_F \in \mathbb{C}^{2 \times 2} \right\}. \quad (68)$$

Here  $|\Delta_{\mathcal{V}}, \Delta_{\mathcal{P}}, \Delta_{\mathcal{R}}| \leq 1$  are real diagonal uncertainty matrices. The entries of the diagonal for each matrix  $\Delta_{\mathcal{V}}, \Delta_{\mathcal{P}}, \Delta_{\mathcal{R}}$  is constructed by repeating the corresponding uncertainty parameter, according to

$$\Delta_{\mathcal{V}} = \begin{bmatrix} \delta_{\mathcal{V}} & & & \\ & \ddots & & \\ & & \ddots & \\ & & & \delta_{\mathcal{V}} \end{bmatrix} \quad \Delta_{\mathcal{P}} = \begin{bmatrix} \delta_{\mathcal{P}} & & & \\ & \ddots & & \\ & & \ddots & \\ & & & \delta_{\mathcal{P}} \end{bmatrix} \quad \Delta_{\mathcal{R}} = \begin{bmatrix} \delta_{\mathcal{R}} & & & \\ & \ddots & & \\ & & \ddots & \\ & & & \delta_{\mathcal{R}} \end{bmatrix} \quad (69)$$

This means that for analysis, the three uncertainty matrices will contain a respective uncertainty parameter for each state, varied simultaneously. This is logical, as it is not realistic that one state is for example perturbed with 20% uncertainty in  $\mathcal{V}$ , while the next state is perturbed with  $-20\%$  uncertainty in  $\mathcal{V}$ . Accounting for uncertainty in that sense would lead to a very conservative controller, which is not desirable. It is however possible that one state is perturbed by for example 10% uncertainty in  $\mathcal{V}$ , but also with  $-10\%$  uncertainty in  $\mathcal{P}$ . Hence, the three uncertainty matrices  $\Delta_{\mathcal{V}}, \Delta_{\mathcal{P}}, \Delta_{\mathcal{R}}$  are varied independently. The last uncertainty matrix  $\Delta_F$  is a performance block, which is necessary to incorporate the performance requirements in the  $M\Delta$ -analysis. Concluding,  $\Delta \in \mathbf{\Delta}$  describes any possible uncertainty block  $\Delta$  from the set containing all possible uncertainty blocks  $\mathbf{\Delta}$ . In order to determine the robust stability of the system, we introduce the smallest perturbation that destabilizes the system which we write as

$$\mu_{\Delta}^{-1}(M) := \min_{\Delta \in \mathbf{\Delta}} \{ \bar{\sigma}(\Delta) : \det(I - M\Delta) = 0 \} \quad (70)$$

Then, the structured singular value  $\mu$  for the system  $M(s)$  is defined as

$$\mu_{\Delta}(M(s)) := \sup_{\omega \in \mathbb{R}} \mu_{\Delta}(M(j\omega)). \quad (71)$$

It is now useful to translate this to a number of requirements used to test the performance and stability characteristics of the system. The requirements of the system are defined as follows:

- Nominal Stability (NS):  $M$  is internally stable
- Robust Stability (RS):  $\|M_{11}\|_{\mu} < 1$  for all  $\Delta \in \mathbf{\Delta}$
- Nominal Performance (NP):  $\|M_{22}\|_{\infty} < \|G\|_{\infty}$
- Robust Performance (RP):  $\|M\|_{\mu} < \|G\|_{\mu}$  for all  $\Delta \in \mathbf{\Delta}$

The three measures relevant for our analysis are robust stability, nominal performance and robust performance. The robust stability of the system is measured by the maximum amount of uncertainty the system can accept without destabilizing. As described before, the value  $\mu$  describes the minimum perturbation that destabilizes the system, so the robust stability then can be described by

$$\delta_{\max} = \frac{1}{\mu} \quad (72)$$

where  $\delta_{\max}$  is the maximum perturbation for which the system is guaranteed to be robustly stable. Nominal performance is, as described in Section III, measured by the energy reduction of the nominal closed-loop system relative to the nominal open-loop system, defined as

$$E = \frac{\|T_{zw}\|_2^2}{\|G_{zw}\|_2^2} \quad (73)$$

Robust performance is measured similarly, but the plant is perturbed while the controller is kept the same. For nominal performance, the closed-loop system is thus described by  $F_l(G, K)$ , and for robust performance the closed-loop system is described by  $F_l(G_\delta, K)$ . Here,  $\delta$  is the parameter that describes the amount of combined uncertainty the system is subject to, still using the vector  $p$  to describe the relative uncertainty of each parameter. The systems robust performance is measured by the perturbed energy reduction  $E_\delta$ , defined as

$$E_\delta = \frac{\|T_{zw}^\delta\|_2^2}{\|G_{zw}^\delta\|_2^2} \quad (74)$$

The objective of the  $\mu$  controller design procedure is now to solve for a controller  $K$

$$\inf_K \sup_{\omega \in \mathbb{R}} \mu[M(P, K)(j\omega)] \quad (75)$$

As this controller cannot be determined analytically, an iterative method called the  $DK$ -iteration has been suggested by Doyle (1985).<sup>23</sup> This method introduces a diagonal constant scalar matrix  $D$  to find an upper bound for the structured singular value

$$\inf_{D \in \mathbf{D}} \bar{\sigma}[DM(P, K)D^{-1}]. \quad (76)$$

The optimisation problem then becomes to find a stabilizing controller  $K$  such that

$$\sup_{\omega \in \mathbb{R}} \inf_{D \in \mathbf{D}} \bar{\sigma}[DM(P, K)D^{-1}(j\omega)] < 1 \quad (77)$$

The controller is then found by minimizing the left hand side of Equation (77) for  $K$  and  $D$  iteratively.  $K$  is found using the optimal  $H_\infty$  controller synthesis described in Section C keeping  $D$  fixed, starting with  $D = I$  and finding  $K$  for

$$\inf_K \left\| F_l(\tilde{P}, K) \right\|_\infty = \inf_K \left\| F_l \left( \begin{bmatrix} D & 0 \\ 0 & I \end{bmatrix} P \begin{bmatrix} D^{-1} & 0 \\ 0 & I \end{bmatrix} K \right) \right\|_\infty \quad (78)$$

The next step in the iteration is to approximate the entries of the matrix  $D(s)$  by curve fitting  $D(j\omega)$ , where  $D(j\omega)$  is found at each frequency of interest  $\omega$  using the following optimization problem:

$$D(j\omega) = \arg \inf_{D \in \mathbf{D}} \bar{\sigma}[DF_l(P, K)D^{-1}(j\omega)] \quad (79)$$

One disadvantage of the  $DK$ -iteration is that it results in rather large controllers. According to [10, pp. 336] the order of the controller resulting from each iteration is equal to the number of states in the plant  $G(s)$ , plus the number of states in the weights, plus twice the number of states in  $D(s)$ . This results in high computational efforts, which makes this method less attractive for a system with large number of states. The current discretization as described in Section B has resulted in 147 states. However, the rest of this chapter shows that this method is implementable for the current system, as the number of states in  $D(s)$  for our controller is relatively low.

## E. Parameter selection

Next to the system being nominally stable, robust stability is the most important requirement. Obviously, nominal and robust performance are objectives that drive the design process, but robust stability is a hard requirement. Due to the feedback configuration, an error in the model is fed back into the controller. This construction will cause the error to grow, potentially destabilizing the system. It is only justifiable to implement a feedback controller if the system is guaranteed to remain stable for the expected perturbations.

The system can be tuned to meet the requirements presented in Section D using three tuning parameters. The first two parameters have also been used to tune the LQG/feedforward controller, the control penalty  $l$  and the signal-to-noise ratio  $\gamma$ . The additional parameter that highly influences the performance of the system is the position of the sensor,  $x_s$ . As stated by Belson et al. (2013), the sensor should be placed close to the sensor, as the sensor must be capable of measuring the effectiveness of the controller. However, if the sensor is placed too close to the actuator, the system can become unstable due to a relatively small

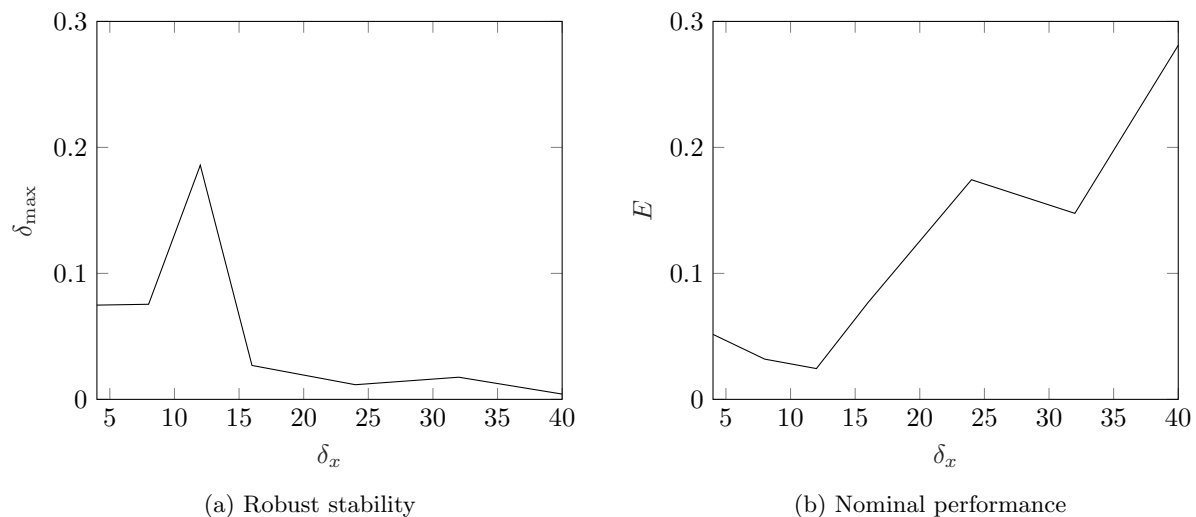


Figure 10: Placing the sensor further downstream decreases the maximum allowed perturbation  $\delta_{\max}$  and the energy reduction  $E$ .

perturbation. If the sensor is placed too far downstream, as shown in Figure 10, the controller cannot control the signal anymore due to the time-delay caused by the time it takes for the signal to reach the sensor. A brief analysis was performed to determine what sensor position should be selected, relative to the position of the actuator at  $x_a = 480$ . The distance between the actuator and sensor is denoted by  $\delta_x$ . For this analysis, the tuning parameters were kept constant at  $l = 1$  and  $\gamma = 1$ . Obviously, each sensor location could be optimized for either maximum performance or stability characteristics, but that would make the relative positions hard to compare. As shown in Figure 10a, the robust stability is highest for  $\delta_x = 12$ . This can be explained by the fact that for low  $\delta_x$ , the controller will need to react very quickly, resulting in an aggressive feedback gain. Hence, a small perturbation can destabilize the system. When  $\delta_x$  is increased, the controller acts less aggressively, increasing the stability of the system. However, for  $\delta_x > 15$ , the sensor cannot correctly sense the actuation, resulting in a loss of stability. Also, from Figure 10b, it becomes evident that the performance of the controller degrades when the sensor is moved downstream. We find that the best robust stability and performance is found for  $\delta_x = 12$ , resulting in the optimal sensor position  $x_s = 492$ . A more extensive study of the actuator and sensor placement could potentially improve both performance and stability, but this is not within the scope of this research.

For the optimal sensor position  $x_s = 492$ , the system now can be tuned using the tuning parameters  $l$  and  $\gamma$ . In Section III, it was shown that for the feedforward configuration, increasing either the control penalty  $l$  or the expected signal-to-noise ratio  $\gamma$  results in a decrease in performance. A similar analysis has been done for the feedback configuration. The results of this analysis are shown in Figure 11, showing how tuning of the parameters affects the robust stability and the nominal performance of the system.

## F. Robust stability

As mentioned before, the implementation of a feedback controller can only be justified when *a priori* stability guarantees are provided. The introduction of the structured singular value  $\mu$  provides such guarantees. The robust stability of the system is influenced by three parameters. As shown in Figure 10a, maximum allowed perturbation is influenced by the relative position of the actuator and sensor. However, when an optimal actuator and sensor configuration has been selected, the control penalty  $l$  and expected signal-to-noise ratio  $\gamma$  can be tuned to achieve the desired performance and requirements. Figure 11 shows a parameter analysis executed for the sensor position  $x = 492$ , where both tuning parameters were varied, measuring the robust stability in terms of the maximum allowed perturbation  $\delta_{\max}$  and the nominal performance in terms of relative energy reduction  $E$ . Figure 11a clearly shows that when  $l$  and  $\gamma$  are increased, the maximum allowed perturbation also increases. This means that for higher  $l$  and  $\gamma$ , the system has very good stability characteristics. As described previously, the feedforward controller is rendered as good as ineffective for a

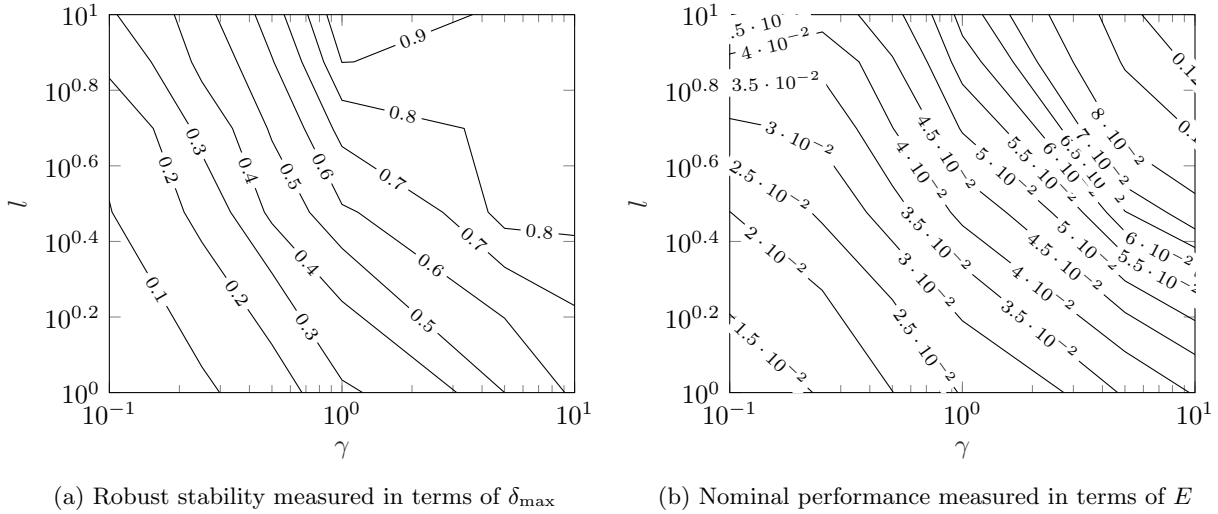


Figure 11: Increasing the control penalty  $l$  and the expected signal-to-noise ratio  $\gamma$  increases the robust stability of the closed-loop system, but decreases the nominal performance of the closed-loop system.

combined uncertainty  $\delta = 0.5$ . For each parameter, this corresponds with the worst-case uncertainty of

$$\delta \begin{bmatrix} p_V \\ -p_P \\ p_R \end{bmatrix} = 0.5 \begin{bmatrix} 4\% \\ -54\% \\ 80\% \end{bmatrix} = \begin{bmatrix} 2\% \\ -27\% \\ 40\% \end{bmatrix} \quad (80)$$

A perturbation of this magnitude is not expected to occur frequently, but if this would be the case, a system designed for such stability requirements could in that case be destabilized. Hence, two design points are selected for further investigation. The first design point is selected focusing on robust stability, and is tuned for  $l = 5$ ,  $\gamma = 5$ , providing a priori stability guarantees for  $\delta_{\max} = 80\%$ . The second design point is selected at  $l = 5$ ,  $\gamma = 0.1$  to show the behaviour of a controller with better performance but worse stability characteristics. Analysis showed that increasing both tuning parameters to much higher values of for example 100 stops increasing the robust stability of the system when the maximum perturbation has reached 85%. This means that the maximum combined perturbation that this system could ever be designed for is 3.4% uncertainty in  $\mathcal{P}$ , 46% uncertainty in  $\mathcal{P}$  and 68% uncertainty in  $\mathcal{R}$ .

### G. Nominal performance

As illustrated in Figure 10b, the relative energy reduction  $E$  of the closed-loop system in nominal setting increases significantly if the sensor is placed far downstream of the actuator. When the sensor is placed close to the actuator, the performance is much better, and the best results are found when the sensor is placed at  $x_s = 492$ . Increasing the control penalty  $l$  and signal-to-noise ratio  $\gamma$  increases the robust stability of the system, but, as can be observed from Figure 11b, decreases the nominal performance of the system. Hence, for design of a robust controller, there always is a trade-off between robust stability and (nominal) performance. If Figures 11a and 11b are compared, we see that the contours follow similar paths. From this we can conclude that the precise combination of the tuning parameters  $l$  and  $\gamma$  does not directly influence the robust stability or performance. In the previous section, two design points were selected at  $l = 5$ ,  $\gamma = 5$  and  $l = 5$ ,  $\gamma = 0.1$ , corresponding with a robust stability of 70% and 20%, respectively. From Figure 11b we see that the controllers designed with this tuning provide a relative energy reduction of  $E = 0.08$  and  $E = 0.035$ . This is a significant loss of performance compared to the LQG controller designed at  $E = 0.008$ . However, this result was expected, as a robust controller cannot outperform an optimal controller in nominal setting.

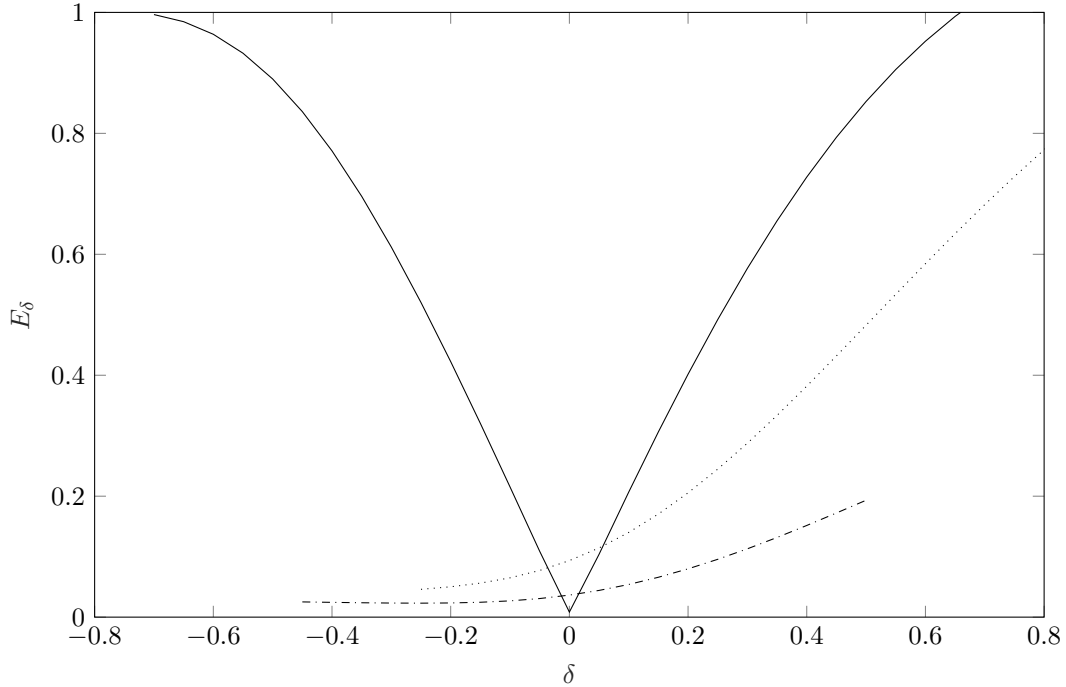


Figure 12: Energy reduction for the LQG controller in feedforward configuration (solid line), the robust feedback controller designed at  $l = 5$ ,  $\gamma = 5$  (dotted line) and the robust feedback controller designed at  $l = 5$ ,  $\gamma = 0.1$  (dashed-dotted line). The relative perturbation vector is selected at  $p = [0.04 \ -0.54 \ 0.8]^T$ . Outside the plotted ranges, the controller is unable to stabilize the perturbed system.

## H. Robust performance

The LQG controller designed in Section III shows excellent nominal performance results and is inherently stable in the presence of uncertainty. Hence, the main goal of the feedback loop is to improve the robust performance of the closed-loop system. As mentioned before, the systems robust performance is measured in the relative energy reduction of a controller designed for the nominal plant, but acting on a perturbed plant. This energy reduction is described by  $E_\delta$ , and the plant is perturbed with the combined relative perturbation vector which has been used throughout this paper:

$$\begin{bmatrix} p_V \\ -p_P \\ p_R \end{bmatrix} = \begin{bmatrix} 4\% \\ -54\% \\ 80\% \end{bmatrix} \quad (81)$$

Figure 12 shows how the performance of the two  $\mu$ -controllers behaves as the plant is perturbed with combined uncertainty  $\delta$ . This figure clearly illustrates the robust behaviour of the controller. As expected, the two robust controllers are much less sensitive to perturbations. The first controller has very good robust stability, however, this comes at the cost of robust performance loss. It still outperforms the  $H_2$  controller, but the second controller is able to keep the energy reduction almost at nominal values. The controller designed at  $l = 5$ ,  $\gamma = 0.1$  shows very good robust performance, hardly increasing in relative energy reduction as the plant is perturbed. Maybe the most important observation that should be made is that the energy reduction of the LQG controller and the second  $\mu$ -controller intersect at a relative combined perturbation of 2%. This corresponds with a perturbation of  $\delta_V p_V = 0.08\%$ ,  $\delta_P p_P = 1.08\%$  and  $\delta_R p_R = 1.6\%$ . Perturbations of this magnitude are almost inevitable in the physical system, which means that  $\delta$  will almost always be greater than 2. Therefore, as long as the robust controller remains stable, the robust controller always outperforms optimal controller. One thing that should be noted when looking at Figure 12, is the fact that for  $\delta < 0$ , the robust performance appears to be even better than the nominal performance. However, this phenomenon is due to the fact that the stability of the open-loop system highly decreases as delta becomes more negative. The stability of the KS equation can be analyzed using the relationship between the frequency  $\omega$  and the

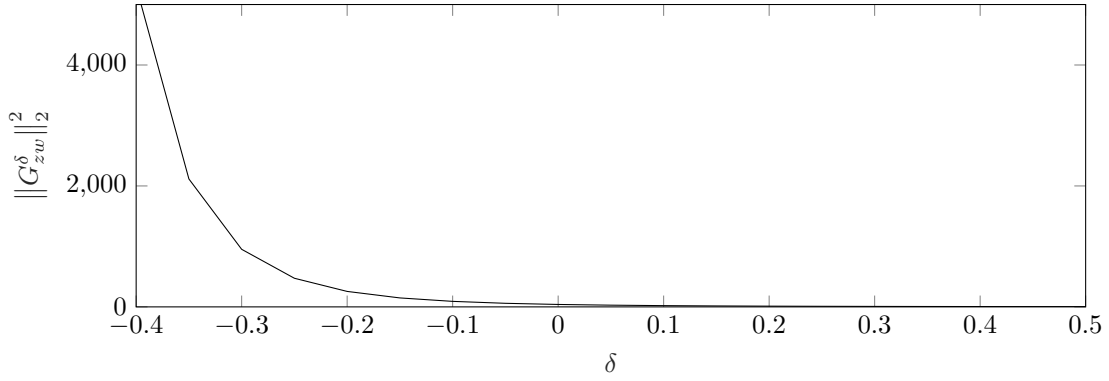


Figure 13: The  $L_2$  norm of the open-loop system as the system is perturbed by  $\delta$  using the relative perturbation vector  $p = [0.04 \ -0.54 \ 0.8]^T$ . The system becomes highly unstable for  $\delta < -0.4$ , which is the reason that the  $\mu$ -controllers are unable to stabilize the system.

spatial wave-number  $\alpha$ , described by

$$\omega = \mathcal{V}\alpha + i \left( \frac{\mathcal{P}}{\mathcal{R}}\alpha^2 - \frac{1}{\mathcal{R}}\alpha^4 \right) \quad (82)$$

where the system is unstable if the imaginary part of Equation (82) is positive.<sup>6</sup> For our current relative perturbation vector, with  $p_{\mathcal{P}} < 0$ , a negative perturbation increases the value of  $\mathcal{P}$  and decreases the value of  $\mathcal{R}$ . Both of these actions increase the value of the imaginary part, which consequently increases the instability of the system. This is illustrated in Figure 13, which shows that as  $\delta$  approaches  $-1$ , the norm of the open-loop system increases asymptotically. As  $H_2$  control cannot destabilize the system, the relative energy reduction can be determined for any value of  $\delta$ . However, analysis showed that a feedback controller cannot stabilize such a turbulent system. This is the reason that the  $\mu$ -controllers are unable to stabilize the system for low values of  $\delta$ , while the LQG controller can.

## V. Results

In this paper, the performance and stability of both feedback and feedforward configurations have been analyzed. The feedforward configuration has shown impressive nominal performance and stability characteristics, but it has been proven that even small perturbations to the plant result in significant performance loss. Hence the possibility for more robust controllers has been explored. The robust feedback configuration does indeed show good results with respect to robust performance, but this seems to come at a loss of nominal performance, and, if the plant is perturbed with enough uncertainty, the system might destabilize. Figure 12 visualizes how the two robust controllers will behave under a range of perturbations compared to the LQG controller. In order to keep the results as general as possible and make sure that the results is not influenced by a certain error signal, the relative energy reduction is once again based on the ratio between the frequency response of the perturbed system and the frequency response of the uncontrolled system, defined by

$$E_\delta = \frac{\|T_{zw}^\delta\|_2^2}{\|G_{zw}^\delta\|_2^2} \quad (83)$$

A range of open-loop systems was generated for  $-80\% \leq \delta \leq 80\%$ , and for each open-loop system the corresponding closed-loop system  $F_l(G_\delta, K)$  was determined. The norm of each perturbed closed-loop system is divided by the norm of the corresponding perturbed open-loop system. For  $\delta < -0.4$ , the open-loop system becomes unstable to the extent that the feedback controllers cannot stabilize the system anymore. However, close observation of Figure 12 shows us that the  $\mu$ -controller designed at  $l = 5$ ,  $\gamma = 0.1$  can keep the system stable up to a perturbation of  $\delta = -45\%$ . If we compare this to the LQG controller, we see that the performance of the feedforward system has degraded to  $E = 0.8$ . From this we can conclude that the perturbation needed to destabilize the system would decrease the performance of the LQG/feedforward

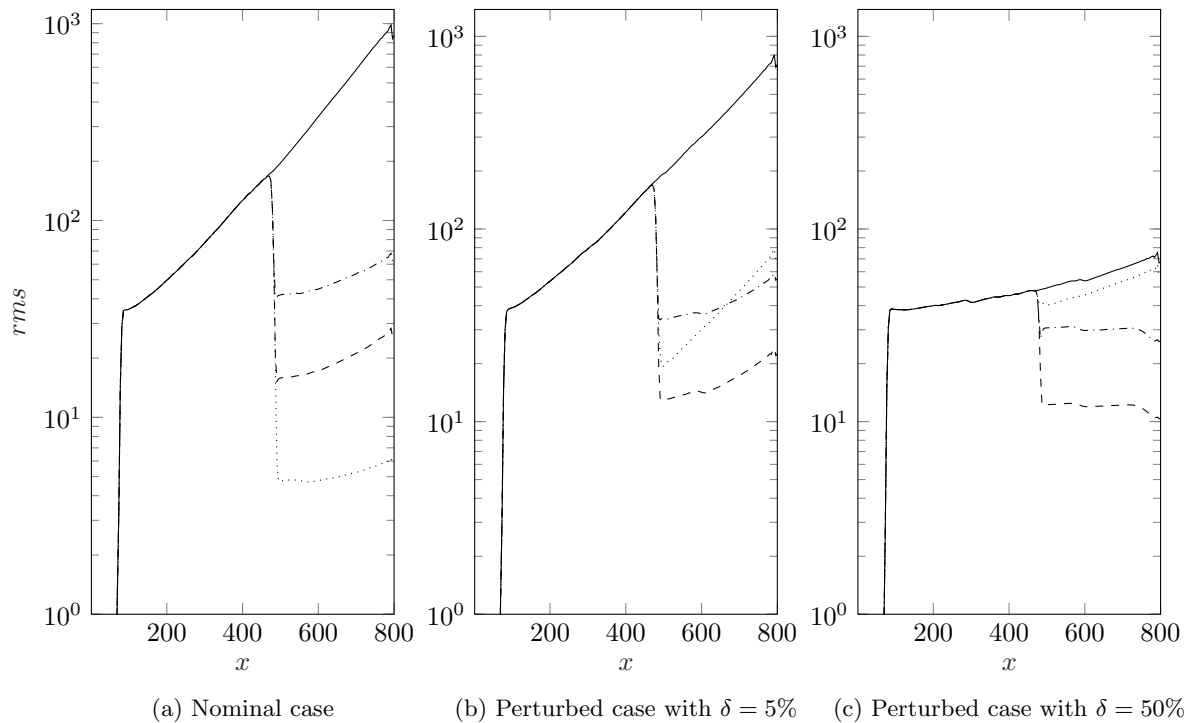


Figure 14: Root mean square over the entire domain for  $x \in [0, 800]$  of the uncontrolled system (solid line), the LQG controller (dotted), the  $\mu$ -controller designed at  $l = 5$ ,  $\gamma = 5$  (dashed-dotted line) and the  $\mu$ -controller designed at  $l = 5$ ,  $\gamma = 0.1$  (dashed line) for a simulation of 2000s.

controller to such an extent, that the risk of destabilizing the system is justified. In order to further analyze the system's performance, the same controllers have been compared in a simulation, where the system was perturbed by a white noise signal with unit variance and zero mean. Figures 14a to 14c show the simulation results where the LQG controller is compared to the robust controllers, examining their performance for the nominal case, a perturbation of 5% and a perturbation of 50%. In order to assess the energy reduction in the system, the root mean square (rms) of the velocity perturbation has been determined over the entire domain, according to

$$rms = \sqrt{\frac{1}{T} \int_0^T |q|^2 dt} \quad (84)$$

The *rms* shows the average size of the perturbation at each location in the domain. Figure 14 shows that the external disturbance enters the system at  $x_d = 80$ , then convectively grows until it reaches the actuator at  $x_a = 480$ , after which it leaves the system at  $x = 800$ . It should be noted that the decreasing growth for the perturbed case ( $\delta = 50\%$ ) is due to the increased stability of the open-loop system (see Figure 13). This increase in stability causes the less aggressive growth shown in Figure 14c. Figure 14a shows that for the nominal case, the LQG controller significantly outperforms the two robust controllers. However, both robust controllers still show a significant energy reduction in the system. Figure 14b shows that even with the slightest perturbation of 5%, the  $\mu$ -controllers outperform the LQG controller. This means that when the system is subject to the very plausible perturbation of 0.16% in the base flow velocity  $\mathcal{V}$ , combined with a perturbation of  $-2.16\%$  in the energy ratio  $\mathcal{P}$  and 3% in the Reynolds number  $\mathcal{R}$ , the robust controllers are the better option. As the plant is perturbed to 50%, we see that the uncertainty introduced into the system renders the LQG controller nearly ineffective. However, the robust controllers are able to maintain performance. This proves that, under the assumption that uncertainty is always present, robust control is more effective than optimal control.

## VI. Conclusions

In this paper the design of a controller in the presence of structured parametric uncertainty has been applied to a parabolic Partial Differential Equation (PDE), the Kuramoto-Sivashinsky equation. In order to allow controller design the model needed to be discretized. This was done using Galerkin projection on a set of multivariate B-splines, resulting in a set of state-space equations. It was shown that this discretization method results in a linear relation between the parameters of the PDE and the state matrix. The structure of the parametric uncertainty is thus defined by the discretization properties of the system.

A Linear Quadratic Gaussian (LQG) controller was then designed using a feedforward configuration, showing excellent nominal performance and inherent robust stability. However, the system was shown to be sensitive to uncertainty in the parameters. As uncertainty is always present in a physical system, it was suggested that a robust controller is bound to achieve a better performance. However, improving the robust performance of the system is not possible using a feedforward configuration, and hence a feedback control design was proposed.<sup>3</sup>

In an attempt to find a more robust controller, the state matrix was decomposed and the nominal parameters were replaced with uncertain parameters, allowing for a set of perturbed plants to be generated. This set of plants was then used to generate a  $\mu$ -controller, using  $DK$ -iterations to find an upper bound on the structured singular value of the closed-loop system. This structured singular value was used to determine the maximum perturbation for which the system is guaranteed to be stable.

An important design parameter of a  $\mu$ -controller in feedback configuration is the distance between the actuator and the sensor. It was shown that if the sensor is placed to far downstream, the feedback loop is rendered ineffective. However, placing the sensor too close to the actuator results in an easily destabilized system. An optimal actuator/sensor combination was determined, and for this configuration a  $\mu$ -controller was designed.

The LQG controller in feedforward configuration was compared to the  $\mu$ -controller in feedback configuration, and it was shown that  $\mu$ -controller outperforms the LQG controller for any perturbation where  $|\delta| > 2\%$ . When the closed-loop system is perturbed, the  $\mu$ -controllers prove to be much less sensitive to this perturbation than the LQG controller. For perturbations where  $|\delta| > 50\%$ , the  $\mu$ -controllers potentially destabilize the system. However, a perturbation that destabilizes the system with the  $\mu$ -controller, the performance of the LQG controller reduces to a relative energy reduction of  $E = 0.8$ , rendering the controller nearly ineffective.

From this we can conclude that a  $\mu$ -controller consequently achieves a better energy reduction, where as the performance of the LQG controller significantly depends on the amount of perturbation present in the system. The  $\mu$ -controller stabilizes the system for a wide range of perturbations, well within the range of what can be expected to occur simultaneously. Hence, a  $\mu$ -controller designed with structured parametric uncertainty in feedback configuration almost always outperforms an LQG controller in feedforward configuration.

## VII. Recommendations

This paper has shown that robust control has much potential in the field of active flow control. One of the drawbacks of robust control methods is the decrease in performance that comes with an increase in robustness. It is suggested that future research should focus on methods that improve performance characteristics of the system. This could be achieved by aggration of multiple actuator/sensor sets, resulting in a performance similar to that of an LQG controller. Another configuration that should be examined is the combination of a mixed feedback-feedforward configuration, where an LQG controller is used to achieve a high performance in the nominal case, and a  $\mu$  controller is used to achieve high performance when the system is perturbed. A last recommendation for further research is to investigate the sensor location. During this study it was noticed that performance and stability characteristics of the system can vary significantly for different actuator/sensor locations. The placement of the sensor with respect to the actuator should be optimized to achieve the maximum stability and performance for both the nominal and perturbed system.

## References

<sup>1</sup>Schlichting, H. and Gersten, K., *Boundary-layer theory*, Springer-Verlag Berlin Heidelberg, 2000.

- <sup>2</sup>Brunton, S. L. and Noack, B. R., “Closed-loop turbulence control: Progress and challenges,” *Applied Mechanics Reviews*, Vol. 67, No. 5, September 2015.
- <sup>3</sup>Sipp, D. and Schmid, P. J., “Linear closed-loop control of fluid instabilities and noise-induced perturbations: A review of approaches and tools,” *Applied Mechanics Reviews*, Vol. 68, No. 2, 2016, pp. 020801.
- <sup>4</sup>Bagheri, S., Henningson, D. S., Hoepffner, J., and Schmid, P. J., “Input-output analysis and control design applied to a linear model of spatially developing flows,” *Applied Mechanics Reviews*, Vol. 62, 2009.
- <sup>5</sup>Bagheri, S., Brandt, L., and Henningson, D. S., “Input-output analysis, model reduction and control of the flat-plate boundary layer,” *Journal of fluid mechanics*, Vol. 620, 2009.
- <sup>6</sup>Fabbiane, N., Semeraro, O., and Bagheri, S., “Adaptive and model-based control theory applied to convectively unstable flows,” *Applied Mechanics Reviews*, Vol. 66, 2014.
- <sup>7</sup>Tol, H. J., Kotsonis, M., de Visser, C. C., and Bamieh, B., “Localized modelling and feedback control of linear instabilities in 2-D wall bounded shear flows,” *APS Division of Fluid Dynamics Meeting Abstracts*, 11 2016.
- <sup>8</sup>Doyle, J. C., “Guaranteed margins for LQG regulators,” *IEEE Transactions on Automatic Control*, Vol. 23, No. 4, 1978, pp. 756–757.
- <sup>9</sup>Belson, B. A., Semeraro, O., Rowley, C. W., and Henningson, D. S., “Feedback control of instabilities in the two-dimensional Blasius boundary layer: the role of sensors and actuators,” *Physics of fluids*, Vol. 25, No. 5, 2013, pp. 54–106.
- <sup>10</sup>Skogestad, S. and Postlethwaite, I., *Multivariate feedback control, analysis and design*, John Wiley & Sons, Ltd, 2nd ed., 2001.
- <sup>11</sup>Bewley, T. R. and Liu, S., “Optimal and robust control and estimation of linear paths to transition,” *Journal of Fluid Mechanics*, Vol. 365, 1998.
- <sup>12</sup>McFarlane, D. C. and Glover, K., *Robust controller design using normalized coprime factor plant descriptions*, Springer, 1990.
- <sup>13</sup>Baramov, L., Tutty, O. R., and Rogers, E., “ $H_\infty$  control of nonperiodic two-dimensional channel flow,” *IEEE Transactions on Control Systems Technology*, Vol. 12, 2004.
- <sup>14</sup>Vinnicombe, G., *Uncertainty and feedback:  $H_\infty$  loop-shaping and the  $\nu$ -gap metric*, World Scientific, 2000.
- <sup>15</sup>Chen, K. K. and Rowley, C. W., “Normalized coprime robust stability and performance guarantees for reduced-order controllers,” *IEEE Transactions on Automatic Control*, Vol. 58, No. 4, April 2013, pp. 1068–1073.
- <sup>16</sup>Tofighi, S. R., Bayat, F., and Merrikh-Bayat, F., “Robust feedback linearization of an isothermal continuous stirred tank reactor: H mixed-sensitivity synthesis and DK-iteration approaches,” *Transactions of the Institute of Measurement and Control*, 2015.
- <sup>17</sup>Schirrer, A., Westermayer, C., Hemedi, M., and Kozek, M., “Robust lateral blended-wing-body aircraft feedback control design using a parameterized LFR model and DGK-iteration,” *Progress in flight dynamics, guidance, navigation, control, fault detection, and avionics*, Vol. 6, EDP Sciences, 2013, pp. 749–766.
- <sup>18</sup>Tol, H. J., de Visser, C. C., and Kotsonis, M., “Model reduction of parabolic PDEs using multivariate splines,” *International Journal of Control*, 2016, pp. 1–16.
- <sup>19</sup>Gu, D. W., Petkov, P. H., and Konstantinov, M. M., *Robust control design with MATLAB®*, Springer Science & Business Media, 2005.
- <sup>20</sup>Sivashinsky, G. I., “Nonlinear analysis of hydrodynamic instability in laminar flamesI. Derivation of basic equations,” *Acta astronautica*, Vol. 4, No. 11-12, 1977, pp. 1177–1206.
- <sup>21</sup>Kuramoto, Y. and Tsuzuki, T., “Persistent propagation of concentration waves in dissipative media far from thermal equilibrium,” *Progress of theoretical physics*, Vol. 55, No. 2, 1976, pp. 356–369.
- <sup>22</sup>Doyle, J. C., Glover, K., Khargonekar, P. P., and Francis, B. A., “State-space solutions to standard  $H_2$  and  $H_\infty$  control problems,” *IEEE Transactions on Automatic control*, Vol. 34, No. 8, 1989, pp. 831–847.
- <sup>23</sup>Doyle, J. C., “Structured uncertainty in control system design,” *Decision and Control, 1985 24th IEEE Conference on*, Vol. 24, IEEE, 1985, pp. 260–265.



**Part II**

**Literature Study**



---

## Chapter 2

---

# Literature Review

This chapter will provide an in depth review of all research done with respect to the subject of this thesis. The objective of this chapter is to provide context to this thesis, as well as to compare the work of other authors and to show how uncertainty returns in the different stages of controller design. Section 2-1 will present a model that is used to model certain fluid flow phenomena and it will further explain the parameters in which uncertainty is expected. Next, Section 2-2 will provide more context to a number of methods used for model reduction, including the discretization method using multivariate B-splines from Tol, Visser, & Kotsonis (2016). Section 2-3 will provide an overview of different control frameworks commonly used for AFC, and will lay ground for the introduction of a robust control framework. Finally, Section 2-4 will provide an in-depth analysis of the different methodologies used within robust control.

### 2-1 Modeling fluid flows

The first step towards the control of fluid flows is finding a model that accurately describes the dynamics of the flow. This model can then be used to design a controller for the system. Fluid flow is commonly modeled using the Navier-Stokes equations. These equations are continuous in both space and time, which often causes them to be highly non-linear and infinite-dimensional. Due to these complexities authors often use simpler models which describe certain phenomena, but are easier to work with. A good example of one of such models is the Kuramoto-Sivashinsky equation described by (Sakthivel & Ito, 2007; Jamal & Morris, 2015; Armaou & Christofides, 2000; Gomes et al., 2016; Fabbiane et al., 2014). This section introduces the mathematical model behind this equation and explains how it is used by different authors to model fluid flow. We will see what parameters are used to model the flow, how these parameters are related to the stability of the model, and to which uncertainty will be introduced later in this preliminary thesis.

### 2-1-1 The Kuramoto-Sivashinky equation

The Kuramoto-Sivashinky equation is a relatively simple PDE, originally used to describe the front flutter in laminar flames. It shows dynamic characteristics such as convection, advection and spatial amplification which can be used to mimic the transition phase in a flow over a flat plate (Gomes et al., 2016). It reproduces the most important stability properties of the flat-plate boundary layer, but avoids the problem of high-dimensionality. In Fabbiane et al. (2014), this model is introduced focusing on flows dominated by convection/advection, with disturbances having little upstream influence and propagating downstream quickly.

#### Mathematical model

The standard KS equation reads:

$$\frac{\partial \tilde{v}}{\partial \tilde{t}} + \tilde{v} \frac{\partial \tilde{v}}{\partial \tilde{x}} = -\eta \frac{\partial^2 \tilde{v}}{\partial \tilde{x}^2} - \mu \frac{\partial^4 \tilde{v}}{\partial \tilde{x}^4} \quad (2-1)$$

where  $\tilde{t}$  is time,  $\tilde{x}$  the spatial coordinate, and  $\tilde{v}$  the velocity. The left side of the equation reads an acceleration and nonlinear convection term, and the right side reads two viscosity terms. By introducing a reference length  $\tilde{l}$  and a reference velocity  $\tilde{V}$ , where

$$x = \frac{\tilde{x}}{\tilde{l}}, \quad v = \frac{\tilde{v}}{\tilde{V}}, \quad t = \frac{\tilde{V}}{\tilde{v}} \tilde{t} \quad (2-2)$$

the equation can be made dimensionless. Introducing two parameters  $\mathcal{R}$  and  $\mathcal{P}$  defined as:

$$\mathcal{R} = \frac{\tilde{V} \tilde{l}^3}{\mu}, \quad \mathcal{P} = \frac{\eta \tilde{l}^2}{\mu} \quad (2-3)$$

the dimensionless form of the KS equation reads:

$$\frac{\partial \nu}{\partial t} + \nu \frac{\partial \nu}{\partial x} = -\frac{1}{\mathcal{R}} \left( \mathcal{P} \frac{\partial^2 \nu}{\partial x^2} + \frac{\partial^4 \nu}{\partial x^4} \right) \quad (2-4)$$

Here,  $\mathcal{R}$  is a Reynolds-number-like coefficient, and  $\mathcal{P}$  controls the ratio between energy production and dissipation. If it is then assumed that the system is close to a steady state solution  $V(x) = V$ , the KS equation can be linearized using the perturbation  $\nu'(x, t)$ :

$$\nu(x, t) = V + \varepsilon \nu'(x, t) \quad (2-5)$$

Combining Equation (2-3) and Equation (2-5) results in the following linearized KS equation:

$$\frac{\partial \nu'}{\partial t} = -V \frac{\partial \nu'}{\partial x} - \frac{1}{\mathcal{R}} \left( \mathcal{P} \frac{\partial^2 \nu'}{\partial x^2} + \frac{\partial^4 \nu'}{\partial x^4} \right) \quad (2-6)$$

This equation is used from here to build a state space system and controller. In order to compare the KS equation to other systems, the stability properties are analysed. It is assumed that the solutions will be traveling wave-like according to:

$$\nu' = \hat{\nu} e^{i(\alpha x - \omega t)} \quad (2-7)$$

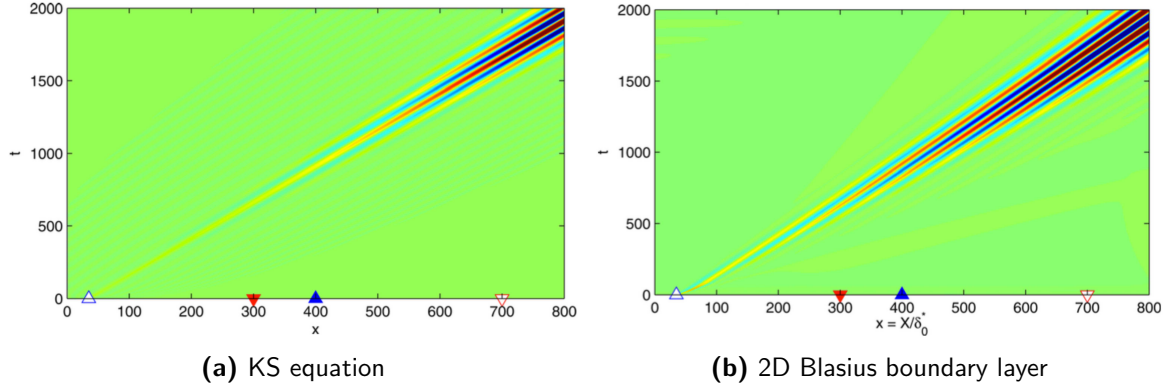


**Figure 2-1:** Comparison between simulations of **(a)** the KS equation and **(b)** the 2D Blasius boundary layer flow by (Fabbiane et al., 2014). The blue triangles show the location of the actuators, and the red triangles represent sensors for state estimation and the control objective.

where  $\alpha \in \mathbb{R}$  and  $\omega = \omega_r + i\omega_i \in \mathbb{C}$ . Substitution now yields the following dispersion relation between the spatial wave-number  $\alpha$  and the temporal frequency:

$$\omega = V\alpha + i \left( \frac{\mathcal{P}}{\mathcal{R}}\alpha^2 - \frac{1}{\mathcal{R}}\alpha^4 \right) \quad (2-8)$$

This equation relates the spatial wave-length of the perturbation described by Equation (2-5) with the temporal stability. The imaginary part of Equation (2-8) is the exponential temporal growth of a wave with wave-number  $\alpha$ . Here, the  $\alpha^2$  term provides a positive destabilizing contribution to  $\omega$ , while the  $\alpha^4$  term has a stabilizing effect. Physically, this means that if more energy is produced than dissipated, the system is temporally unstable. However, if the energy production parameter  $\mathcal{P}$  is low enough ( $\mathcal{P} < \alpha^2$ ), the system will become temporally stable.

### Flow characteristics

The Kuramoto-Sivashinsky equation was originally designed to model the front flutter in laminar flames. The convective instability property of the equation causes the localized initial perturbation to travel upstream while growing exponentially until it leaves the domain (Figure 2-1a). This is due to the outflow boundary condition on the right side of the domain:

$$\left. \frac{\partial^3 v'}{\partial x^3} \right|_{x=L} = 0, \quad \left. \frac{\partial v'}{\partial x} \right|_{x=L} = 0 \quad (2-9)$$

On the left side, the boundary condition is fixed and unperturbed:

$$v'|_{x=0} = 0, \quad \left. \frac{\partial v'}{\partial x} \right|_{x=0} = 0 \quad (2-10)$$

Moreover, Fabbiane et al. (2014) shows that using these boundaries and setting the parameters at  $\mathcal{R} = 0.25$ ,  $\mathcal{P} = 0.05$  and,  $V = 0.4$  the KS equation closely models the two-dimensional Blasius boundary layer at  $\text{Re} = 1000$ . As shown in Figure 2-1, there is hardly any difference

between the two simulations. However, the KS equation has a fixed wave-shape traveling downstream, whereas the Blasius boundary layer has the wavecrests travel faster than the wave-packet itself. This shows that, in contrast to the Blasius boundary layer, the KS equation is indeed not dispersive.

According to Jamal & Morris (2015), it is shown that "under certain assumptions, a controller that stabilizes a finite-dimensional approximation of the linearized KS equation will locally stabilize the nonlinear infinite-dimensional KS equation." This means that even if a low-order approximation is used to design a controller and a high-order approximation to simulate the model, the system will remain stable. One of the key differences between the approach of Fabbiane et al. (2014) and the approach of Jamal & Morris (2015) is that Fabbiane et al. (2014) uses coupled parameters, such that  $\mathcal{R}$  affects both the second-order and fourth-order term in Equation (2-6). The difference is that in Fabbiane et al. (2014),  $\mathcal{R}$  becomes a Reynolds-number-like coefficient affecting both energy production and dissipation, while in Jamal & Morris (2015) this parameter only affects the fourth-order term relating the parameter directly to the instability of the problem. When using the linearized KS equation,  $\mathcal{R}$  only scales the imaginary part of Equation (2-8) and thus, for  $\mathcal{R} > 0$ , cannot stabilize the flow. The steady state velocity  $V$  merely determines the speed of the wave-packet, thus the flow is unstable for  $\mathcal{P} > \alpha^2$ . Sakthivel & Ito (2007) introduce an instability parameter which only scales the fourth order element in the KS equation, and have added scalable uncertainty to this parameter to tackle the problem of robustness in the non-linear KS equation. They derived a robust boundary control using Lyapunov based stabilization achieving robustness despite including uncertainty in  $\mathcal{R}$ .

## 2-2 Model reduction methods

Fluid flows are often modeled using high-dimensional and non-linear governing equations. Model reduction is a methodology used to find approximate models of these high-dimensional dynamical systems. However, during these methods, the initial PDE from Section 2-1-1 undergoes several transformations and its parameters with it. The goal of this thesis is to find out how these parameters are transformed and how they will end up after model reduction and discretization. In order to investigate this problem, a deeper understanding of the methods commonly used in active flow is necessary. This section introduces three methods of model reduction: Proper Orthogonal Decomposition (POD), balanced truncation and a combination of the two, Balanced POD (BPOD). These methods can all be classified as projection methods as they involve projection of the PDE onto a subspace. Rowley (2005) provides a detailed description of the three methods and how they are related, which is summarized in the first few subsections. Next, this review provides a summary of the new method for discretization based on Galerkin projection using multivariate B-splines presented by Tol, Visser, & Kotsonis (2016). Further on in this Preliminary Thesis, Chapter 3 will provide a mathematical background for these methods.

### 2-2-1 Reduced order modeling

Three well-known methods of model reduction are Proper Orthogonal Decomposition (POD), balanced truncation and balanced POD. The POD method is commonly used in the fluid me-

chanics community and obtains a lower-dimensional approximation by projection of the full non-linear system onto a set of basis functions. These basis functions are obtained using empirical data by taking snapshots of the system. Balanced truncation was developed by the control theory community as a tool to make approximations of stable and linear input-output systems using the observability and controllability Gramians of the system. This method has been used on some fluid problems but it becomes computationally intractable when the system is high-dimensional which is often the case when modeling fluid flows. Rowley (2005) has introduced a new method for model reduction which combines POD and balanced truncation. This Balanced POD (BPOD) method uses empirical Gramians to compute balancing transformations for very large systems. Hence it combines the advantages of both methods while remaining computationally tractable. The mathematical background to these methods are described in Sections 3-1-1 to 3-1-3.

### 2-2-2 The multivariate B-spline

A new methodology for model reduction was introduced by Tol, Visser, & Kotsonis (2016). This model uses general geometries based on multivariate splines to generate reduced order models of linear parabolic partial differential equations. This method results in a state-space description of a high-order model, which can then directly be used for balanced truncation without needing empirical data to calculate the observability and controllability Gramians. It was shown that this discretization method results in a linear relation between the parameters of the PDE and the state matrix, which can be used to describe the structure of real uncertainty. This method is extensively described in Section 3-1-4.

### 2-2-3 Use in literature

The model reduction methods described in this chapter can all be classified as projection methods. These methods are based on the projection of a state-space system onto a different subspace. Bagheri et al. (2009) analyzes three different subspaces: a subspace based on the least stable eigenmodes, the POD modes and the balanced eigenmodes. His results clearly indicate that the balanced modes result in a much smaller error compared to the POD modes and the least stable eigenmodes. Bagheri et al. (2009) states that this is due to the fact that the spatial support of the balanced modes is achieved with a relatively low number of modes, accurately capturing input-output behaviour. Barbagallo et al. (2009) also included BPOD model reduction in his comparison, and concludes that BPOD combines the computational ease of POD and the low number of modes needed for reasonable accuracy of balanced truncation. The reason for this is clearly stated by Ilak & Rowley (2008), who shows that BPOD models outperform POD models due to the inclusion of dynamically important, low-energy modes but also due to the bi-orthogonal projection used in BPOD, approximating the best possible solution in the space spanned by the modes. Barbagallo et al. (2009) also make the interesting observation that POD modes show improved robustness when used to design reduced-order controllers. Another interesting observation has been made by Chen & Rowley (2013), who relate the upper bound on the error when using balanced truncation with the  $\nu$ -gap used to determine the robustness of a perturbed system. The combination of the two methods results in the possibility to make *a priori* guarantees about the model robustness of the system, which will be discussed later in Section 2-4.

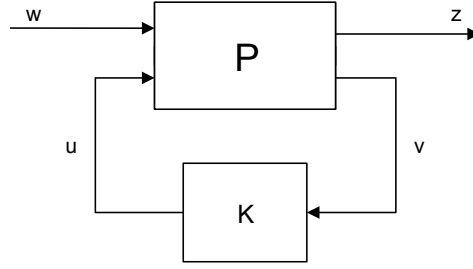


**Figure 2-2:** The generic control configuration is used to generalize the control problem, where  $\mathbf{P}$  represents the generalized plant,  $\mathbf{K}$  the feedback controller,  $\mathbf{u}$  the control variables,  $\mathbf{v}$  the measured variables,  $\mathbf{w}$  the external disturbances and  $\mathbf{z}$  the error signals used for controller optimization.

## 2-3 Control frameworks

After model reduction has taken place a controller can be synthesized. During the past decades a transition was made from optimal controllers to robust controllers, both of which are introduced in this section. Both control frameworks treated in this section are implemented using straight-forwards algorithms, and do not take into account structured uncertainty. However, as these methods are very common in literature, they will be presented as a starting point to the contribution of this thesis. This section will start with a general introduction to control frameworks, after which the basis for these frameworks is introduced. This section will end with a review of how these frameworks are applied in literature.

### 2-3-1 Generic control configuration

In order to explain the differences between optimal and robust control frameworks we introduce a general formulation as described by Figure 2-2. The system of this generic control configuration can be described by:

$$\begin{bmatrix} z \\ v \end{bmatrix} = P(s) \begin{bmatrix} w \\ u \end{bmatrix} = \begin{bmatrix} P_{11}(s) & P_{12}(s) \\ P_{21}(s) & P_{22}(s) \end{bmatrix} \quad (2-11)$$

where the state-space realization of  $P$  is defined as

$$P = \left[ \begin{array}{c|cc} A & B_1 & B_2 \\ \hline C_1 & D_{11} & D_{12} \\ C_2 & D_{21} & D_{22} \end{array} \right] \quad (2-12)$$

and where  $u$  are the control variables,  $v$  the measured variables,  $w$  the external disturbances and  $z$  the error signals which are used to optimize the controller. The closed-loop transfer function of the system is given by

$$F_l(P, K) = P_{11} + P_{12}K(I - P_{22}K)^{-1}P_{21} \quad (2-13)$$

The two control frameworks involve minimization of the  $\mathcal{H}_2$  and  $H_\infty$  norms of  $F(P, K)$ . The following assumptions are made:

(A1)  $(A, B_2, C_2)$  is stabilizable and detectable.

(A2)  $D_{12}$  and  $D_{21}$  have full rank.

(A3)  $\begin{bmatrix} A - j\omega I & B_2 \\ C_1 & D_{21} \end{bmatrix}$  has full column rank for all  $\omega$ .

(A4)  $\begin{bmatrix} A - j\omega I & B_1 \\ C_2 & D_{21} \end{bmatrix}$  has full row rank for all  $\omega$ .

(A5)  $D_{11} = 0$  and  $D_{22} = 0$ .

(A6)  $D_{12} = \begin{bmatrix} 0 \\ I \end{bmatrix}$  and  $D_{12} = [0 \quad I]$

(A7)  $D_{12}^T C_1 = 0$  and  $B_1 D_{21}^T = 0$ .

(A8)  $(A, B_1)$  is stabilizable and  $(A, C_1)$  is detectable.

Assumption A1-A4 and A8 are necessary for a solution to exist, and Assumption A5-A7 significantly simplify the problem with respect to solving of the Ricatti equations. A detailed description of these frameworks can be found in (Skogestad & Postlethwaite, 2001, pp. 362-369), of which a brief summary will be presented in this section. First, the  $H_2$  control framework will be presented, after which the  $H_\infty$  control framework will be presented introducing the concept of robust control.

### 2-3-2 $H_2$ -controller

The  $H_2$  control framework is based on the  $H_2$  norm of the transfer function described in Equation (2-13). The  $H_2$  norm of a system is the sum of the energies of the output of the system:

$$\|F_l(s)\|_2 = \sqrt{\frac{1}{2\pi} \int_0^\infty \text{tr}(F(j\omega)^H F(j\omega)) d\omega} \quad (2-14)$$

The  $H_2$  optimal control framework has as main objective to find the stabilizing controller which minimizes  $\|F_l(s)\|_2$ , which is the energy in the transfer function. Hence, this control framework does not aim to improve the robustness of the system towards uncertainty.

One of the most common controllers used for  $H_2$  control is the Linear Quadratic Gaussian (LQG) controller. It introduces additive white Gaussian noise to the model and combines an observer having incomplete state information and a controller designed using quadratic costs. The controller synthesis consists of a Kalman filter and a Linear Quadratic Regulator (LQR) which can easily be combined due to the separation principle. An extensive description of the controller design procedure can be found in Section 3-2.

### 2-3-3 $H_\infty$ -controller

The  $H_\infty$  control framework was developed due to a need for more robust controllers as the LQG-controller does not provide any guaranteed stability margins. This is due to the fact that the  $H_2$ -norm only gives an average measure of all frequencies, while the  $H_\infty$ -norm of the

weighted sensitivity  $\|w_P S\|_\infty < 1$  actually provides a guarantee on the boundedness of the transfer function over all frequencies. The  $H_\infty$  control problem is to minimize the  $H_\infty$  norm described by

$$\|F_l(P, K)\|_\infty = \max_{\omega} \bar{\sigma}(F_l(P, K)(j\omega)). \quad (2-15)$$

Minimizing the norm of Equation (2-15) results in minimizing the maximum singular value of  $F_l(P, K)$ , instead of minimizing the average energy of over the transfer function. Physically, this results in a lower maximum gain over the transfer function, but also results in a lower overall performance. The singular values of a matrix  $G$  are the square roots of the eigenvalues of  $G^H G$ , where  $G^H$  is the complex conjugate transpose of  $G$ :

$$\sigma_i(G) = \sqrt{\lambda_i(G^H G)} \quad (2-16)$$

Doyle et al. (1989) has provided an algorithm for minimizing Equation (2-15) under Assumptions (A1-A8). Even though most of these assumptions are met by most control problems, controller synthesis using this algorithm results in a suboptimal  $H_\infty$  controller. Methods described in Section 2-4 are, for some applications, more thorough but also more complicated to implement.

### 2-3-4 Controller synthesis in literature

The controller synthesis methods described in this section are commonly used in literature related to AFC. Especially the LQG controller is often used as it comes with both ease of implementation, best possible performance and closed-loop stability guarantees, but is very sensitive to errors in the knowledge of the model. This is very important, because, as Kim & Bewley (2007) states, increasing the Reynolds number comes with increasing difficulty to stabilize the system. Hence they focus on characterizing the fundamental limitations in fluid systems. When designing an LQG controller, one of the challenges is the decision on actuator and sensor placement. Bagheri et al. (2009) state that the sensor locations should overlap with unstable global modes and that actuators should coincide with the corresponding adjoint modes. However, Chen & Rowley (2011) present a method which uses a gradient of the  $H_2$  squared norm to determine optimal sensor and actuator placements and applies this to the Ginzburg-Landau equation. Another challenge with LQG controllers is that they provide no guarantees with respect to robustness of the system. Fabbiane et al. (2014) suggest that the robustness issue may be solved using model-free methods such as LMS and X-Filtered LMS. However, as these systems can become unstable, Fabbiane et al. (2014) expect future developments to head to hybrid models where these techniques are combined.

The need for a robust solution is growing fast. As Fabbiane et al. (2015) clearly point this out in a statement with respect to optimal control techniques: "Although these studies provide important insight into performance limitations ... they remain at a proof-of-concept level, since any deviation of the design conditions can destabilize the controller." This necessity has led to the introduction of robust  $H_\infty$  control frameworks. As shown by Sipp & Schmid (2016),  $H_\infty$  control methods can even extend the operating range in terms of the Reynolds number. However, Bagheri et al. (2009) show that when accounting for robustness, compromises have to be made between  $H_2$  control and  $H_\infty$  control unfluencing performance of the overall system. Lauga & Bewley (2004) add to this that for increasing Reynolds numbers,  $H_\infty$  control methods show better performance than  $H_2$  control methods with respect

to both worst-case noise rejection, and even Gaussian noise rejection. Especially the latter is interesting, as  $H_2$  control methods are based on the idea of adding Gaussian noise to the system.

Robustness can be accounted for using different methods. Starting from  $H_2$  control, a generalized  $H_\infty$  controller synthesis algorithm has been developed by Doyle et al. (1989) which is very similar to the  $H_2$  controller synthesis algorithm. These methods differ merely in the latter taking into account worst-case disturbances in the objective function. Bewley & Liu (1998) introduce a convenient method of scaling three scalar parameters which allows for adjusting of closed-loop characteristics. Changing these parameters shifts the objective from accounting for noise in  $H_2$  control to accounting for worst-case disturbances in  $H_\infty$  control. Lauga & Bewley (2001) show that the use of such  $H_\infty$  controller synthesis methods are of particular importance near the stabilizability limit of the system. However, this generalized method does not take into account actual parametric uncertainty in the model, which lies at the basis of the concept of robust control. The next chapter will discuss some advanced robust control methods that do take into account this uncertainty which should potentially result in less conservative controllers.

## 2-4 Robust control

For the past three decades, control frameworks such as the frameworks described in Section 2-3 have been implemented for AFC applications. First,  $H_2$  optimal control was applied in aerospace applications, where the model dynamics are often well known, yielding good results. When control problems such as LQG were applied to systems where less knowledge was available, these controllers performed less. Hence, the focus shifted to more robust  $H_\infty$  optimal control solutions. However, as the synthesis of these controllers often need simplifications, a deeper understanding of uncertainties and how they need to be modeled was needed. This section will elaborate on what uncertainties can be found when modeling fluid flows and on how this knowledge can be applied to improve controller robustness.

### 2-4-1 Uncertainties

Uncertainties arise from differences between the actual system and the model of the system used to build a controller. These uncertainties can be caused by the model not being precise enough, or by external disturbances acting on the real system. Bobba (2004) was one of the first to point out different types of uncertainty, which were then categorized by Jones et al. (2015) according to:

- (i) Model uncertainty: this type of uncertainty comes in two forms. (Skogestad & Postlethwaite, 2001, pp. 255) divides this type of uncertainty in parametric (real) uncertainty and dynamic (frequency-dependant) uncertainty.
- (i) Disturbance uncertainty: this type of uncertainty arises from the lack of precise knowledge of the disturbances occurring in the real experiment.

The focus of robust control lies on model uncertainty. Model uncertainty can originate from different sources. (Skogestad & Postlethwaite, 2001, pp. 255) list the following sources as main causes for uncertainty:

- Parameters in the model which are only known approximately
- Parameters in the model which vary due to nonlinearities
- Imperfect measurement devices
- High frequency deviations from the linear model
- Neglected dynamics due to model reduction
- Differences between synthesized controller and implemented controller

These sources for model uncertainty can be classified as either parametric uncertainty or dynamic uncertainty. Disturbance uncertainty includes the lack of knowledge on boundary conditions and lack of knowledge of the initial conditions but also small disturbances like impurities, Coriolis force or acoustic forcing, etc. These uncertainties are seen as external signals that can be incorporated into the model using weighted signals. A good example of this method is presented by Baramov et al. (2004)

### Parametric uncertainty

Parametric uncertainty is real and is represented by  $\Delta$  which is a real scalar satisfying  $|\Delta| < 1$ . In a simple case where state-space matrices depend linearly on these parameters, such a perturbation could be represented according to

$$A_p = A + \Sigma\delta_i A_i, \quad B_p = B + \Sigma\delta_i B_i, \quad C_p = C + \Sigma\delta_i C_i, \quad D_p = D + \Sigma\delta_i D_i$$

Parametric uncertainty is often avoided. (Skogestad & Postlethwaite, 2001, pp. 258) lists the following reasons:

1. It requires a large effort to model parametric uncertainty.
2. The uncertainty model becomes deceiving, as it provides a very detailed description of an approximated model.
3. The exact model structure is required, so dynamic uncertainty cannot be dealt with.
4. Real perturbations are required, which increases the difficulty of controller synthesis.

Hence, parametric uncertainty in the form of real perturbations are often represented as complex perturbations. They can then be lumped together into a single complex perturbation which often describes them more more accurately. As (Skogestad & Postlethwaite, 2001, pp. 260-261) shows, varying multiple parameters in the transfer function creates so-called uncertainty discs on the Nyquist plot, having complex mathematical descriptions. These discs are then approximated using additive uncertainty according to

$$G_p(s) = G(s) + w_A(s)\Delta_A(s); \quad |\Delta_A(j\omega)| \leq 1\forall\omega \quad (2-17)$$

where  $G(s)$  is the nominal plant model and  $G_p(s)$  the perturbed plant model. For reduce-then-design methods such as described in Section 2-2 there are no known references as to how parametric disturbances can be modeled. The main difference between this parametric 'unstructured' uncertainty and parametric 'structured' uncertainty is that the perturbation matrix  $\Delta$  is full, instead of partially empty.

### Dynamic uncertainty

Dynamic uncertainty is usually due to high frequency disturbances and thus represented in the frequency domain. These complex perturbations are normalized such that  $\|\Delta\|_\infty \leq 1$ . Dynamic uncertainty is usually represented using either feedforward or feedback forms. The feedforward forms include additive uncertainty, multiplicative input uncertainty and multiplicative output uncertainty and are defined as

$$G_p = G + w_A \Delta_A \quad (2-18)$$

$$G_p = G(I + w_I \Delta_I) \quad (2-19)$$

$$G_p = (I + w_O \Delta_O)G \quad (2-20)$$

respectively. The feedback forms include inverse additive uncertainty, inverse multiplicative input uncertainty and inverse multiplicative output uncertainty and are defined as

$$G_p = G(I - w_{iA} \Delta_{iA} G)^{-1} \quad (2-21)$$

$$G_p = G(I - w_{iI} \Delta_{iI})^{-1} \quad (2-22)$$

$$G_p = (I - w_{iO} \Delta_{iO})^{-1} G \quad (2-23)$$

respectively. The block diagrams for these representations are shown in Figure 2-3. Unstructured multiplicative output uncertainty is often used to obtain a simple uncertainty description. However, as plants increase in complexity, uncertainty should be implemented as it occurs physically using one of the other forms. The inverse forms are used for dealing with unstable plant poles. Green & Limebeer (2012) states that one of the disadvantages of the additive representation is that the error in  $G$  differs from the error in a compensated loop  $GK$ . Therefore it is difficult to take into account the effect of the perturbation on the compensated loop  $GK$ . According to Zhou et al. (1996), this results in "an additive noise model [being] entirely inappropriate for capturing uncertainty arising from variations in the material properties of physical plants." Next to the models described in Figure 2-3, there is a coprime factorization model which aims to combine the useful properties of the models described above. This model is further elaborated on in Section 3-3-3.

### 2-4-2 Generalized robust control problem

When more knowledge is obtained on the structure and type of uncertainty of the model, more advanced and less conservative robust control methods can be applied. For the robust control problem, a similar control configuration as shown in Figure 2-2 is introduced by Figure 2-4. This model can be described using the following state space configuration:

$$\begin{bmatrix} z \\ v \end{bmatrix} = P(s) \begin{bmatrix} w \\ u \end{bmatrix} \quad (2-24)$$

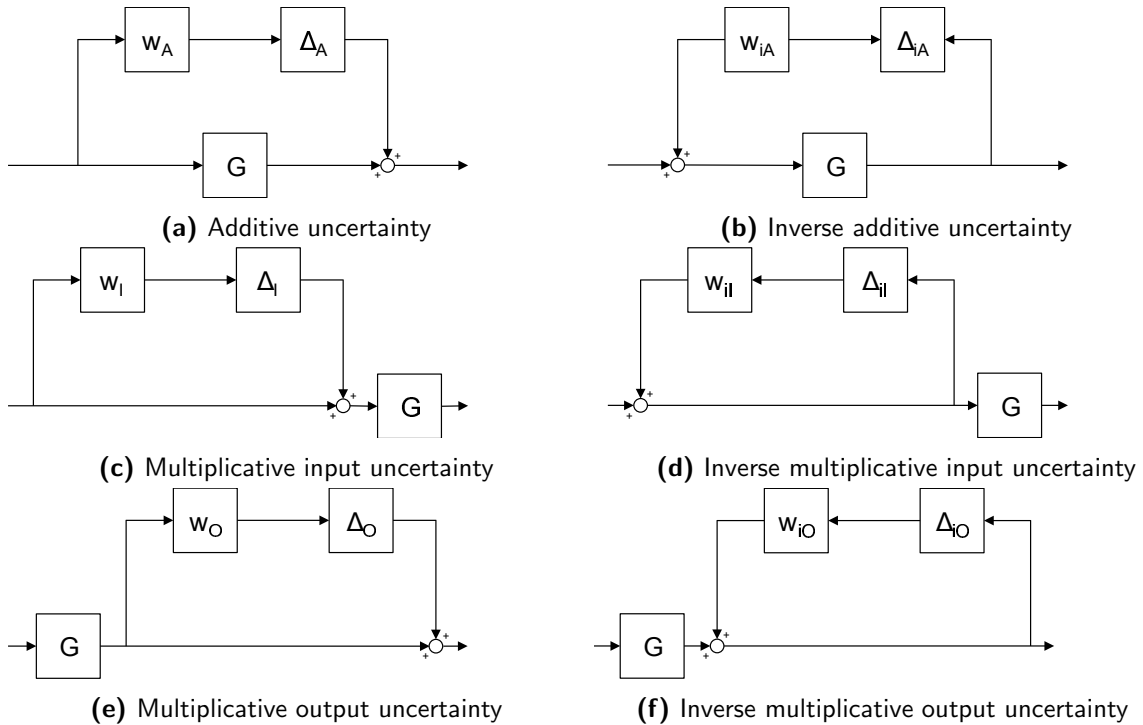


Figure 2-3: Representations used for analysis

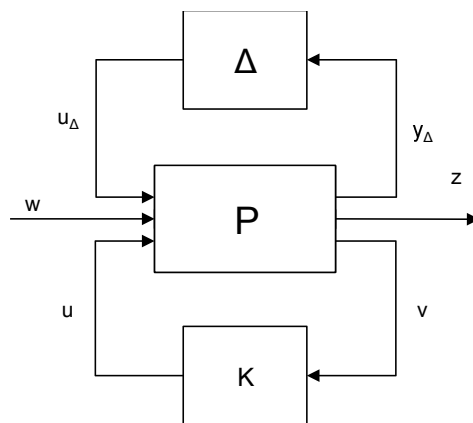
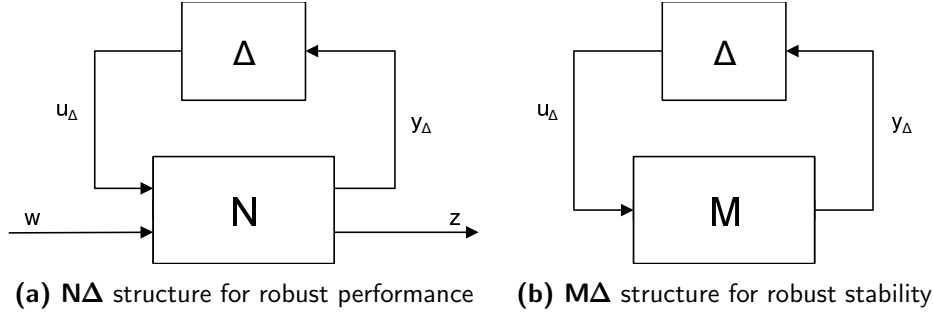


Figure 2-4: The standard representation of an uncertain system, where **P** represents the generalized plant, **K** the feedback controller, **Δ** the uncertainty block, **u** the control variables, **v** the measured variables, **w** the external disturbances and **z** the error signals used for controller optimization.



**Figure 2-5:** Representations used for analysis

where the corresponding plant can be defined as

$$P = \begin{bmatrix} P_{11} & P_{12} \\ P_{21} & P_{22} \end{bmatrix} = \begin{bmatrix} 0 & W_2 \\ W_1 & G \end{bmatrix} \quad (2-25)$$

The closed loop transfer function of this system is then given by

$$F_u(P, \Delta) = P_{22} + P_{21}\Delta(I - P_{11}\Delta)^{-1}P_{12} = G + W_1\Delta W_2 \quad (2-26)$$

When analyzing robust performance or stability issues, the plant as shown in Figure 2-4 is often slightly adapted. For robust performance analysis the  $N\Delta$  structure (Figure 2-5a) is used and for robust stability analysis the  $M\Delta$  structure (Figure 2-5b) is used. The nominal plant  $N = F_l(P, K)$  has previously been described as a function of the general plant  $P$  and the feedback gain  $K$ . The  $N\Delta$  structure is then used to describe the relationship between  $N$  and  $\Delta$  and the uncertain closed-loop transfer function from  $w$  to  $z$ ,  $z = Fw$  according to

$$F = F_u(N, \Delta) \triangleq N_{22} + N_{21}\Delta(I - N_{11}\Delta)^{-1}N_{12} \quad (2-27)$$

The  $M\Delta$  structure describing the transfer function from the output to the input of the perturbation is then given by  $M = N_{11}$ .

## 2-5 Comparing robust control methods

The controller design methods described earlier in this chapter are focussed on optimal control and on general robustness to uncertainty. The structure of the uncertainty and the way it appears in the physical system is not accounted for, resulting in either non-robust or over-conservative designs. Good examples are the methods as presented by Bewley & Liu (1998) and Lauga & Bewley (2001), which do not take into account the effect of parametric uncertainty, which results in a potentially conservative controller. If the physical process is carefully observed, more knowledge of the uncertainty can be obtained, which can be used to improve the controllers with respect to their robustness.

The signal-based approach is one of the simpler methods which uses weighed signals to represent uncertainty in the model (for a detailed description, see Section 3-3-2). A good example of this method is applied in Baramov et al. (2004), where four external inputs are used to model uncertainty. The first input disturbs the co-prime factor model, the second generates

flow disturbance measured at the far upstream sensor and the third and fourth input are measurements noises. These inputs are then filtered and introduced into the system using a configuration similar to that in Figure 3-1a. The simulation results showed that the disturbances could be kept at a low level, however, the results were not compared with other (robust) control methods. A similar design method was applied by Baramov et al. (2002), where the results were compared with an LQG controller. It was shown that the LQG controller reacted faster but had a much larger overshoot than the  $H_\infty$  controller. Examination of transfer functions  $T_{wz}$  showed that the LQG controller is much more vulnerable to modeling errors than its  $H_\infty$  counterpart.

In Section 3-3-3 the  $H_\infty$  loop-shaping approach is presented. This more advanced two step method is extensively described by Chen & Rowley (2013), who provide useful mathematical properties of  $\nu$ -gap and introduces the connection between balanced truncation and  $H_\infty$  loop shaping. Flinois & Morgans (2016) implement  $H_\infty$  loop shaping for ERA reduced order model but shows that even though a controller designed using the loop-shaping approach is robust enough to stabilise the system, it does not always yield stabilizing results at off-design Reynolds numbers. This method is also applied by Jones et al. (2015) to design a controller robust to dynamic model uncertainty but then using model refinement instead of model reduction.

The structured singular value approach as described in Section 3-3-1 has not been encountered in literature with respect to AFC applications. However, this methodology has proven successful for other problems. Tofighi et al. (2015) provide a good example of both mixed-sensitivity synthesis and DK-iteration approaches for robust feedback linearization of an isothermal continuous stirred tank reactor. However, this reactor is modeled using a state-space system that allows for easy implementation of parametric uncertainty:

$$\dot{z} = \begin{bmatrix} -\frac{k_1}{2}x_{10}^{-\frac{1}{2}} & 0 \\ 0 & \frac{k_2(x_{20}-1)}{(x_{20}+1)^3} \end{bmatrix} + \begin{bmatrix} 1 & 1 \\ \frac{C_{B1}-7.07}{100} & \frac{C_{B2}-7.07}{100} \end{bmatrix} w \quad (2-28)$$

where real parametric uncertainty ranges were considered of 20% for  $k_1$ , 30% for  $k_2$ , 20% for  $C_{B1}$  and 20% for  $C_{B2}$  from the corresponding nominal values. The controllers were both able to effectively reach the design goals at presence of the modeled uncertainty, proving the value of modeling for parametric uncertainty. However, Schirrer et al. (2013) also shows the difficulty arising when modeling for parametric uncertainty in more complex system. When attempting to design a robust controller for blended wing body aircraft using structured uncertainty, it was found that a highly parametrized Linear Fractional Representation (LFR)  $F_u(M, \Delta)$  results to be prohibitively complex for  $\mu$  analysis and synthesis. After performing a few iterations of the *DGK*-design (similar to the *DK*-iteration approach) the order of the controller increased above 1000, which rendered the attempt numerically and computationally infeasible. However, using a reduced-accuracy parameterized LFR of order 30 a significant loss of performance was encountered, but the resulted in a robust controller nonetheless.

From the literature can be concluded that signal-based and loop-shaping approaches can be effective methods to improve the controller robustness. However, these designs can lead to sub-optimal controllers. The structured singular value approach shows potential for simpler systems, where parametric uncertainty is taken into consideration. However, literature shows that high-dimensionality can be problematic with respect to the implementation of such methods. The objective for this thesis is to design a control framework for systems discretized

using the Multivariate B-Spline method, which in general have a lower dimension. Hence, the structured singular value approach has the potential to construct a robust controller which is far less conservative but still very robust.



**Part III**

**Methodology**



---

# Chapter 3

---

## Methodology

This chapter provides more detail to the methods introduced in Chapter 2. The preliminaries introduced here will be used later during the thesis to either examine the behaviour structured uncertainty for reduced order models or to design robust controllers. Section 3-1 provides a mathematical background for the three model reduction methods and also summarizes the new model reduction method of Tol, Visser, & Kotsonis (2016). Section 3-2 provides a more detailed description of the  $H_2$  and  $H_\infty$  controller synthesis methods and Section 3-3 describes the advanced robust control methods described in Section 2-4.

### 3-1 Reduced Order Models

In the previous chapter, three model reduction methods have been introduced. This section provides the reader with a mathematical description of these methods. Section 3-1-1 describes the POD method, Section 3-1-2 describes the balanced truncation method and Section 3-1-3 describes the combination of these two methods, the BPOD. Finally, a detailed description is provided of the Multivariate B-spline method in Section 3-1-4.

#### 3-1-1 Proper Orthogonal Decomposition

POD is an approximation method which projects a set of data,  $x(t)$  that lies in a vector space  $\mathcal{V}$  unto a finite-dimensional subspace  $\mathcal{V}_r$  which has a fixed dimension,  $r$ . For simplicity we assume  $\mathcal{V} = \mathbb{R}^n$ , which means that the infinite-dimensional fluid flow have already been discretized in space. For the infinite-dimensional case, see Rowley et al. (2004).

The aim of POD is to find a subspace  $\mathcal{V}_r$  such that the error between  $\mathcal{V}$  and  $\mathcal{V}_r$  is minimized. We can then define the projection  $P_r : \mathbb{R}^n \rightarrow \mathbb{R}^r$  which project the dataset from  $\mathcal{V}$  to  $\mathcal{V}_r$ . The problem then becomes to minimize the total error

$$\int_0^T \|x(t) - P_r x(t)\| dt. \quad (3-1)$$

To this end we introduce the following  $n \times n$  matrix:

$$R = \int_0^T x(t)x(t)^* dt, \quad (3-2)$$

where  $x(t)^*$  is the transpose of  $x(t)$ . We then find the eigenvalues and eigenvectors of the matrix  $R$ , which are given by

$$R\varphi_k = \lambda_k\varphi_k, \quad \lambda_1 \geq \dots \geq \lambda_n > 0 \quad (3-3)$$

In fluid flow problems, the size of this eigenvalue problem is often computationally intractable. In Sirovich (1987), a method to transform the eigenvalue problem and decrease its size was introduced. This snapshot method is elaborated on in Section 3-1-3. The eigenvectors  $\varphi_k$  found in Equation (3-3) are chosen orthonormal which is possible because  $R$  is symmetric, positive-semidefinite and all the eigenvalues  $\lambda_k$  are real and non-negative. The optimal subspace  $P_r$  of dimension  $r$  is then given by

$$P_r = \sum_{k=1}^r \varphi_k\varphi_k^* \quad (3-4)$$

The eigenvectors  $\varphi_k$  are called the POD modes and they consist of the first  $r$  eigenvectors of  $R$ . Using these eigenvectors, we can now form a ROM by projecting the system dynamics  $\dot{x}(t) = f(x(t))$  unto the previously defined subspace:

$$\dot{x}_r(t) = P_r f(x_r(t)) \quad (3-5)$$

where  $x_r(t) \in \text{span}\{\varphi_1, \dots, \varphi_r\}$  and can be written as

$$x_r(t) = \sum_{j=1}^r a_j(t)\varphi_j. \quad (3-6)$$

Combining Equations (3-4) to (3-6) and multiplying by  $\varphi_k^*$  yields the following set of Ordinary Differential Equations (ODEs):

$$\dot{a}_k(t) = \varphi_k^* f(x_r), \quad k = 1, \dots, r. \quad (3-7)$$

These ODEs can then be used as a ROM to describe the evolution of  $x_r(t)$ . The POD modes in Equation (3-7) describe only the largest eigenvalues of the system. Physically this means that they maximize the average energy in the projection of the data unto the subspace spanned by the modes. However, this is not always optimal for describing a fluid flow, since low energy modes can be critical to the flow dynamics. This problem can be solved using balanced truncation, which is described later in this section.

### 3-1-2 Balanced truncation

Balanced truncation is a method for model reduction introduced by Moore (1981). Instead of maximizing the energy of the projection as with POD, balanced truncation aims for a hierarchy based on the controllability and observability of the modes. Balanced truncation starts with defining the controllability and observability Gramians of a stable linear input-output system

$$\begin{aligned} \dot{x} &= Ax + Bu \\ y &= Cx + Du \end{aligned} \quad (3-8)$$

where  $x(t) \in \mathbb{R}^n$  is the state vector,  $u(t) \in \mathbb{R}^p$  is the input vector and  $y(t) \in \mathbb{R}^q$  is the output vector. The controllability and observability Gramians are then defined as follows:

$$\begin{aligned} W_c &= \int_0^\infty e^{At} B B^* e^{A^*t} dt \\ W_o &= \int_0^\infty e^{At} C^* C e^{A^*t} dt \end{aligned} \quad (3-9)$$

Both Gramians are symmetric and positive-semidefinite, and can be calculated by solving the following Lyapunov equations:

$$\begin{aligned} A W_c + W_c A^* + B B^* &= 0 \\ A^* W_o + W_o A + C^* C &= 0 \end{aligned} \quad (3-10)$$

The two Gramians measure the degree to which each state is either excited by an input or the degree to which each state excites future outputs, respectively. Balanced truncation means that a transformation  $T$  is found which balances the controllability and observability properties of the system so they are equal and diagonal:

$$T^{-1} W_c (T^{-1})^* = T^* W_o T = \Sigma = \text{diag}(\sigma_1, \dots, \sigma_n). \quad (3-11)$$

This balancing transformation exists as long as the system is both controllable and observable. The diagonal elements  $\sigma_1 \geq \dots \geq \sigma_n \geq 0$  of  $\Sigma$  are called the Hankel Singular Values (HSVs) of the system and are independent of the coordinate system. The transformation  $T$  is found using:

$$W_c W_o T = T \Sigma^2 \quad (3-12)$$

A balanced realisation can be found by a change of coordinates  $x = Tz$ , which can then be partitioned as

$$A_b = \begin{bmatrix} A_{11} & A_{12} \\ A_{21} & A_{22} \end{bmatrix}, B_b = \begin{bmatrix} B_1 \\ B_2 \end{bmatrix}, C_b = [C_1 \quad C_2], \Sigma = \begin{bmatrix} \Sigma_1 & 0 \\ 0 & \Sigma_2 \end{bmatrix} \quad (3-13)$$

where  $\Sigma_1$  and  $\Sigma_2$  contain the HSVs and  $\Sigma_1$  is an  $r \times r$  matrix containing the most controllable/observable modes. The ROM of order  $r$  is then constructed using  $G_r(s) = (A_{11}, B_1, C_1, D)$  where  $D$  is collected straight from Equation (3-8). Instead of aiming to maximize the energy in the projection, balanced truncation aims to keep modes of dynamical importance.

Another important property of balanced truncation is that there is an upper bound on the error of a given order truncation described by

$$\|G(s) - G_r(s)\|_\infty < 2 \sum_{j=N_r+1}^n \sigma_j \quad (3-14)$$

One of the uses of this upper bound will be elaborated on later in Section 3-3-3.

### 3-1-3 Balanced Proper Orthogonal Decomposition

Model reduction using POD is a very efficient way to approximate a model based on a dataset  $x(t)$ . However, with fluid flows, the eigenvalue problem described in Equation (3-3) can be a challenge due to high dimensionality of the problem. Balanced truncation has similar problems when calculating the Gramians. Hence, some methods have been developed to make these problems computationally tractable.

### Snapshot method for POD

Sirovich (1987) found that if the dataset  $x(t)$  is provided discretely as snapshots  $x(t_j)$  at  $t_1, \dots, t_m$ , the dimension of the problem can be reduced from  $n$  to  $m$ . Since the data is discretized, we can write Equation (3-2) as

$$R = \sum_{j=1}^m x(t_j)x(t_j)^* \delta_j \quad (3-15)$$

where  $\delta_j$  are the quadrature weighing coefficients. The data can then be written in matrix format of size  $m \times n$

$$X = [x(t_1)\sqrt{\delta_1} \quad \dots \quad x(t_m)\sqrt{\delta_m}] \quad (3-16)$$

so that we can rewrite  $R = XX^*$ . The eigenvalue problem then becomes

$$X^*Xu_k = \lambda_k u_k, \quad u_k \in \mathbb{R}^m, \quad (3-17)$$

which has exactly the same eigenvalues as Equation (3-3). The POD modes are then given by

$$\varphi_k = Xu_k/\sqrt{\lambda_k}. \quad (3-18)$$

### Snapshot method for balanced truncation

When using balanced truncation, difficulties arise when computing high-dimensional systems. This is due to the fact that the matrices in the Lyapunov equations (Equation (3-10)) are too large, so analytical calculation of the Gramians (Equation (3-9)) becomes computationally intractable. In order to cope with this problem, Moore (1981) introduced a method very similar to the snapshot method as presented by Sirovich (1987) by calculating the exact balanced truncation for finite dimensional systems.

The controllability Gramian is computed by writing the input matrix  $B = [b_1, \dots, b_p]$  and then determining the state responses to unit impulses according to  $x_p = e^{At}b_p$ . The controllability Gramian is then given by

$$W_c = \int_0^\infty (x_1(t)x_1(t)^* + \dots + x_p(t)x_p(t)^*)dt. \quad (3-19)$$

For the observability Gramian this procedure can be followed analogously, but using the adjoint system

$$\dot{z} = A^*z + C^*v \quad (3-20)$$

where  $C^* = [c_1, \dots, c_q]$ . The input responses then become  $z_q = e^{A^*t}c_q$ , and the observability Gramian is given by

$$W_o = \int_0^\infty (z_1(t)z_1(t)^* + \dots + z_q(t)z_q(t)^*)dt. \quad (3-21)$$

If the simulated responses are also provided in a discrete dataset, the integral from Equation (3-19) can be written as quadrature sums and be stacked in a matrix as

$$X = [x_1(t_1)\sqrt{\delta_1} \quad \dots \quad x_1(t_m)\sqrt{\delta_m} \quad \dots \quad x_p(t_1)\sqrt{\delta_1} \quad \dots \quad x_p(t_m)\sqrt{\delta_m}] \quad (3-22)$$

Analogously a matrix  $Y$  can be formed for the integral from Equation (3-21), resulting in the following equations for the Gramians:

$$\begin{aligned} W_c &= XX^* \\ W_o &= YY^* \end{aligned} \quad (3-23)$$

Comparing Equation (3-16) and Equation (3-22) clearly shows the relation between POD and balanced truncation. Balanced truncation is similar to POD in a sense that for the POD dataset consists only of unit impulses and that the observability Gramian is used for inner product.

### Balanced POD

In order to cope with these problems of high-dimensionality Rowley (2005) introduced the Balanced POD method. In this method, instead of determining the transformation matrix  $T$  using the eigenvalue problem of Equation (3-12),  $T$  is determined by finding the Singular Value Composition (SVD) of the two snapshot matrices  $Y^*X$  of Equation (3-23) according to:

$$Y^*X = U\Sigma V^* = \begin{bmatrix} U_1 & U_2 \end{bmatrix} \begin{bmatrix} \Sigma_1 & 0 \\ 0 & 0 \end{bmatrix} \begin{bmatrix} V_1^* \\ V_2^* \end{bmatrix} = U_1 \Sigma_1 V_1^* \quad (3-24)$$

where  $\Sigma_1 \in \mathbb{R}^{r \times r}$  is invertible,  $r$  is the rank of  $Y^*X$ , and  $U_1^*U_1 = V_1^*V_1 = I_r$ . The balancing transformation and its inverse can then be written as:

$$T_1 = XV_1\Sigma_1^{-1/2}, \quad S_1 = \Sigma_1^{-1/2}U_1^*Y^* \quad (3-25)$$

Rowley (2005) proves that if  $r = n$ , the matrix  $\Sigma_1$  contains the Hankel singular values, and if  $r < n$ , the columns of  $T_1$  contain the first  $r$  columns of the balancing transformation and the columns of  $S_1$  contain the first  $r$  columns of the inverse transformation. Brunton & Noack (2015) show how these transformations can transform the generalized plant of Equation (3-8) into a balanced ROM:

$$\begin{aligned} A_r &= S_1^*AT_1 \\ B_r &= S_1^*B \\ C_r &= C^*T_1 \\ D_r &= D \end{aligned} \quad (3-26)$$

#### 3-1-4 Galerkin projection and the multivariate B-spline

In Section 2-2 the concept of POD is introduced as a method of model reduction. This methodology projects a set of data that lies in a vector space  $\mathcal{V}$  onto a subspace  $\mathcal{V}_r$ . The projection described by Equations (3-5) and (3-7) is also referred to as a Galerkin projection. In Tol, Visser, & Kotsonis (2016) a new methodology is presented that uses Galerkin projection to project a PDE onto a general geometry using multivariate B-splines to derive a finite set of ODEs. This section will provide a brief overview of this methodology. For a detailed analysis is referred to Tol, Visser, & Kotsonis (2016).

### Multivariate B-spline approximation

First the system of equations is reduced to a finite set of coupled ODEs using Galerkin projection. In order to do this, the state equations of the PDE need to be formulated in a weak condition:

Find  $y(x, t) \in \mathcal{L}^2(0, T; \mathcal{H}^k(\Omega))$

$$\int_{\Omega} \frac{\partial y(x, t)}{\partial t} v(x) dx = \int_{\Omega} \left( Ly(x, t) + g(x)u(t) \right) v(x) dx \quad (3-27)$$

$$L_{\Gamma} y(x, t) = g_{\Gamma}(x)u_{\Gamma}(t), \quad \text{on } \Gamma_T \quad (3-28)$$

$\forall v \in \mathcal{V}_0$  and  $t \in [0, T]$ , with  $\mathcal{H}^k(\Omega)$  the standard Sobolev space consisting of all functions whose spatial derivatives up to the k-th order exist in the weak sense and are in  $\mathcal{L}^2(\Omega)$  and with  $\mathcal{V}_0$  the space of test functions  $v(x)$

$$\mathcal{V}_0 = \{v \in \mathcal{H}^k(\Omega) : L_{\Gamma} v = 0\} \quad (3-29)$$

The spline approximation of Equation (3-27) can now be defined. Let  $\mathcal{T}$  be the triangulation of the domain  $\Omega$  and let  $\mathcal{S}$  be a spline subspace consisting of spline functions which are  $C^r$  inside  $\Omega$ . A finite approximation of  $y$  in  $\Omega$  can then be represented by

$$y^N(x, t) = s(x, t) \quad (3-30)$$

The spline approximation of Equation (3-27) with respect to spatial variables is  $s(\cdot, t) \in \mathcal{S}$  which must satisfy the boundary conditions approximately such that

$$\int_{\Omega} \frac{\partial s(x, t)}{\partial t} s_v(x) dx = \int_{\Omega} \left( Ls(x, t) + g(x)u(t) \right) s_v(x) dx \quad (3-31)$$

$\forall s_v \in \mathcal{S}_0$  and  $t \in [0, T]$ , where  $\mathcal{S}_0 = \mathcal{S} \cap \mathcal{V}_0$ . The implementation to this is quite easy, however, the construction of a basis for  $\mathcal{S}_0$  and  $\mathcal{V}_0$  is difficult. To solve this, discontinuous piecewise polynomial functions are used over a triangulation combined with the smoothness properties and boundary conditions as side constraints.

### Implementation of side constraints

The splines in Equation (3-31) are represented using the B-form of splines using the vector formulation from Visser et al. (2009):

$$s(x, t) = B^d(x)c(t) \quad (3-32)$$

The spline function can now be identified by its B-coefficients  $c(t)$  which are the time-varying coefficients of the global vector of B-form basis polynomials. The differential operator acting on  $s$  can be written in terms of a single degree basis polynomial of the form

$$L[B^d(x)c(t)] = \sum_{|\alpha| \leq k} a_{\alpha}(x) B^d(x) \mathbb{T}c(t) \quad (3-33)$$

The side constraints, namely the smoothness of  $s$  and the discrete constraints for the boundary conditions, can be expressed by a linear system of the form

$$\begin{bmatrix} H \\ R \end{bmatrix} c(t) = \begin{bmatrix} 0 \\ G \end{bmatrix} u_\Gamma(t) \quad (3-34)$$

where the continuity conditions are represented by  $H$ , the boundary conditions are represented by  $R$ , and the interpolation between the boundary  $\Gamma$  and the boundary control input  $u_\Gamma$  is represented by  $G$ . Using definitions for a velocity mass matrix  $M$  and a bending matrix  $K$  from Tol, Visser, & Kotsonis (2016) and Equations (3-32) and (3-33), the problem of Equation (3-31) can be rewritten to

$$\begin{aligned} c_v^T M \dot{c}(t) &= c_v^T K c(t) + c_v^T F u(t) \\ H c(t) &= 0 \\ R c(t) &= G_\Gamma u_\Gamma(t) \end{aligned} \quad (3-35)$$

where  $c_v(t)$  is the B-coefficient vector of the test function  $s_v \in \mathcal{S}_0$ ,  $F$  contains the contribution of the in domain forcing model and  $u_\Gamma$  represents the control input.

### Transformation to state space

The system of Equation (3-35) needs to be solved for  $\dot{c}(t)$ . This is done by using a null space approach, significantly reducing the size of the system and transforming the system to state space format. In order to do that Equation (3-34) needs to be rewritten as

$$Q c(t) = \bar{G}_\Gamma u_\Gamma(t). \quad (3-36)$$

Then let  $V$  be a basis for  $\text{null}(Q)$  such that  $QV = 0$  and let  $c_p(t) = C_p u_\Gamma(t)$  be a particular solution of Equation (3-36). The general solution for Equation (3-36) can then be written as

$$c(t) = V \tilde{c}(t) + C_p u_\Gamma(t) \quad (3-37)$$

with  $\tilde{c} \in \mathbb{R}^{N-R^*}$  the coordinate vector of  $c$  relative to the basis for  $\text{null}(Q)$  and with  $R^*$  the rank of  $Q$ . Since  $Q c_v = 0$  for all B-coefficient vectors  $c_v$ , the solution set for  $c_v$  can be written as  $c_v = V \tilde{c}_v$ . Substituting this and Equation (3-37) into Equation (3-36) and reordering gives

$$(V^T M V) \dot{\tilde{c}}(t) = V^T [K V \tilde{c}(t) + K C_p u_\Gamma(t) + F u(t) - M C_p \dot{u}_\Gamma(t)] \quad (3-38)$$

Defining the following matrices

$$\begin{aligned} A &= (V^T M V)^{-1} V^T K V, & A_\Gamma &= (V^T M V)^{-1} V^T K C_p \\ B_c &= (V^T M V)^{-1} V^T F, & B_\Gamma &= -(V^T M V)^{-1} V^T M C_p \end{aligned}$$

Equation (3-38) can be written as

$$\dot{\tilde{c}}(t) = A \tilde{c}(t) + A_\Gamma u_\Gamma(t) + B_c u(t) + B_\Gamma \dot{u}_\Gamma(t) \quad (3-39)$$

This can be written in state space format as

$$\begin{bmatrix} \dot{\tilde{c}} \\ \dot{u}_\Gamma \end{bmatrix} = \begin{bmatrix} A & A_\Gamma \\ 0 & 0 \end{bmatrix} \begin{bmatrix} \tilde{c} \\ u_\Gamma \end{bmatrix} + \begin{bmatrix} B_c \\ 0 \end{bmatrix} u + \begin{bmatrix} B_\Gamma \\ 1 \end{bmatrix} \dot{u}_\Gamma \quad (3-40)$$

## 3-2 Control framework synthesis

This section will provide a more detailed description of the two control frameworks introduced in Section 2-3. First the LQG problem is described in detail, introducing the separation principle, after which an algorithm is introduced that synthesizes a controller for the generalized robust control problem. This algorithm is also used for some of the advanced robust control frameworks described in Section 3-3.

### 3-2-1 The LQG problem

The objective of the  $H_2$  control problem is often solved using the LQG problem, which is a special case of  $H_2$  optimal control. For the LQG problem the plant model is defined as

$$\dot{x} = Ax + Bu + w_d \quad (3-41)$$

$$y = Cx + w_n \quad (3-42)$$

where  $w_d$  and  $w_n$  are both white noise processes. Here Assumption (A5) is used to make  $P_{11}$  strictly proper and thus to simplify the algorithm. In order to solve the LQG problem, a controller  $u = K(s)y$  needs to be found such that

$$J = E \left\{ \lim_{T \rightarrow \infty} \frac{1}{T} \int_0^T [x^T Q x + u^T R u] dt \right\} \quad (3-43)$$

where  $Q = Q^T \geq 0$  and  $R = R^T \geq 0$ . If we define the error signal  $z$  as

$$z = \begin{bmatrix} Q^{\frac{1}{2}} & 0 \\ 0 & R^{\frac{1}{2}} \end{bmatrix} \begin{bmatrix} x \\ u \end{bmatrix} \quad (3-44)$$

and the stochastic inputs as

$$\begin{bmatrix} w_d \\ w_n \end{bmatrix} = \begin{bmatrix} W^{\frac{1}{2}} & 0 \\ 0 & V^{\frac{1}{2}} \end{bmatrix} w \quad (3-45)$$

we can represent the LQG problem as an  $H_2$  optimal control problem, resulting in the cost function

$$J = E \left\{ \lim_{T \rightarrow \infty} \frac{1}{T} \int_0^T z(t)^T z(t) dt \right\} \quad (3-46)$$

The generalized plant from Equation (2-12) can now be written as

$$P = \left[ \begin{array}{c|cc} A & B_1 & B_2 \\ \hline C_1 & D_{11} & D_{12} \\ C_2 & D_{21} & D_{22} \end{array} \right] = \left[ \begin{array}{c|cc|c} A & W^{\frac{1}{2}} & 0 & B \\ \hline Q^{\frac{1}{2}} & 0 & 0 & 0 \\ 0 & 0 & 0 & R^{\frac{1}{2}} \\ \hline C & 0 & V^{\frac{1}{2}} & 0 \end{array} \right] \quad (3-47)$$

### The separation principle

Solving the LQG problem can be split up in two independent problems using the separation principle as described in (Skogestad & Postlethwaite, 2001, pp. 354). The first step is to determine the optimal controller for a deterministic LQR problem and the second step is to determine the optimal state estimator. The final step is then to combine the optimal state estimator and the optimal state feedback into a LQG controller:

1. The control feedback  $K$  is computed using a simple LQR controller to optimize the objective function described by Equation (3-43). This is done by solving the Riccati equation such that the control signal is equal to  $u(t) = -Kx(t)$ , where

$$K = R^{-1}B^T X \quad (3-48)$$

and  $X = X^T \geq 0$  is the solution to the algebraic Riccati equation

$$A^T X + XA - XBR^{-1}B^T X + Q = 0 \quad (3-49)$$

2. The next step is to compute the estimation feedback gain  $L$  using a Kalman estimator. The Kalman filter has the following structure:

$$\dot{\hat{x}} = A\hat{x} + Bu + L(y - C\hat{x}) \quad (3-50)$$

The optimal estimation feedback gain is given by

$$L = YC^T V^{-1} \quad (3-51)$$

where again we find  $T = Y^T \geq 0$  using the algebraic Riccati equation

$$YA^T + AY - YC^T V^{-1} CY + W = 0 \quad (3-52)$$

3. The last step is to combine steps 1 and 2 to create the following compensator:

$$\begin{aligned} \dot{\hat{x}} &= (A + BK + LC)\hat{x} + Ly \\ u &= K\hat{x} \end{aligned} \quad (3-53)$$

The closed-loop dynamics can now be described as

$$\frac{d}{dt} \begin{bmatrix} x \\ x - \hat{x} \end{bmatrix} = \begin{bmatrix} A - BK & BK \\ 0 & A - LC \end{bmatrix} \begin{bmatrix} x \\ x - \hat{x} \end{bmatrix} + \begin{bmatrix} I & 0 \\ 0 & -I \end{bmatrix} \begin{bmatrix} w_d \\ w_n \end{bmatrix} \quad (3-54)$$

This system provides an optimal control signal  $u$  proportional to the estimate flow  $\hat{x}$  using signals from the measurement  $y$ .

#### 3-2-2 General $H_\infty$ algorithm

The algorithm presented by Doyle et al. (1989) is rather similar to the algorithm of Section 2-3-2. However, this algorithm does not minimize an objective function, as much as tries to find a bound for the objective function of Equation (2-15) according to  $\|F_l(P, K)\|_\infty < \gamma$ . Both algorithms require the solutions of two Riccati equations and they both have steps which can be separated from each other:

1. The optimal state feedback controller  $F_\infty$  is found by solving the Riccati equation, such that the control signal is equal to

$$u = F_\infty x(t) \quad (3-55)$$

where  $F_\infty = -(D_{12}^T D_{12})^{-1} B_2^T X_\infty$  and  $X_\infty \geq 0$  is a solution to the algebraic Riccati equation

$$A^T X_\infty + X_\infty A + C_1^T C_1 + X_\infty (\gamma^{-2} B_1 B_1^T - B_2 B_2^T) X_\infty = 0 \quad (3-56)$$

such that  $A + (\gamma^{-2} B_1 B_1^T - B_2 B_2^T) X_\infty$  is stable.

2. Then, the optimal estimator  $L_\infty$  is given by

$$\begin{aligned} \dot{\hat{x}}(t) &= A\hat{x}(t) + L_\infty [y(t) - C_2 \hat{x}(t)], & \hat{x}(0) &= 0 \\ \hat{z}(t) &= C_1 \hat{x}(t) \end{aligned} \quad (3-57)$$

where  $L_\infty = Y_\infty C_2^T (D_{21} D_{21}^T)^{-1}$  and  $Y_\infty > 0$  is a solution to the algebraic Riccati equation

$$A Y_\infty + Y_\infty A^T + B_1 B_1^T + Y_\infty (\gamma^{-2} C_1^T C_1 - C_2^T C_2) Y_\infty = 0 \quad (3-58)$$

such that  $A + Y_\infty (\gamma^{-2} C_1^T C_1 - C_2^T C_2)$  is stable.

3. If for the two Riccati solutions  $X_\infty$  and  $Y_\infty$  holds that

$$\rho(X_\infty Y_\infty) < \gamma^2 \quad (3-59)$$

where  $\rho(X_\infty Y_\infty)$  denotes the maximum eigenvalue of  $XY$ , we can write  $Z_\infty = (I - \gamma^{-2} X_\infty Y_\infty)$ .

Combining these steps results in the following state estimator and state feedback:

$$\dot{\hat{x}} = A\hat{x} + B_1 \gamma^{-2} B_1^T X_\infty \hat{x} + B_2 u + Z_\infty L_\infty (C_2 \hat{x} - y) \quad (3-60)$$

$$u = F_\infty \hat{x} \quad (3-61)$$

The algorithm in presented above constructs a controller which achieves the  $H_\infty$  bound for a given  $\gamma > 0$ . Optimizing the controller is done by iteration on  $\gamma$  trying to find the minimum achievable  $H_\infty$  norm  $\gamma_{\min}$ . This can be done by performing a bisection, testing each value of  $\gamma$  for whether it is greater or smaller than  $\gamma_{\min}$ .

### 3-3 Advanced robust control methods

In the previous chapter a comparison was made between the different robust control methods that use information about the uncertainty to design less conservative controllers. This section provides a more detailed description about these methods. Section 3-3-1 describes the structured singular value synthesis, a method using structured uncertainty, Section 3-3-2 describes the signal-based approach which uses weighed external signals to introduce uncertainty into the model and Section 3-3-3 describes the two-step loop-shaping approach used to account for dynamic uncertainty.

### 3-3-1 Structured singular value synthesis

A very powerful method to for structured uncertainty is the structured singular value or  $\mu$ -synthesis, extensively described by (Skogestad & Postlethwaite, 2001, pp. 335-345). The structured singular value can be considered a special type of the maximum singular value  $\bar{\sigma}$ . Even more, if the uncertainty is structured using one block, we can say that  $\mu(M) = \bar{\sigma}(M)$ . The structured singular value synthesis is a valuable method or a specific type of structured uncertainty with a plant of the shape

$$G_p(s) = G(s) + W_1 \begin{bmatrix} \Delta_1 & 0 \\ 0 & \Delta_2 \end{bmatrix} W_2, \quad \Delta \in \mathbf{\Delta}_s(\rho) \quad (3-62)$$

where  $\mathbf{\Delta}_s(\rho)$  is defined as the set of general structured norm-bounded uncertainty with norm-bound equal to  $\rho > 0$ , represented by

$$\mathbf{\Delta}_s(\rho) = \{ \Delta = \text{block diag}(\Delta_1, \dots, \Delta_s), \quad \Delta_i \in H_\infty^{r_i \times r_i}, \|\Delta_i\|_\infty \leq \rho \}. \quad (3-63)$$

where  $H_\infty^{r_i \times r_i}$  is defined as the set of stable  $r_i \times r_i$  transfer functions with a bounded  $H_\infty$  norm. The problem then becomes to find a controller such that the control system in Figure 2-4 is stable for all uncertainties  $\Delta \in \mathbf{\Delta}_s(\rho)$ . This is equivalent to

$$\det(I - M\Delta) \neq 0, \quad \forall \omega \text{ and } \Delta \in \mathbf{\Delta}_s(\rho) \quad (3-64)$$

In contrast to Section 2-3-3 where the  $H_\infty$  norm described by Equation (2-15) was minimized, this problem cannot readily be solved by an algorithm. Instead, Doyle (1982) has introduced the structured singular value  $\mu(M)$  of  $M$ . It is defined by introducing the smallest value of the uncertainty magnitude (or spectral radius)  $\rho$  such that there exists  $\Delta \in \mathbf{\Delta}_s(\rho)$  which destabilizes the plant:

$$\rho_{\min}(M) = \min \{ \rho \mid \det(I - M\Delta) = 0 \text{ for some } \Delta \in \mathbf{\Delta}_s(\rho) \} \quad (3-65)$$

That means that for all  $\rho < \rho_{\min}(M)$  the plant is stable. The structured singular value is then defined as

$$\mu(M) = \rho_{\min}(M)^{-1} \quad (3-66)$$

The structured singular value synthesis (or  $\mu$ -synthesis) now consists of finding a stabilizing controller such that the structured singular value of the closed loop system satisfies

$$\sup_{\omega} \mu(F(j\omega)) < \rho^{-1} \quad (3-67)$$

Since there is no algorithm to compute the structured singular value, an upper bound on  $\mu$  is computed. This is done using the  $DK$ -iteration with the  $N\Delta$  structure which provides an upper bound  $D$  according to

$$\mu(N) \leq \min_{D \in \mathcal{D}} \bar{\sigma}(DND^{-1}) \quad (3-68)$$

The algorithm tries to find the controller that minimizes the peak value over the frequency of this upper bound according to

$$\min_K \left( \min_{D \in \mathcal{D}} \|DN(K)D^{-1}\|_\infty \right) \quad (3-69)$$

The iterations minimize Equation (3-69) by alternating between keeping either  $D$  or  $K$  fixed, and minimizing for the other. This minimization is done using the  $H_\infty$  controller synthesis as described in Section 2-3-3. One of the biggest disadvantages of the  $DK$ -iteration is that it results in rather large controllers. According to (Skogestad & Postlethwaite, 2001, pp. 336) the order of the controller resulting from each iteration is equal to the number of states in the plant  $G(s)$ , plus the number of states in the weights, plus twice the number of states in  $D(s)$ . This makes this methodology not very attractive for AFC purposes, as fluid models, even after model reduction, often cope with relatively large plants.

### 3-3-2 Signal based approach

In the signal-based approach the aim is to minimize the energy in certain external input signals. This approach combines model uncertainty and external signals affecting the system. The external signals are then weighted as they enter the model so that the disturbances closely match the physical system, as shown in Figure 3-1a. The signal based approach can be solved using the general  $H_\infty$  algorithm described in Section 2-3-3 by modifying the general control configuration by

$$w = \begin{bmatrix} d \\ r \\ n \end{bmatrix} \quad z = \begin{bmatrix} z_1 \\ z_2 \end{bmatrix} \quad v = \begin{bmatrix} r_s \\ y_m \end{bmatrix} \quad u = u \quad (3-70)$$

This problem can be converted to the  $S/KS$  mixed sensitivity approach by setting  $G_d = W_d = I$  and  $W_i = W_n = 0$ . The mixed sensitivity approach is based on the shaping of transfer functions, in particular the sensitivity function  $S = (I + GK)^{-1}$  and the complementary sensitivity function  $T = I - S$  where  $T$  is the closed loop transfer function described by  $T = GK(I + GK)^{-1}$ . This approach minimizes

$$\left\| \begin{bmatrix} W_e S \\ W_u K S \end{bmatrix} \right\|_\infty \quad (3-71)$$

As can be seen in Figure 3-1a, the general signal based approach does not contain any model uncertainty. Hence, this problem is solved as a general  $H_\infty$  control problem. However, when implementing model uncertainty, the signal based control problem is converted into a robust performance problem (Figure 3-1b), where the structured singular value needs to satisfy

$$\mu(M(j\omega)) < 1, \forall \omega. \quad (3-72)$$

This problem can be solved using the  $\mu$ -synthesis approach presented in Section 3-3-1, where  $M(j\omega)$  describes the transfer function between  $[d \ r \ n \ \delta]^T$  and  $[z_1 \ z_2 \ \epsilon]^T$ .

### 3-3-3 $H_\infty$ loop-shaping

This section describes the  $H_\infty$  loop-shaping design method as proposed by McFarlane & Glover (1990). This methodology consists of two steps combining classical loop-shaping with  $H_\infty$  robust stabilization. In the first step the plant is augmented using

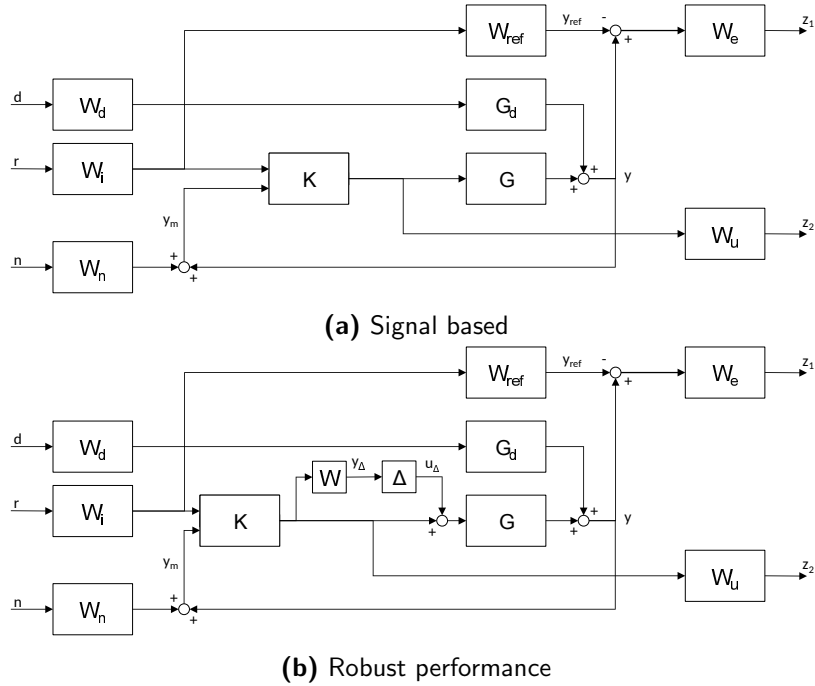


**Figure 3-1:** The signal based  $H_\infty$  control problem can be transformed to a robust performance problem by introducing a multiplicative dynamic uncertainty model. The inputs  $\mathbf{d}$ ,  $\mathbf{r}$  and  $\mathbf{n}$  describe the disturbances, set points and noise signals, respectively. The outputs  $\mathbf{z}_1$  and  $\mathbf{z}_2$  represent the error and the control signals.

pre- and post-compensators to shape the singular values of the open-loop frequency response. The shaped plant  $G_s$  is then given by

$$G_s = W_2 G W_1 \tag{3-73}$$

as is shown in Figure 3-2. The second step consists of a general robust stabilization of the shaped plant  $G_s$  with a normalized coprime factorization  $G_s = M_s^{-1} N_s$ , synthesizing a controller  $K_s$ . The feedback controller for the plant  $G$  can then be obtained using

$$K = W_1 K_s W_2 \tag{3-74}$$

Finally, the  $\nu$ -gap as proposed by Vinnicombe (2000) is introduced as a useful tool to provide bounds on the closed loop performance.

### Open-loop augmentation

The first step in the  $H_\infty$  loop-shaping design approach is to shape the singular values of the open-loop frequency response. (Skogestad & Postlethwaite, 2001, pp. 382-383) provides a detailed and extended walkthrough for this approach, which is summarized here:

1. Scale the outputs so that equal magnitudes of cross-coupling into each of the outputs is equally undesirable, and scale the inputs by a given percentage of their expected range of operation.

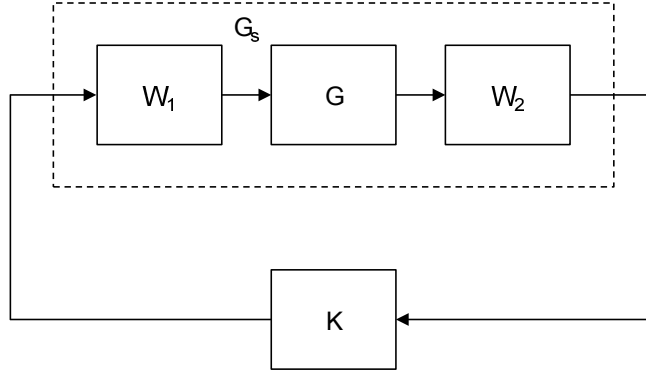


**Figure 3-2:** The shaped plant  $G_s$  given by pre- and post-compensators  $W_1$  and  $W_2$

2. Order the inputs and outputs so that the plant is as diagonal as possible.
3. Select the elements of the diagonal compensators so that the singular values of  $W_2GW_1$  are desirable:
  - high gain at low frequencies
  - roll-off rates of 20 dB/decade at desired bandwidths
  - higher roll-off rates at high frequencies

(Skogestad & Postlethwaite, 2001, pp. 384) provide some additional options to align the singular values and to provide control over actuator usage, but these are not described here.

### Coprime factorization

The shaped plant  $G_s$  can be stabilized by first determining the normalized left coprime factorization of the plant:

$$G_s = M^{-1}N \quad (3-75)$$

The perturbed plant model  $G_p$  can then be written as

$$G_p = (M + \Delta_M)^{-1}(N + \Delta_N) \quad (3-76)$$

The objective is then to stabilize the family of perturbed plants defined by:

$$G_p = \left\{ (M + \Delta_M)^{-1}(N + \Delta_N) \mid \left\| \begin{bmatrix} \Delta_N & \Delta_M \end{bmatrix} \right\|_\infty < \epsilon \right\} \quad (3-77)$$

where  $\epsilon > 0$  is the stability margin which is to be maximized. The stability property for the perturbed feedback system is robust if and only if the nominal feedback system is stable and

$$\gamma_K \triangleq \left\| \begin{bmatrix} K \\ I \end{bmatrix} (I - GK)^{-1} M^{-1} \right\|_\infty \leq \frac{1}{\epsilon} \quad (3-78)$$

The lowest achievable value of  $\gamma_K$  can be determined using

$$\gamma_{\min} = (1 + \rho(XZ))^{1/2} = \epsilon_{\max}^{-1} \quad (3-79)$$

where  $\rho(XZ)$  represents the maximum eigenvalue of the the two solutions to the Ricatti equation. They can be found for a minimal state-space realization of  $G$  using

$$(A - BS^{-1}D^TC)Z + Z(A - BS^{-1}D^TC)^T - ZC^TR^{-1}CZ + BS^{-1}B^T = 0 \quad (3-80)$$

where  $R = I + DD^T$  and  $S = I + D^TD$ , and

$$(A - BS^{-1}D^TC)^TX + X(A - BS^{-1}D^TC) - XBS^{-1}B^TX + C^TR^{-1}C = 0. \quad (3-81)$$

The controller that satisfies Equation (3-78) is given by

$$K = \left[ \frac{A + BF + \gamma^2(L^T)^{-1}ZC^T(C + DF)}{B^TX} \mid \frac{\gamma(L^T)^{-1}ZC^T}{-D^T} \right] \quad (3-82)$$

$$F = -S^{-1}(D^TC + B^TX) \quad (3-83)$$

$$L = (1 - \gamma^2)I + XZ \quad (3-84)$$

### The $\nu$ -gap metric

The resulting normalized coprime factor stability margin can be combined with the  $\nu$ -gap metric to provide bounds on the closed-loop performance Vinnicombe (2000). In order to do this we introduce the  $\nu$ -gap metric  $\delta_\nu(G, G_p)$ , with  $G$  the nominal plant and  $G_p$  the perturbed plant, defined by Vinnicombe (2000) as

$$\delta_\nu(G, G_p) \triangleq \inf_{\substack{\Delta_N, \Delta_M \in \mathcal{L}^\infty \\ \text{wno}|M + \Delta_N| = \eta(G_p)}} \left\| \begin{bmatrix} \Delta_N \\ \Delta_M \end{bmatrix} \right\|_\infty \quad (3-85)$$

where,  $\text{wno } g(s)$  is the Counter-Clock Wise (CCW) winding number around 0 as  $s$  follows the CCW Nyquist D-contour,  $|\cdot|$  is the determinant and  $\eta(G)$  is the number of poles on the right-hand-plane of  $G$ . The  $\nu$ -gap as described in Equation (3-85) represents the closeness of the nominal plant  $G$  and the perturbed plant  $G_p$ . The  $\nu$ -gap can be calculated using

$$\delta_\nu(G, G_p) = \left\| (I + G_p G_p^*)^{-1/2} (G - G_p) (I + G^* G)^{-1/2} \right\| \quad (3-86)$$

where  $(X^* X)^{-1/2}$  is the Hermitian square root of the matrix  $X^* X$ , satisfying  $((X^* X)^{-1/2})^2 = X^* X$ . Equation (3-86) only holds under two conditions:

1.  $|I + G_p^*(j\omega)G(j\omega)| \neq 0$  for all  $\omega \in \mathbb{R}$ ,
2.  $\text{wno}|I + G_p^*G_p| + \eta(G) - \eta(G_p) - \eta_0(G_p) = 0$ , where  $\eta_0(G)$  denotes the number of pure imaginary poles of  $G$ .

otherwise  $\delta_\nu(G, G_p) = 1$ . The interesting thing about the  $\nu$ -gap is that it is closely related to the closeness between a high-dimensional model  $G$  and a reduced order model  $G_r$ . Namely, if the robust stability margin of Equation (3-79) is significantly larger than  $\delta_\nu(G, G_r)$ , robust closed-loop performance is guaranteed. This is readily implemented for models where model reduction methods such as balanced truncation have been used, as they have an analytic upper bound on the  $H_\infty$  norm of the error. As we see in Section 3-1-2, balanced truncation has the upper bound

$$\|G - G_r\|_\infty \leq 2 \sum_{k=r+1}^n \sigma_k(G). \quad (3-87)$$



## **Part IV**

# **Conclusions and Recommendations**



---

## Chapter 4

---

# Conclusion

The goal of this thesis was to develop a robust control framework for the KS equation using structured parametric uncertainty. The research question was divided into four subquestions regarding the structure of the uncertainty, the control method implementation, the performance of the robust controller and stability of the robust controller.

To answer the first question, it was shown that this discretization method results in a linear relation between the parameters of the PDE and the state matrix. By use of the state-modeling framework from Tol, de Visser and Kotsonis (2016), explicit finite dimensional representations can be obtained for all differential operators in the KS equation (Tol, Visser, & Kotsonis, 2016). These representations determine how the parameters from the equation are mapped to the state space equations, defining the structure in which the uncertainty appears in the model. The linear relation between the parameters and the state matrix allow for parametric decomposition of the state matrix. The parametric uncertainty can then be accounted for in the model using Linear Fractional Transformations (LFTs).

An LQG controller was then designed using a feedforward configuration, showing excellent nominal performance and inherent robust stability. However, the system was shown to be sensitive to uncertainty in the parameters. As uncertainty is always present in a physical system, it was suggested that a robust controller is bound to achieve a better performance. However, in a feedforward configuration a robust control design is impossible, and hence a feedback control design was proposed.

The parametric uncertainty was accounted for in the model using the structure defined by the differential operators, proving that is possible to account for structured parametric uncertainty for flow control applications. The state matrix was decomposed and the nominal parameters were replaced with uncertain parameters, allowing for a set of perturbed plants to be generated. This set of plants was then used to generate a  $\mu$ -controller. This method is recommended by Skogestad & Postlethwaite (2001) for structured parametric uncertainty.  $\mu$ -synthesis uses  $DK$ -iterations to find an upper bound on the structured singular value of the closed-loop system. This structured singular value could be used to determine the maximum perturbation for which the system is guaranteed to be stable.

One of the more important design considerations when designing a feedback controller is the distance between the actuator and the sensor. It was shown that if the sensor is placed too far downstream, the feedback loop is rendered ineffective. However, placing the sensor too close to the actuator results in a quickly destabilized system. An optimal actuator/sensor combination was determined, and for this configuration two  $\mu$ -controllers were designed, yielding a controller accounting for structured parametric uncertainty.

The LQG controller in feedforward configuration was compared to the  $\mu$  controller in feedback configuration, and it was shown that  $\mu$  controller outperforms the LQG controller for any perturbation where  $|\delta| > 2\%$ . When the closed-loop system is perturbed, the  $\mu$ -controllers prove to be much less sensitive to this perturbation than the LQG controller. For perturbations where  $|\delta| > 50\%$ , the  $\mu$ -controllers potentially destabilize the system. However, a perturbation that destabilizes the system with the  $\mu$ -controller, the performance of the LQG controller reduces to a relative energy reduction of  $E = 0.8$ , rendering the controller nearly ineffective. From this we can conclude that a  $\mu$ -controller consequently reduces the energy in the system, while the performance of the LQG controller significantly depends on the amount of uncertainty present in the system. A  $\mu$  controller designed with structured parametric uncertainty is hence expected to provide much better results than an LQG controller in feedforward configuration.

---

## Chapter 5

---

# Recommendations

This thesis has shown that robust control has much potential in the field of active flow control. One of the drawbacks of robust control methods is the decrease in performance that comes with an increase in robustness. It is suggested that future research should be focused around methods that improve performance characteristics of the system.

A very obvious method of performance improvement is the aggration of multiple actuator/sensor sets. The interesting question, however, is how the combination of sensors will influence the systems stability. During this research it became evident that the placing of the sensor with respect to the actuator has a strong influence on the stability and performance characteristics. The placement of the sensor with respect to the actuator should be optimized to achieve the maximum stability and performance for both the nominal and perturbed system, which could easily be combined with a study to how the aggregated sensor/actuator couples should be placed with respect to eachother.

Another configuration that should be explored is the combination of a mixed feedback-feedforward configuration, where an LQG controller is used to achieve a high performance in the nominal case, and a  $\mu$  controller is used to achieve high performance when the system is perturbed. However, as shown in this research, feedforward is very sensitive to model error, so the combination of the two controllers might even show worse performance and stability characteristics.



---

# Bibliography

- Armaou, A., & Christofides, P. D. (2000, March). Feedback control of the kuramoto-sivashinsky equation. *Physica D*, *137*(1), 49-61.
- Bagheri, S., Henningson, D. S., Hoepffner, J., & Schmid, P. J. (2009). Input-output analysis and control design applied to a linear model of spatially developing flows. *Applied Mechanics Reviews*, *62*.
- Baramov, L., Tutty, O. R., & Rogers, E. (2002). Robust control of linearized poiseuille flow. *Journal of guidance, control, and dynamics*, *25*(1), 145–151.
- Baramov, L., Tutty, O. R., & Rogers, E. (2004).  $H_\infty$  control of nonperiodic two-dimensional channel flow. *IEEE Transactions on Control Systems Technology*, *12*.
- Barbagallo, A., Sipp, D., & Schmid, P. J. (2009). Closed-loop control of an open cavity flow using reduced-order models. *Journal of Fluid Mechanics*, *641*, 1–50.
- Bewley, T. R., & Liu, S. (1998). Optimal and robust control and estimation of linear paths to transition. *Journal of Fluid Mechanics*, *365*.
- Bobba, K. M. (2004). *Robust flow stability: theory, computations and experiments in near wall turbulence*. Unpublished doctoral dissertation, Citeseer.
- Brunton, S. L., & Noack, B. R. (2015, September). Closed-loop turbulence control: Progress and challenges. *Applied Mechanics Reviews*, *67*(5).
- Chen, K. K., & Rowley, C. W. (2011, August).  $H_2$  optimal actuator and sensor placement in the linearised complex ginzburg-landau system. *Journal of Fluid Mechanics*, *681*, 241-260.
- Chen, K. K., & Rowley, C. W. (2013, April). Normalized coprime robust stability and performance guarantees for reduced-order controllers. *IEEE Transactions on Automatic Control*, *58*(4), 1068-1073.
- Doyle, J. C. (1982, November). Analysis of feedback systems with structured uncertainties. *IEE Proceedings*, *129*(6), 242-250.

- Doyle, J. C., Glover, K., Khargonekar, P. P., & Francis, B. A. (1989). State-space solutions to standard  $h_2$  and  $h_\infty$  control problems. *IEEE Transactions on Automatic control*, *34*(8), 831–847.
- Fabbiane, N., Semeraro, O., & Bagheri, S. (2014). Adaptive and model-based control theory applied to convectively unstable flows. *Applied Mechanics Reviews*, *66*.
- Fabbiane, N., Simon, B., Fischer, F., Grundmann, S., Bagheri, S., & Henningson, D. S. (2015). On the role of adaptivity for robust laminar flow control. *Journal of Fluid Mechanics*, *767*.
- Flinois, T. L. B., & Morgans, A. S. (2016). Feedback control of unstable flows: a direct modelling approach using the eigensystem realisation algorithm. *Journal of Fluid Mechanics*, *793*, 41–78.
- Gomes, S. N., Papageorgiou, D. T., & Pavliotis, G. A. (2016). Stabilizing non-trivial solutions of the generalized kuramotosivashinsky equation using feedback and optimal control. *IMA Journal of Applied Mathematics*.
- Green, M., & Limebeer, D. J. N. (2012). *Linear robust control*. Courier Corporation.
- Gu, D. W., Petkov, P. H., & Konstantinov, M. M. (2005). *Robust control design with matlab®*. Springer Science & Business Media.
- Ilak, M., & Rowley, C. W. (2008). Modeling of transitional channel flow using balanced proper orthogonal decomposition. *Physics of Fluids*, *20*(3), 34–103.
- Jamal, R. al, & Morris, K. (2015). Output feedback control of the kuramoto-sivashinsky equation. In *2015 54th ieee conference on decision and control (cdc)* (p. 567–571).
- Jones, B. L., Heins, P. H., Kerrigan, E. C., Morrison, J. F., & Sharma, A. S. (2015). Modelling for robust feedback control of fluid flows. *Journal of Fluid Mechanics*, *769*.
- Kim, J., & Bewley, T. R. (2007). A linear systems approach to flow control. *Annual Review of Fluid Mechanics*, *39*.
- Kuramoto, Y., & Tsuzuki, T. (1976). Persistent propagation of concentration waves in dissipative media far from thermal equilibrium. *Progress of theoretical physics*, *55*(2), 356–369.
- Lauga, E., & Bewley, T. R. (2001).  $H_\infty$  control of linear global instability in models of non-parallel wakes. In *Tsfp digital library online*.
- Lauga, E., & Bewley, T. R. (2004). Performance of a linear robust control strategy on a nonlinear model of spatially developing flows. *Journal of Fluid Mechanics*, *512*, 343–374.
- McFarlane, D. C., & Glover, K. (1990). *Robust controller design using normalized coprime factor plant descriptions*. Springer.
- Moore, B. C. (1981). Principal component analysis in linear systems: Controllability, observability, and model reduction. *IEEE Transactions on Automatic Control*, *29*, 17–32.
- Rowley, C. W. (2005). Model reduction for fluids, using balanced proper orthogonal decomposition. *International Journal of Bifurcation and Chaos*, *15*(03), 997–1013.

- Rowley, C. W., Colonius, T., & Murray, R. M. (2004). Model reduction for compressible flows using pod and galerkin projection. *Physica D: Nonlinear Phenomena*, 189(1), 115–129.
- Sakthivel, R., & Ito, H. (2007, March). Non-linear robust boundary control of the kuramoto-sivashinsky equation. *IMA Journal of Math*, 24(1), 47-55.
- Schirrer, A., Westermayer, C., Hemedi, M., & Kozek, M. (2013). Robust lateral blended-wing-body aircraft feedback control design using a parameterized lfr model and dgk-iteration. In *Progress in flight dynamics, guidance, navigation, control, fault detection, and avionics* (Vol. 6, pp. 749–766).
- Sipp, D., & Schmid, P. J. (2016). Linear closed-loop control of fluid instabilities and noise-induced perturbations: A review of approaches and tools. *Applied Mechanics Reviews*, 68(2), 020801.
- Sirovich, L. (1987). Turbulence and the dynamics of coherent structures parts i-iii. *Quarterly of applied mathematics*, 45(3), 561–590.
- Sivashinsky, G. I. (1977). Nonlinear analysis of hydrodynamic instability in laminar flames. derivation of basic equations. *Acta astronautica*, 4(11-12), 1177–1206.
- Skogestad, S., & Postlethwaite, I. (2001). *Multivariate feedback control, analysis and design* (Second ed.). John Wiley & Sons, Ltd.
- Tofighi, S. R., Bayat, F., & Merrikh-Bayat, F. (2015). Robust feedback linearization of an isothermal continuous stirred tank reactor: H mixed-sensitivity synthesis and dk-iteration approaches. *Transactions of the Institute of Measurement and Control*.
- Tol, H. J., Kotsonis, M., Visser, C. C. de, & Bamieh, B. (2016, 11). Localized modelling and feedback control of linear instabilities in 2-d wall bounded shear flows. *APS Division of Fluid Dynamics Meeting Abstracts*.
- Tol, H. J., Visser, C. C. de, & Kotsonis, M. (2016). Model reduction of parabolic pdes using multivariate splines. *International Journal of Control*, 1–16.
- Vinnicombe, G. (2000). *Uncertainty and feedback:  $H_\infty$  loop-shaping and the  $\nu$ -gap metric*. World Scientific.
- Visser, C. C. de, Chu, Q. P., & Mulder, J. A. (2009). A new approach to linear regression with multivariate splines. *Automatica*, 45(12), 2903-2909.
- Zhou, K., Doyle, J. C., Glover, K., et al. (1996). *Robust and optimal control* (Vol. 40). Prentice hall New Jersey.

